B. Karthikeyan
G. Gnanakumar
A. Therasa Alphonsa

Nano Metal Oxides

Engineering and Biomedical Applications

Springer

Nano Metal Oxides

B. Karthikeyan · G. Gnanakumar ·
A. Therasa Alphonsa

Nano Metal Oxides

Engineering and Biomedical Applications

Springer

B. Karthikeyan
Department of Chemistry
Annamalai University
Chidambaram, Tamil Nadu, India

G. Gnanakumar
Department of Physical Chemistry
Madurai Kamaraj University
Madurai, Tamil Nadu, India

A. Therasa Alphonsa
PG & Research Department of Chemistry
Government Arts College, C-Mutlur
Chidambaram, Tamil Nadu, India

ISBN 978-981-19-9443-2 ISBN 978-981-19-9444-9 (eBook)
https://doi.org/10.1007/978-981-19-9444-9

This Springer imprint is published by the registered company Springer Nature Singapore Pte Ltd.
The registered company address is: 152 Beach Road, #21-01/04 Gateway East, Singapore 189721, Singapore

Contents

Part I
Introduction to Nanomaterials

Chapter 1
Introduction of Metal Oxides and Impact of Nanosize

In many fields of chemistry, physics, and materials research, metal oxides are crucial. The variety of oxide compounds that may be created by the metal elements is enormous. With an electrical structure that may have a metallic, semiconductor, or insulator property, they can adopt a huge variety of structural shapes. Oxides are employed in technical processes to create fuel cells, sensors, piezoelectric devices, microelectronic circuits, coatings to protect surfaces from corrosion, and catalysts. Making nanostructures or nanoarrays with unique features in comparison to those of bulk or single particle species is an aim in the developing area of nanotechnology. Due to their small size and many corner or edge surface sites, oxide nanoparticles may display unusual physical and chemical characteristics. Three significant classes of fundamental characteristics in any material are anticipated to be influenced by particle size. The first one includes the structural properties, namely the cell parameters and lattice symmetry. Typically, bulk oxides are reliable, stable, and have crystal structures that are well characterized. However, it is important to take into account the increasing significance of surface free energy and stress as particle size decreases. Changes in thermodynamic stability associated with size can lead to modifications in cell parameters and/or structural transformations, and in extreme cases, the nanoparticle can vanish as a result of interactions with its environment and a high surface free energy. A nanoparticle has to have a low surface free energy in order to show mechanical or structural stability. This need has the effect of making phases that are poorly stable in bulk materials very stable in nanostructures. These structural changes have been seen in the oxides of TiO_2, VO_x, Al_2O_3, or MoO_x. For instance, structural aberrations brought on by size have been seen in nanoparticles of Al_2O_3, NiO, Fe_2O_3, ZrO_2, MoO_3, and Y_2O_3 as well as alterations in cell characteristics. The growing number of surface and interface atoms causes stress/strain and corresponding structural disturbances as the particle size decreases. In addition to this "intrinsic" strain, there may also be "extrinsic" strain connected to a specific synthesis technique that may be partly eased by annealing or calcination. Non-stoichiometry is another frequent occurrence. On the other hand, interactions with the substrate on which the nanoparticles are supported might make things more difficult and lead

B. Karthikeyan et al., *Nano Metal Oxides*,
https://doi.org/10.1007/978-981-19-9444-9_1

to structural phase changes or perturbations that are not present in the oxide's bulk state. The electrical characteristics of the oxide are connected to the second significant influence of size. The existence of distinct, atom-like electronic states causes the nanostructure to create the so-called quantum size or confinement effects in any material. These states may be seen from the perspective of the solid state as a superposition of bulk-like states with a concurrent rise in oscillator strength. Experiments on oxides have also shown further broad electronic effects of quantum confinement relating to the energy shift of exciton levels and optical band gap. The long-range effects of the Madelung field, which are absent or restricted in a nanostructured oxide, are a crucial consideration when dealing with the electrical characteristics of a bulk oxide surface. When switching from big periodic structures to tiny clusters or aggregates—which must essentially be seen as being somewhat small for ionic solids and much larger for covalent ones—theoretical studies for oxides demonstrate a redistribution of charge. In systems with partial ionic or covalent character, the degree of ionicity or covalency in a metal–oxygen bond may, however, greatly rely on size; an increase in the ionic component of the metal–oxygen bond in parallel with the size lowering has been postulated. 15 The solid's physical and chemical characteristics, which make up the third category of attributes affected by size in a basic categorization, are plainly driven by its structural and electrical properties. Many oxides have limited reactivity and broad band gaps in their bulk state. Reduced average oxide particle size does, in fact, alter the band gap's size, which has a significant impact on conductivity and chemical reactivity. Due to their significance in chemistry, surface characteristics make up a unique subset of the topics covered in this chapter. Chemical reactions between solid–liquid or solid–gas may typically be contained to the solid's surface and/or subsurface areas. As was already established, the two-dimensional (2D) character of surfaces has important structural consequences—typically a reconstruction or rearrangement of bulk geometries—as well as electrical ones, such as the occurrence of mid-gap states. When it comes to 2D-infinite surfaces, surface properties of nanostructured oxides are significantly altered, resulting in solids with novel sorption or acid/base properties. Additionally, the existence of O vacancies or undercoordinated atoms (such as corners or edges) in an oxide nanoparticle should result in particular geometrical configurations and occupied electronic states that are above the valence band of the corresponding bulk material, thereby enhancing the chemical activity of the system. In this chapter, we will examine the synthesis of nanoparticulated oxides, their key physicochemical characteristics, and then devote the last section to a number of well-known oxides. The impact of the fundamental nanostructure, such as the primary particle size, on structural and electrical characteristics and how these affect other industrially relevant features will get special consideration.

1.1 Introduction

Metal oxides are crucial in a variety of fields of chemistry, physics, and materials science. A wide variety of oxide compounds may be created by the metal elements.

These are capable of adopting a huge variety of structural geometries with electronic structures that may have metallic, semiconductor, or insulator characteristics. Oxides are employed in technology to make fuel cells, sensors, piezoelectric devices, microelectronic circuits, coatings to prevent corrosion on surfaces, and catalysts. Making nanostructures or nanoarrays with unique features in comparison to bulk or single particle species is an aim in the developing area of nanotechnology. Due to their small size and many corner or edge surface sites, oxidized nanoparticles might display unusual physical and chemical characteristics. Any material's three key groupings of fundamental characteristics are anticipated to be influenced by particle size. Lattice symmetry and cell parameters are included in the first one, which includes structural features. Typically, bulk oxides are reliable, stable, and have distinct crystal structures. The growing significance of surface free energy and stress with shrinking particle size must be taken into account, though. Changes in thermodynamic stability associated with size can lead to modification of cell parameters and/or structural changes, and in extreme cases, the nanoparticle can vanish due to interactions with its surrounding environment and a high surface free energy. A nanoparticle's surface free energy must be low for it to exhibit mechanical or structural stability. This need has the effect of causing phases with poor stability in bulk materials to become very stable in nanostructures. In TiO_2, VO_x, Al_2O_3, or MoO_x oxides, this structural phenomenon has been seen. Examples of size-induced structural distortions linked to changes in cell characteristics include nanoparticles of Al_2O_3, NiO, Fe_2O_3, ZrO_2, MoO_3, and Y_2O_3. Stress/strain and ensuing structural changes are produced when the particle size decreases due to the growing number of surface and contact atoms. In addition to this "intrinsic" strain, there may also be "extrinsic" strain connected to a specific synthesis technique that might be partly eased by annealing or calcination. Additionally, non-stoichiometry is a frequent occurrence. However, interactions with the substrate that the nanoparticles are supported on may exacerbate the situation and lead to structural disturbances or phases that are not present in the oxide's bulk form. The second significant impact of size is connected to the oxide's electrical characteristics. The existence of discrete, atom-like electronic states causes the so-called quantum size or confinement effects, which are produced by the nanostructure in any material. These states may be seen as a superposition of bulk-like states from the perspective of the solid state, with a corresponding rise in oscillator strength. The energy shift of exciton levels and optical band gap are two more broad electronic effects of quantum confinement that have been experimentally investigated on oxides. The long-range effects of the Madelung field, which are absent or severely constrained in a nanostructured oxide, are a crucial consideration when dealing with the electrical characteristics of a bulk oxide surface. Theoretical studies for oxides demonstrate a redistribution of charge upon transitioning from large periodic structures to small clusters or aggregates, which must roughly be regarded as relatively small for ionic solids while significantly larger for covalent ones. However, in systems with partial ionic or covalent character, the degree of ionicity or covalency in a metal-oxygen bond may greatly rely on size; it has been claimed that the ionic component of the metal-oxygen bond increases concurrently with the decrease in size. The solid's physical and chemical

characteristics—the third set of qualities affected by size in a straightforward classification are evidently driven by its structural and electrical characteristics. Many oxides have large band gaps and little reactivity in their bulk state. When the size of an oxide particle decreases, the band gap changes in size, which has a significant impact on the conductivity and chemical reactivity. Due to their significance in chemistry, surface characteristics are a rather unique category featured in this topic. Chemical reactions involving solid–liquid or solid–gas can frequently be restricted to the surface and/or subsurface regions of the solid. As was already mentioned, surfaces' two-dimensional (2D) nature has significant structural and electronic effects, such as the presence of mid-gap states and the typical rearrangement or reconstruction of bulk geometries. The surface properties of nanostructured oxides are significantly altered in comparison to 2D-infinite surfaces, resulting in solids with novel sorption or acid/base properties. In addition, the presence of undercoordinated atoms (such as corners or edges) or O vacancies in an oxide nanoparticle should result in specific geometrical arrangements and occupied electronic states that are located above the valence band of the corresponding bulk material, thereby enhancing the chemical activity of the system. This chapter will examine the synthesis of nanoparticulated oxides, as well as some of their most important physicochemical characteristics. The final section of the chapter will concentrate on several well-known oxides. We will pay close attention to how the primary nanostructure, such as primary particle size, affects structural and electronic properties and how these affect other industrially relevant properties.

1.2 Key Terms

(a) **Nanoscience and nanotechnology**—Nanoscience and nanotechnology are the sciences and technologies that deal with particles with sizes ranging from 1 to 100 nm.

(b) **Measurement-based classification of nanomaterials**—Nanomaterials are divided into three classes based on the reduction in size of materials in different dimensions.

S.No.	Size reduction in various coordinates	Size (nm)	Examples
1	3 dimensions	< 100	Nanoparticles, quantum dots
2	2 dimensions	< 100	Nanotubes, nanowires, nanofibres
3	1 dimension	< 100	Thin films, coatings

(c) **Pore diameter-based classification**

The majority of characteristics that are crucial for adsorption and diffusion applications depend on this value, making it a useful method for categorizing nanoporous materials. A typical diameter of 1–100 nm is indicated by the prefix

nano-. When molecules from different materials interact, this spectrum of their properties is significantly altered. In reality, the size of molecules that may diffuse inside a pore depends on its diameter, and information on diffusion and interaction properties can be obtained by comparing the dimensions of a pore and a guest molecule. Both the molecule–wall interaction and the molecule–molecule contact should be noticeable if the two dimensions are the same. As opposed to molecule–molecule interaction, there will be less of it during the diffusion process if the guest molecules are smaller than the pore size. According to the IUPAC definition, there are three main kinds of nanoporous materials depending on the size of their pores:

Microporous materials ($d < 2$ nm)—The pores in these materials are quite small. They can only host small molecules like gases or linear molecules, and their diffusion kinetics are sluggish, and their interaction properties are high. They are common in gas purification systems, membrane filters, and gas storage materials.

Mesoporous materials ($2 < d < 50$ nm)—Big molecules, such as aromatic systems or enormous polymeric monomers, may fit within the pores of these materials because of their large pore diameters. Capillarity typically contributes to the capillary-induced diffusion kinetics of the adsorbed molecules, with pore filling occurring after an initial contact with the pore wall. These gadgets may be used as liquid or vapour adsorbing systems as well as polymerization nanoreactors.

Example: MCM-41, MCM48, SBA15 and carbon mesoporous materials, etc.

Macroporous systems ($d > 50$ nm)—The interactions with pore walls in the case of extremely tiny guest molecules often take a backseat to interactions with other molecules. Small biological molecules or extremely big molecules like polyaromatic systems may be hosted in the pores of these materials, and interactions with the pore walls are often secondary to interactions with other molecules. These materials are primarily used as matrices to hold functional molecules, as scaffolds to graft functional groups, such as catalytic centres, and as sensing materials due to the fast diffusion of chemical species in the pore system.

Example: Carbon microtubes, porous gels, and porous glasses.

(d) **Nanomaterials synthetic techniques**:

(i) **Bottom-up approach**—The bottom-up approach is the construction of nanostructures from small components such as atoms or molecules.

Ex: Chemical vapour deposition, sol–gel process, chemical reduction methods, etc.

(ii) **Top-down approach**—The top-down approach is the method of creating nanostructures by starting with larger structures and breaking them down to nanoscale.

Ex: Lithography, ball milling, epitaxy, etc.

(e) **Porosity**—The ratio of pore volume to total volume is known as porosity. The difference between the total volume and the solid volume called the pore volume.

(f) **Pore diameter**—Pore diameter is the average or effective diameter of the apertures in a membrane, screen, or other porous material. Porous materials are divided into three kinds based on the pore diameter range.

(i) **Microporous materials**—They are material shaving the average pore diameter less than 2 nm.

Ex: Zeolites, organic frameworks, and surgical tape.

(ii) **Mesoporous materials**—They are materials having the average pore diameter in the range of 2–50 nm.

Ex: Mobile crystalline materials (MCM-41), Mesoporous molecular sieves, xerogels, silica, alumina, titanium oxide and niobium oxide materials.

(iii) **Macroporous materials**—They are materials having the average pore diameter greater than 50 nm.

Ex: Porous glasses and aerogels.

(g) **Wafer**—A wafer is a semiconductor or substrate material that is thinly sliced.

(h) **Sol**—It is a colloidal suspension of extremely small solid particles suspended in a liquid media. For example, ink and blood.

(i) **Gel**—Gel is a colloidal suspension of very minute liquid particles in a solid medium, such as agar, gelatin, jelly, or toothpaste.

(j) **Aerogel**—A porous, very light synthetic material known as an aerogel, is created by substituting a gas for the liquid component of a gel. Examples include carbon aerogel, alumina aerogel, and silica aerogel. The best insulator and lightest solid is silica aerogel. It has a surface area of 1000 m^2/gm, a porosity of 95%, and an average pore size of 2–50 nm.

(k) **Xerogel**—A xerogel is a solid created from a gel by drying with unrestricted shrinkage.

(l) **Surface area**—The surface area is the accessible or observable area of a solid surface per unit mass of material.

(m) **Nanomaterials Characterization Techniques**

S.No.	Techniques	Information acquired
1	Scanning electron microscopy (SEM) with energy-dispersive X-ray spectroscopy	Surface topography (upto 10 nm) and composition
2	Transmission electron microscopy (TEM)	Surface morphology (up to 0.2 nm)
3	Atomic force microscopy	Identification of individual surface atoms
4	Particle size analyser	Particle size distribution
5	FT-Raman Spectra	Distinguish single called carbon nanotubes and multiwalled carbon nanotubes
6	Photoluminescence spectra	CNT chirality or asymmetry determination

(continued)

(continued)

S.No.	Techniques	Information acquired
7	X-ray photoelectron spectroscopy	Electronic state of the element

(n) **Chiral**—A chiral molecule is one with non-superimposable mirror images (i.e. enantiomers).
Example: A carbon having four different substituents.
(o) **Helicity**—It is a type of axial chirality, or non-superimposable mirror images with respect to an axis. Protein folding is a good example.

1.3 Size-Dependent Properties

The following are some of the different properties that are drastically affected as a result of a size reduction in at least one dimension:

(a) Reactivity and catalysis are two chemical properties.
(b) Melting point temperature is a thermal characteristic.
(c) Electrical conduction is an electronic property.
(d) Optical properties include light absorption and scattering.
(e) Magnetization is one of the magnetic properties.

1.3.1 Chemical Properties

- Nanoscale materials have the following properties based on the surface area to volume effect:
  (a) A larger overall surface area.
  (b) An increase in the number of atoms that can be accessed on the surface.
  (c) The catalytic activity of such huge numbers of surface atoms is increased.
  (d) Surface catalytic properties that are different/tunable as a function of form, size, and composition.
- As a result, nanoscale catalysts can boost the speed, selectivity, and efficiency of a wide range of chemical reactions (Fig. 1.1).

1.3.2 Thermal Properties

- A substance's melting point directly correlates with its binding strength. Surface effects may be disregarded since bulk materials have a low surface-to-volume ratio.

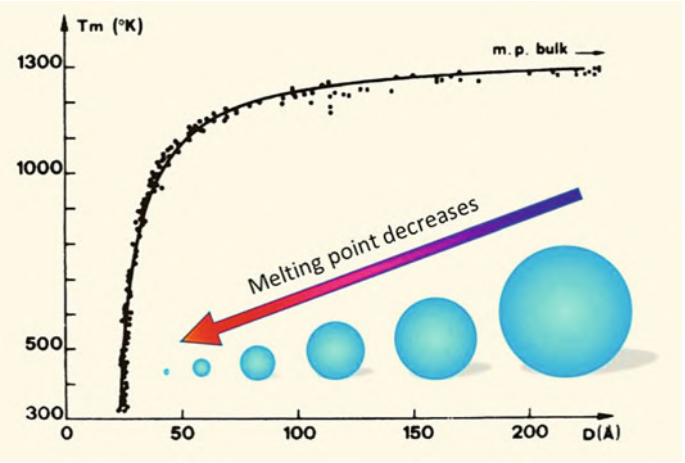

Fig. 1.1 Effect of particle size on the reaction rate

- However, when particle size diameters go smaller, the melting temperature of nanomaterials drops. This is due to the fact that surface atoms in nanoscale materials are more free to move since their bonds are not directed in a direction parallel to the surface plane (Fig. 1.2).

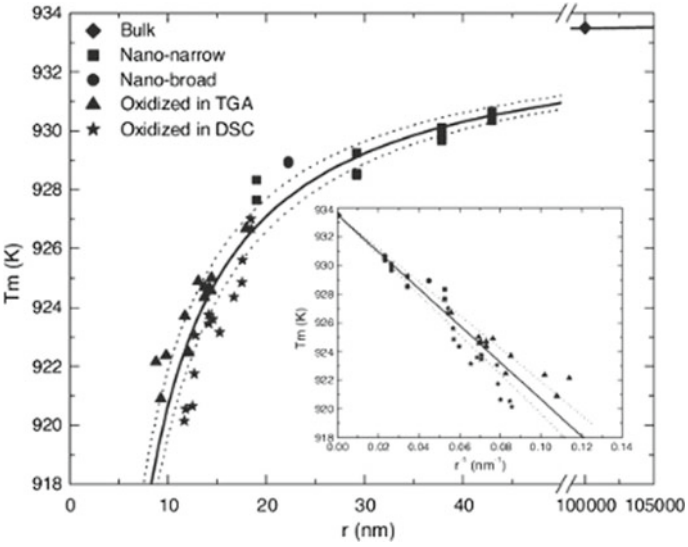

Fig. 1.2 Effect of particle size on the melting point

1.3.3 Electronic Properties

- Electron conduction is delocalized in bulk materials, meaning electrons can travel freely in all directions.
- The quantum effect takes over when the scale is decreased to the nanoscale. Because all of the dimensions of zero-dimensional nanomaterials are at the nanoscale, electrons are trapped in three-dimensional space. As a result, no electron delocalization (movement freedom) occurs.
- Electron confinement occurs in 2D space for one-dimensional nanomaterials; hence, electron delocalization happens along the axis of nanotubes/nanorods/nanowires.
- Electron confinement replaces energy bands with discrete energy states, causing conducting materials to behave as either semiconductors or insulators.

1.3.4 Optical Properties

The emission of visible light can be adjusted by modifying the nanoscale dimensions due to quantum confinement in nanomaterials. The emission of peak in nanomaterials changes towards shorter wavelengths as their size decreases (blue shift) (Fig. 1.3).

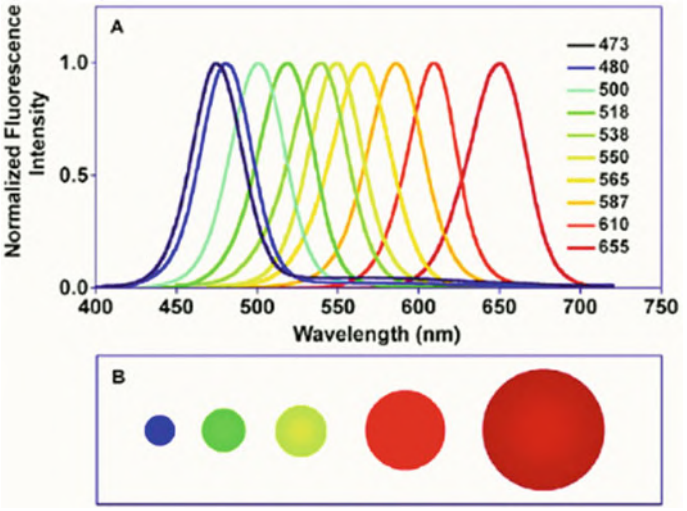

Fig. 1.3 Effect of particle size on photoluminescence

1.3.5 *Magnetic Properties*

- The value magnetization is also influenced by the size of magnetic nanoparticles. The influence of particle size on the saturation magnetization of zinc ferrite is depicted in Fig. 1.4. Below a grain size of 20 nm, the magnetization increases considerably. As a result, by reducing the particle size of a granular magnetic material, the quality of magnets made from it can be improved.

1.4 Nanoparticle Synthesis

- Nanoparticles are particles or powders with a particle size of less than 100 nm.

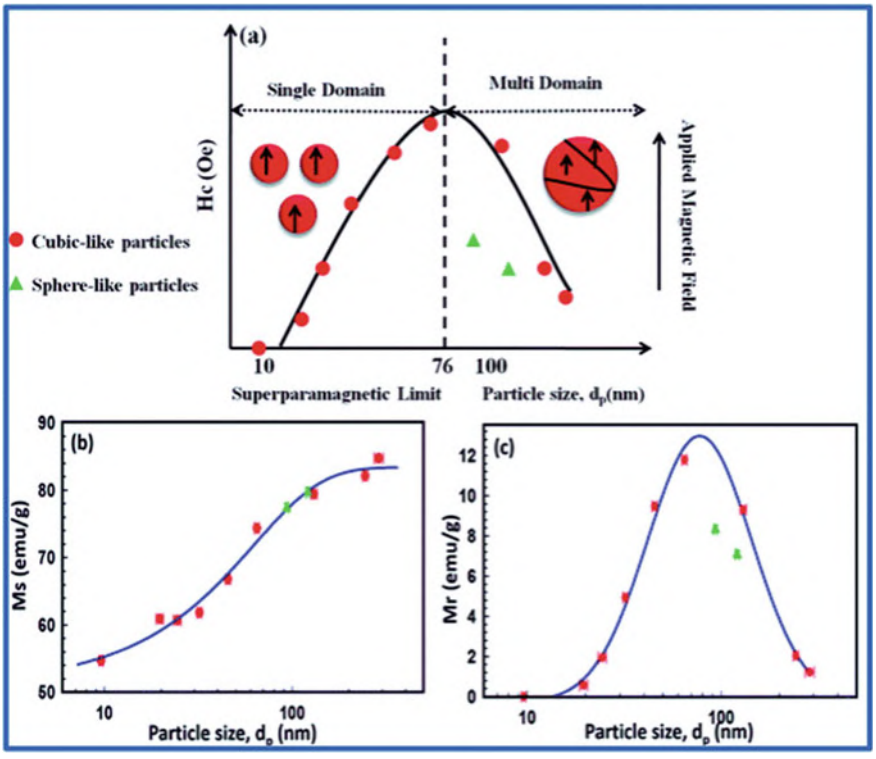

Fig. 1.4 Effect of particle size on the saturation magnetization

1.4.1 Chemical Reduction Method for Synthesis of Nanoparticles

- At ambient temperature, group VIB metal halides such as $CrCl_3$, $MoCl_3$, and WCl_4 can be reduced to their corresponding metals using $NaBEt_3H$ (sodium triethoxy boron hydride) and toluene as the solvent.

$$MCl_3 + xNaBEt_3H \xrightarrow{\text{Toluene}} M + xNaCl + xBEt_3 + x/2H_2$$

$$CrCl_3 + 3NaBEt_3H \xrightarrow{\text{Toluene}} Cr + 3NaCl + 3BEt_3 + 3/2H_2$$

$$MoCl_3 + 3NaBEt_3H \xrightarrow{\text{Toluene}} Mo + 3NaCl + 3BEt_3 + 3/2H_2$$

when M = W, then $x = 4$,

$$WCl_4 + 4NaBEt_3H \xrightarrow{\text{Toluene}} W + 4NaCl + 4BEt_3 + 2H_2$$

Nanoparticle Characteristics:

(i) Surface area expands as particle size decreases. This boosts the nanoparticles' catalytic activity.

(ii) Particle size reduction from micron to nanometre scale affects optical characteristics.

For example, micron-sized CdS appears red, 6 nm-sized CdS appears orange, 4 nm-sized CdS appears yellow, and 2 nm-sized CdS appears white.

(iii) Particle size reduction from micron to nanometre scale has an impact on thermal parameters such as melting point and thermal conductivity.

1.5 Nanoparticles Are Used in a Variety of Applications

(a) Silver nanoparticles are utilized in surgical equipment, refrigerators, air conditioners, and water purifiers because of their antimicrobial qualities.

(b) Gold nanoparticles are used in catalytic synthesis of silicon nanowires, sensors carrying the drugs and in the detection of tumours.

(c) ZnO nanoparticles are used in electronics, ultraviolet (UV) light emitters, piezoelectric devices, and chemical sensors.

(d) TiO_2 nanoparticles are used as photocatalyst and sunscreen cosmetics (UV blocking pigment).

(e) Nanoparticles of antimony–tin–oxide (ATO) and indium–tin–oxide (ITO) are utilized in automobile windows, liquid crystal displays, and solar cell preparations.

1.6 Diversity: Nanowires

Nanowires are solid wire formations that are cylindrical in shape and have a diameter of less than 100 nm and a length of a few micrometres. It is a quantum mechanically one-dimensional structure when the diameter of a nanowire is equal to the electron's de Broglie wavelength in the plane perpendicular to the growth direction. Nanowires are solid wire formations that are cylindrical in shape and have a diameter of less than 100 nm and a length of a few micrometres. It is a quantum mechanically one-dimensional structure when the diameter of a nanowire is equal to the electron's de Broglie wavelength in the plane perpendicular to the growth direction. The simplicity with which we may alter the band gap, a crucial variable in creating devices for certain applications, is one exciting aspect of nanowires. Because the band gap widens as the diameter of the nanowire shrinks, they may produce visible light very effectively. Because nanowires have a large surface area to volume ratio, surface chemistry affects the band gap of these materials. In addition, the band gap might change depending on the passivation on the nanowire surface. A well-known method for the creation of nanowires via gas phase reactions is the vapour–liquid–solid process. Any substance used to make nanowires has to dissolve in catalyst nanoparticles. Gold nanoparticles are used to create silicon nanowires because silicon vapour is soluble in them. Iron nanoparticles are used to create gallium nitride nanowires because gallium and nitrogen, the reactants, are soluble in these particles.

1.6.1 Silicon Nanowire Synthesis (Vapour–Liquid–Solid Mechanism)

The production of silicon whiskers from the gas phase when a liquid gold droplet was deposited on a silicon substrate was explained in 1964 using the vapour–liquid–solid process. Nanowires and other one-dimensional objects may develop thanks to a process called the VLS. Direct adsorption of a gas phase onto a solid surface often results in a slow growth of a crystal. This is overcome in the VLS process by the addition of a catalytic liquid alloy phase, which may quickly adsorb a vapour to supersaturation levels, at which point nucleated seeds at the liquid–solid border can crystallize. The physical properties of the nanowires produced in this manner are controlled by the size and physical properties of the liquid alloy.

It uses two-step procedures. The vapour phase (SiH_4 reactants) diffuses into the gold liquid phase in the first step (catalyst nanoparticles).

- In the second stage, the gold liquid phase experiences supersaturation of Si reactants, resulting in the formation of Si solid phase (nanowire).

Figure 1.5 shows the vapour–liquid–solid mechanism of Si Nanowires. The substrate is first covered with gold nanoparticles and then heated in a furnace until it liquidizes. The precursor silane (SiH_4) is introduced simultaneously into the furnace,

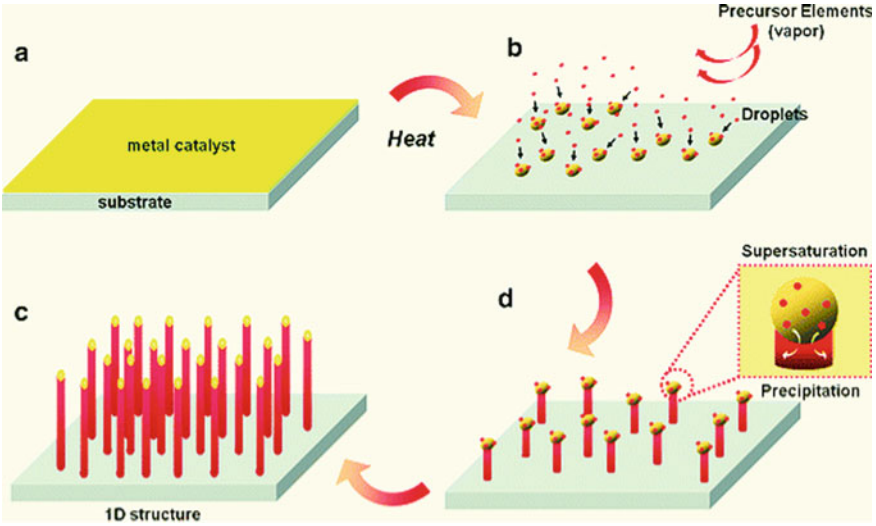

Fig. 1.5 Vapour–liquid–solid mechanism of Si nanowires

where it vaporizes to produce silicon vapour. During the process, silicon vapour diffuses and dissolves in the molten gold nanoparticles. When the silicon concentration approaches supersaturation, the excess material (silicon) precipitates and forms as nanowires.

The VLS mechanism's catalyst must meet the following requirements.

- The catalyst must be inert to the reaction products (non-reacting) (during synthesis).
- The catalytic agent's solid solubility in the solid and liquid phases of the substrate material is poor.
- At the nanowire growth temperature, it must form a liquid solution with the crystalline material to be formed.

1.6.2 Applications of Nanowires

- Field effect transistors, light emitting diodes, biosensors, optical switches, solar cells, and photodetectors are all examples of electron devices that utilize nanowires.
- Copper is being phased out of computers and electronics in favour of nanowires.
- Self-assembled nanowires (NWs) offer a high degree of chemical tailoring flexibility, making them ideal building blocks for nanosized devices, such as communication systems and the creation of nanotechnologies and biosensors.
- Vapour–liquid–solid (VLS) is a common nanowire development method in which metal is typically used as a catalyst.

1.7 Nanoporous Materials

All of the pores in nanoporous materials have a diameter of less than 100 nanometres. In nature, there are various nanoporous and other nanostructured materials. Zeolites are naturally nanoporous minerals that have been employed as catalysts in the petroleum industry for decades; however, most zeolites utilized today are manufactured. Like zeolites, activated carbon is a nanoporous material that has been utilized for a very long period.

Synthesis of Nanoporous Materials By Sol–Gel Process:

According to the sol–gel process, "Formation of an oxide network through polycondensation reactions of a molecular precursor in a liquid."

1.7.1 Precursors

Metal alkoxides M (OR) are the precursors employed in the sol–gel technique for the creation of nanoporous materials. They easily form gels when mixed with water.

Examples

- Tetramethoxysilane [$Si(O_3CH_4)$]
- Tetraethoxysilane [$Si(O_2C_5H_4)$]
- Tetrabutoxytitanate
- [$Ti(O_4C_9H_4)$].

Process (Synthesis of silicaaerogel)

There are four basic steps in this procedure.

1. Precursors are hydrolysed.
2. Condensation is followed by polycondensation.
3. Gelation.
4. Drying under supercritical conditions.

1. **Hydrolysis**

   It happens when water is added to any of the precursor materials, resulting in silanol (Si–OH) particles.

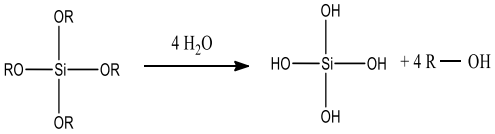

2. **Condensation**

Self-condensation of silanol group's results in siloxane linkages that are filled with water and alcohol by-products.

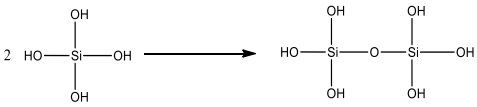

3. **Polycondensation**

The condensation process continues to form polycondensed silica gel with Si–O–Si linkages.

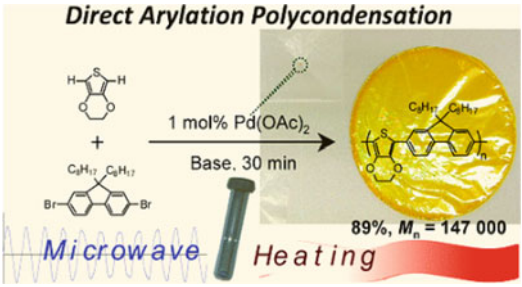

4. **Drying**

- In an autoclave, the gels are dried under extreme conditions. To extract liquid from silica.
- Sol–gel and generate the network structure of silica aerogel, a critical pressure of 78 bar, and critical temperatures of 294 °C were utilized (Fig. 1.6).

Advantages of Sol–Gel Process

- It produces a thin bond layer that enables strong adhesion between the topcoat and the metallic substrate.
- It creates a substantial layer of corrosion protection.
- In a gel state, it is simple to shape materials into complex geometries.
- At low temperatures (usually 200–600 °C), it may sinter.
- It is an easy, affordable, and effective method of creating high-quality coatings.

Applications of Sol–Gel Process

- It may be used as a casting material for investment casting or as a way to make ultra-thin metal oxide coatings for a range of ceramics industry applications.
- Sol–gel-derived materials are used widely in a variety of fields, including separation, electronics, energy, space, (bio)sensors, and medicine (e.g. controlled drug release) (e.g. chromatography).
- One of the most significant uses of sol–gel technology is zeolite synthesis.

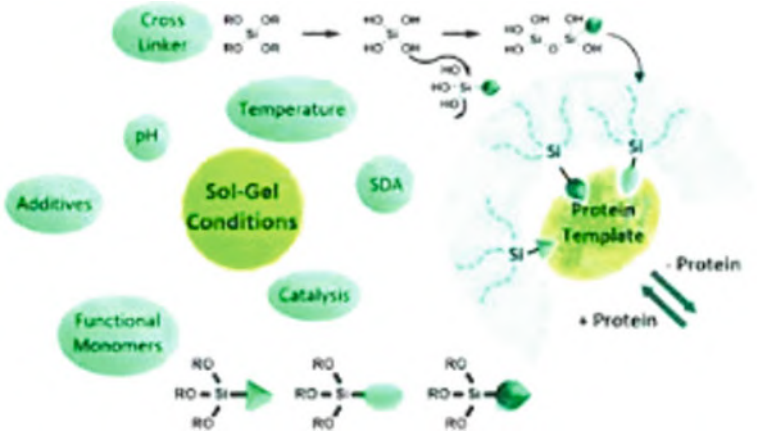

Fig. 1.6 Sol–gel process

- The silicalite sol generated by this procedure is highly stable, and other components (metals, metal oxides) may easily be added to the finished product.
- Other products produced using this process include reverse osmosis ceramic membranes, microfiltration, ultrafiltration, and nanofiltration.

Properties and Applications of Nanoporous Materials

- In nanoporous materials, a porous structure is supported by a regular organic or inorganic framework.
- Examples of nanoporous solids include zeolites, activated carbon, metal organic frameworks, ceramics, silicates, aerogels, pillared materials, various polymers, and inorganic porous hybrid materials.
- The three subclasses of nanoporous materials are microporous materials (less than 2 nm), mesoporous materials (2–50 nm), and macroporous materials (greater than 50 nm).
- Recently, it has been discovered that nanoporous materials provide intriguing candidates for a variety of multifunctional applications, including catalysis, ion exchange, gas storage, low density magnetic storage, and others.
- Nonporous materials are also important in science and technology because of their capacity to absorb and interact with atoms, ions, and molecules on their expansive inner surfaces and pore space.
- Nonporous materials have a surface area of 500–1000 m^2/gm, which boosts catalytic activity.
- Due to their weak thermal conductivity, they are used as thermal insulators.
- They are widely employed in membrane technology due to their high porosity (90–99%).
- They are made of thin materials (density: 0.003–0.8 gm/cc).

1.8 Synthesis of Nanomaterials By Chemical Vapour Deposition (CVD)

Principle

On a substrate that is maintained at a certain temperature, films, coatings, wires, and tubes are deposited using the chemical vapour deposition (CVD) technique. Transport of reactant gases to the substrate causes them to split into various products that disperse on the surface and experience certain chemical reactions at the right location, nucleating and developing to create the required films, coatings, wires, and tubes.

Precursors

The common precursors used in CVD reactions are.

- Metal hydrides—SiH_4, GeH_4
- Metal halides—$TiCl_4$, $TaCl_5$, WF_6
- Metalorganics—$AlMe_3$, $AlBu_3$, $Fe(CO)_5$, $Ni(CO)_4$.

CVD Reactions

- Thermal Decomposition (Pyrolysis): Silicon deposition from SiH_4 at 650 °C

$$SiH_4(g) \rightarrow Si(s) + 2H_2(g)$$

- Reduction: W-deposition at 300 °C

$$WF_6(g) + 3H_2 \rightarrow W(s) + 6HF(g)$$

- Oxidation: SiO_2 deposition at 450 °C

$$SiH_4(g) + O_2 \rightarrow SiO_2(s) + 2H_2(g)$$

Types of CVD

Temperatures of 300–1200 °C are commonly employed in CVD. Thermal, light, plasma, and other types of heat input are all possibilities. As a result, a variety of CVD procedures have emerged.

S.No.	Name of the CVD	Source of thermal energy
1	Thermal activated CVD	IR radiation, RF heating
2	Photo assisted CVD	Arc lamps, CO laser, Nd:YAGlaser, Argon ion laser
3	Plasma assisted CVD	RF diode, microwave
4	Metalorganic CVD	It uses organometallic as precursors

Mechanism

For every kind of CVD, the system follows a five-step procedure

- Precursor transport into reactors.
- Precursor absorption and diffusion on the substrate.
- Chemical reactions on the substrate.
- Film deposition and growth.
- Transport of unreacted precursors and by-products.

Advantages

- CVD can deposit any element or compound.
- Versatile-CVD can deposit any element or compound.
- CVD creates extremely dense films.
- Cost-effective in production since multiple goods can be covered at once.
- Coatings and free-standing structures.
- Creates complex net or near-net shapes.
- Self-cleaning—extremely high purity deposits (> 99.995% purity).
- Conforms uniformly to substrate surface contours.
- Controllable thickness and shape.
- Produces alloys.
- Uses high length-to-diameter ratios to coat interior passageways.
- Coat many components at the same time.
- Powder coats.

Applications

- CVD may be used to create nanotubes and nanowires.
- In microelectronics, CVD may be used to make metal films and hard coatings.
- Among other things, CVD may be used to create dielectrics, energy conversion devices, and semiconducting devices.
- On a surprisingly large variety of industrial components, such as aviation and land gas turbine blades, timing chain pins for the automobile sector, radiant grills for gas cookers, and components of chemical plants, CVD processes are used to fend off diverse attacks by carbon, oxygen, and sulphur.
- Surface alterations to reduce or improve adhesion.
- Microarray silane/Substrate adhesion photoresist adhesion to semiconductor wafer adhesion (DNA, gene, protein, antibody, tissue).
- BioMEMS includes a biosensor covering to reduce “drift” in device performance.
- Promote biocompatibility of manmade and natural materials. Copper capping has an anticorrosive covering.

1.9 Physical Vapour Deposition

Physical vapour deposition processes can generate nanomaterials in the form of thin films, multilayer films, nanoparticles, and nanotubes.

Definition

Physical vapour deposition (PVD) is a technique for converting a metal, ceramic, or chemical into a gaseous state and depositing it on a substrate's surface.

PVD methods are categorized into three categories in general:

1. Evaporation.
2. Sputtering.
3. Laser ablation or pulsed laser deposition.

Evaporation

In this process, refractory metals including W, Ta, and Mo are often used as source materials. In the evaporation process, the substrate and the source materials (to be deposited) are both put within the vacuum chamber (10^{-6} to 10^{-7} torr). For the molecules in the chamber to evaporate and move about freely, the vacuum is necessary. A 10 keV electron beam is produced using an electron cannon (e-gun). In order to produce enough vapour to deposit on the wafer or substrate, this beam is concentrated on the source material. Figure 1.7 displays a schematic representation of an evaporation system.

Sputtering

The raw materials in this process are often an alloy, a ceramic, or a compound. In the sputtering process, surface atoms of the chosen source material are affected by a high energy atom in ionized state, often Ar^+. To create uniform coatings, the knocked-out atoms are subsequently deposited as vapour on the substrate's surface (Fig. 1.8).

Laser Ablation or Pulsed Laser Deposition

A thin-film deposition technique for putting materials on surfaces is pulsed laser deposition (PLD). The basic system includes target and substrate carriers that are mounted in a vacuum chamber. An excimer laser is used to energize a target's surface in order to produce a deposition plume. Usually, the plume is aimed towards the substrate, where it deposits a thin layer. The quantity of material ablated is proportional to each laser pulse, allowing for exact regulation and control of the deposition rate. Figure 1.9 displays the design for pulsed laser deposition.

Advantages

- PVD employs a vacuum atmosphere to produce ultrapure films or particles, and by carefully monitoring the production parameters, it may also provide excellent structural control.
- Materials with attributes superior to the substrate material may be used.

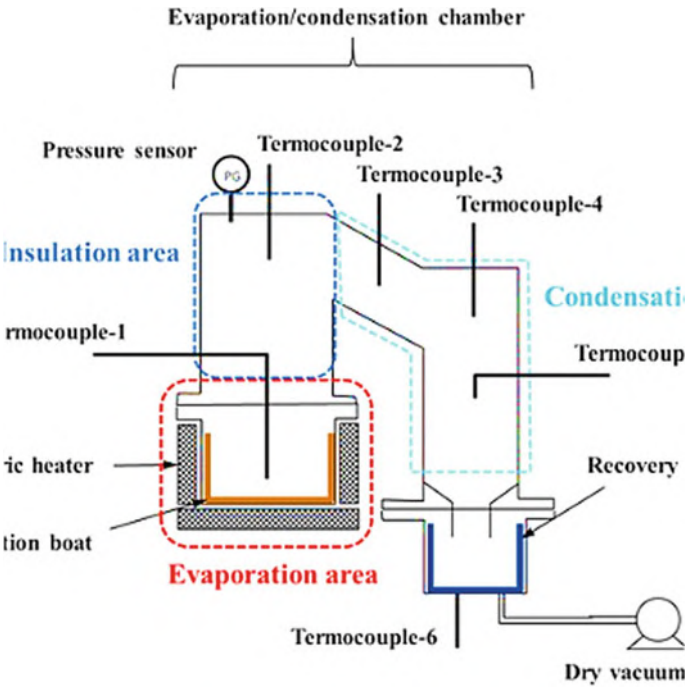

Fig. 1.7 Schematic diagram of evaporation equipment

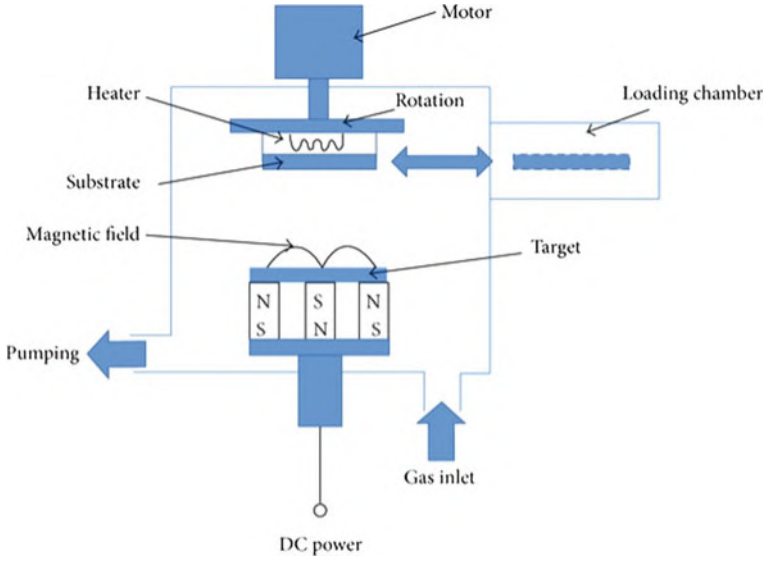

Fig. 1.8 Schematic diagram of sputtering equipment

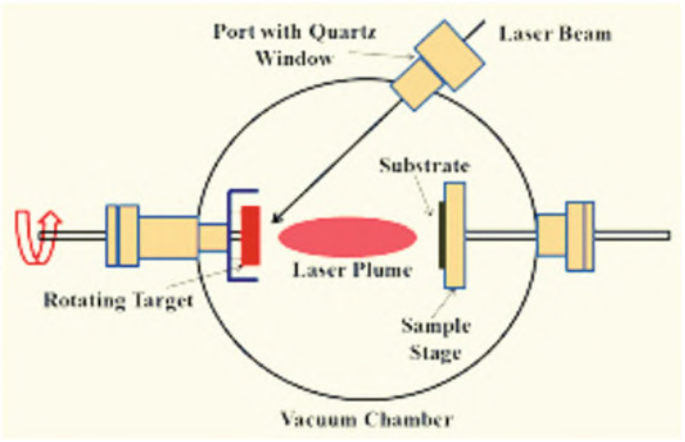

Fig. 1.9 Schematic diagram of pulsed laser deposition

- The procedure is more ecologically friendly than electroplating and may be used with almost any kind of inorganic material, as well as certain organic compounds.

Disadvantages

- Because PVD operates at low pressures, deposition is more difficult and costs more to produce.
- Coating undercuts and other surface features is especially difficult since it is a line-of-sight method.
- Expensive initial outlay.
- Some procedures need the employment of skilled operators because to their high vacuum and temperature requirements.
- Operations requiring extreme heat demand the use of sufficient cooling systems. Coating deposition is often gradual.

Applications

- PVD is used to deposit various metals, alloys, or compounds in the form of coatings or films for the following applications.
- Optics is the study of light (Ex: Antireflection coatings) Electronics (Electronics) (Ex: Metal contacts).
- PVD coatings are commonly used to improve hardness, wear resistance, and oxidation resistance (e.g. hard coatings on tools).

PVD Coatings Use in a Wide Range of Applications Such as:

- Aerospace
- Automotive
- Surgical/Medical dies and moulds for all manner of
- Material processing

- Cutting tools
- Fire arms3030.

1.10 Nanomaterial Applications

To ensure that humanity continues to evolve, new materials with new qualities are needed in many aspects of our daily lives today. Numerous new discoveries have been made as a result of the development of nanomaterials. Nanomaterials with attractive electrical, optical, magnetic, thermal, and catalytic characteristics have attracted a lot of interest because of their many applications in physics, chemistry, biology, medicine, material science, and transdisciplinary disciplines. Nanomaterials are made up of extremely small particles, have a large surface area that speeds up the interaction between them and their environment, and lack of point flaws, giving them ten times the strength of steel. These properties give rise to the ability of even a gramme of nanomaterial to outperform a large number of conventional substances. Nowadays, nanomaterials are used in many different industries, such as:

- Production technologies
- Military engineering
- Nuclear power engineering
- Electronic equipment
- Protection of materials surface
- Medicine and biotechnology.

Production Technologies:

- Using nanoparticles in composites as components of multiple functionalities is crucial and feasible currently.
- Adding nanopowders to steel and alloy manufacturing reduces porosity and improves the range of mechanical qualities.
- The presence of superplasticity in nanostructured aluminium and titanium alloys makes their employment in the fabrication of complex shapes and as a connecting layer in the welding of various solid-state materials promising.
- The use of very large specific surface nanopowders as catalysts in a variety of chemical processes is encouraged.

Military Engineering:

- Ultra-fine powders are employed in a range of radar absorption coatings for aircraft created employing “Stealth” technology, as well as potential kinds of explosives and incendiaries.
- Specialized ammunition that is intended to destroy an opponent’s power systems uses carbon nanofibres.

Nuclear Power Engineering:

- The development of nuclear power engineering required the use of ultra-fine particles. In industrial procedures, these powders are often employed to separate uranium isotopes. The likelihood of developing nuclear energy by lowering natural uranium consumption on a global scale is essentially dependent on this development. Most of this is achieved by deepening the combustion of nuclear fuel. Researchers are exploring the potential for making porous nuclear materials with coarse-grained topologies to achieve this. These nanoparticles will support the high retention of fission products.

Material Surface Protection:

- In some circumstances, high water and oil repellency qualities of the material surface are required for reliable operation. Car windows, glass planes and ships, protective apparel, liquid storage tanks in the walls, and building structure are all examples of such items. At this time, titanium oxide nanoparticles with diameters ranging from 20 to 50 nm, as well as a polymer binder, are being developed. This coating significantly lowers the surface's wet ability in water, oil, and alcohol solutions.

Medicine and Biotechnology:

The following are a few examples of successful nanotechnology applications:

1. **Drug (molecule) delivery to the target**: In cancer therapy, a variety of issues, including as drug degradation and interactions with biological components, will be resolved by tailored drug delivery. It is possible to improve the selectivity of drug absorption by tumour cells, control pharmacokinetics, and raise drug bioavailability in tumour cells. In addition to delivering drugs to cells, nanoparticles may also do so.
2. **Nanomaterials for treatment and prosthetics**: Nanomaterials' unique features enable the creation of a variety of implants and dentures. Nanotechnology can be used to create implants that are safe, biocompatible, and long-lasting.
3. **Diagnostics**: Thanks to improved technology, the development of nanotechnology in biomedicine has facilitated the capture of images, characterization, and analysis of biological material with a high level of resolution. The creation of magnetic nanoparticles is essential for the development of biosensors. The most often used nanoparticles are iron oxide nanoparticles that have been coated with various polymers. Additionally, several biospecific ligands may change the surface. As a consequence, the iron oxide nanoparticles' shell prevents them from coming into contact chemically with chemicals found in cells and tissues. Some nanomaterials, such as nanotubes and nanoparticles, are also used in diagnostics as electrochemical sensors.
4. **Electronic equipment**: In order to advance nanotechnology in electronics, carbon nanotubes were employed. They are able to create flexible and transparent electronics by not just replacing transistors but also adding new mechanical and optical properties to cutting-edge electronic circuits. Since nanotubes

are more mobile and do not confine light to a small layer, the experimental matrix integrated circuit may be bent without losing its electrical functionality. Another example of nanotechnology's use in electronics is the creation of a novel kind of hard disc. The enormous magneto resistance effect, often referred to as the GMR-effect by certain sources, was discovered by Peter Gruenberg and Albert Fret, who shared the 2007 Nobel Prize in Physics for it. Based on this phenomenon, it is possible to create magnetic field sensors that can read data from a hard drive with atomic density precision. Another possible use for nanomaterials is the production of solar cells. The energy collected by a battery using solar cells made of nanowires rather than conventional metal wires might be increased by 15 times. The characteristics of conductor nanoscale for light absorption are special. Solar cell manufacturing using nanostructured materials may increase efficiency while cutting prices. Silver nanoparticles are utilized in medical equipment, refrigerators, air conditioners, and water purifiers because of their antimicrobial characteristics.

- Gold nanoparticles are utilized in the catalytic production of silicon nanowires, drug-delivery sensors, and tumour detection.
- Electronics, ultraviolet (UV) light emitters, piezoelectric devices, and chemical sensors all require ZnO nanoparticles.
- Photocatalysts and sunscreen cosmetics contain TiO_2 nanoparticles (UV blocking pigment).
- Nanoparticles of antimony–tin–oxide (ATO) and indium–tin–oxide (ITO) are utilized in automobile windows, liquid crystal displays, and solar cell preparations.
- Nanoscale structures and materials, such as nanoparticles, nanowires, nanofibres, and nanotubes, have been investigated for use in a variety of biological applications, including biosensing, biological separation, molecular imaging, and/or anticancer therapy, due to their novel properties and functions that differ significantly from their bulk counterparts.
- Their high volume-to-surface ratio, surface tailor ability, enhanced solubility, and multifunctionality open up a plethora of novel biomedical possibilities.
- Nanomaterials' inherent optical, magnetic, and biological capabilities provide unparalleled potential to investigate and manage complicated biological processes for biomedical applications.
- These materials are used in water purification, wastewater treatment, environmental remediation, food processing and packaging, industrial and home applications, medicine, and the development of smart sensors, to name a few.
- Nanomaterials are also used in crop protection and agriculture production.
- Nanomaterials made of metals, semiconductors, carbon, or polymeric species, structured into nanoparticles and nanotubes, have been extensively studied for their ability to improve the efficiencies of electrochemical biosensors as electrode modification materials.

1.11 Carbonnanotubes

Nanotechnology in electronics has been promoted using carbon nanotubes. They are able to create flexible and transparent electronics by adding additional mechanical and optical elements to cutting-edge electronic circuits in addition to replacing transistors. The nanotubes are more mobile and do not confine the light in a small layer, allowing the experimental matrix integrated circuit to be bent without compromising its electrical capabilities. Another example of the use of nanotechnology in electronics is the creation of a new kind of hard disc. The enormous magneto resistance effect, or GMR-effect as some writers like to call it, was discovered by Peter Gruenberg and Albert Fret and was awarded the 2007 Nobel Prize in Physics. Based on this phenomenon, magnetic field sensors may be created that can read data from a hard drive with atomic density precision. Manufacturing solar cells is another possible use for nanomaterials. The amount of energy a battery receives from solar cells may be increased by 15 times if nanowires were used in place of conventional metal wires. Conductor nanoscale has special capabilities for absorbing light. Solar cell production may be made more cost-effectively and efficiently by using nanostructured materials.

Types of Carbon Nanotubes

A carbon nanotube is a tube-shaped material with a diameter that is measured in nanometres and is made of carbon. The structure of a carbon nanotube may be seen by rolling up a sheet of graphene, which is a planar-hexagonal arrangement of carbon atoms arranged in a honeycomb lattice. A single layer of graphite sheet is called graphene. The lengths, thicknesses, helicity kinds, and layer counts of carbon nanotubes vary, as well as their forms and sizes. CNTs are available in a range of sizes, with diameters between 1 nm and 50 nm. Nanotubes typically have a length of a few microns, although recent advances have enabled them to reach centimetre lengths. Two groups of carbon nanotubes are distinguished.

1. **Single-wall carbon nanotubes (SWCNT)**:

Single-wall carbon nanotubes (SWNT) are graphite tubes with capped ends. They only have one cylindrical wall. A SWNT's structure can be envisioned as a single-atom-thick layer of graphite called graphene that is rolled into a seamless cylinder.

The diameter of most SWNTs is typically around 1 nm. However, the tube length can be thousands of times longer. SWNT are more malleable than MWNT, but they are also more difficult to produce. Without breaking, they can be twisted, flattened, and bent into small circles or around acute curves

2. **Multiwalled carbon nanotubes (MWCNT)**:

There are two structural models for walled carbon nanotubes. In the Russian Doll paradigm, a carbon nanotube contains another nanotube (the inner nanotube has a smaller diameter than the outer nanotube). In the Parchment model, a single graphene sheet is repeatedly wrapped around itself to resemble a scroll of paper. The

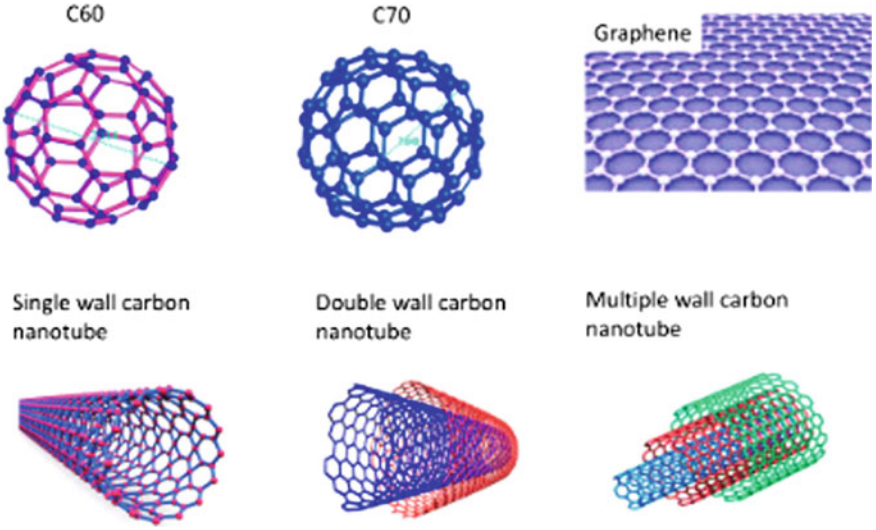

Fig. 1.10 Fullerene (C60) single-wall CNT multiwall CNT preparation of carbon nanotubes

most fundamental kind of MWNT is a double-walled carbon nanotube (DWNT). The outside walls of multiwalled carbon nanotubes may shield the inner carbon nanotubes from chemical interactions with outside materials, despite the fact that they share many characteristics with single-walled carbon nanotubes. The tensile strength of single-walled nanotubes is lower than that of multiwalled nanotubes. MWNT generally comes in diameters between 5 and 50 nm. Similar to the space between graphene layers in graphite, the interlayer spacing in MWNT is about 3.39Ao. Making MWNT is simpler than SWNT.

However, because of its greater complexity and variety, the structure of MWNT is less well known. The material's appealing qualities might be compromised by structural issues (Fig. 1.10).

There are various methods for making single-wall and multiwall carbon nanotubes, each with its own set of benefits and drawbacks. They can be divided into two sorts based on whether they need to be kept at high or medium temperatures.

Laser ablation, arc discharge, and chemical vapour deposition are three significant ways for producing high-quality CNT (CVD). Several types of microcarbon structures, such as carbon onions, carbon nanohorns, and carbon nanotubes, have recently been synthesized using arc discharge in liquid media. This is a low-cost strategy because it does not necessitate the purchase of expensive equipment.

Electric Arc Discharge method or Plasma Arcing

Electric arc discharge is the most common method for making carbon nanotubes. An electric arc is produced by plasma discharge, which results from the electrical breakdown of a gas. An very high temperature produced by the arc, which develops between two conducting electrodes in a gaseous environment, has the power to melt

or vaporize almost anything. A schematic illustration of the CNT producing arc discharge device is shown in Figure 1.11. This method, which employs two graphite electrodes, has a normal spacing between the two rod tips of 1–2 mm. The cathode and anode are both made of pure graphite. A hole is drilled in the anode, and the mixture of graphite powder and metal catalyst powder, such as iron, cobalt, nickel, or yttrium, is then placed within. The chamber is then filled with a rarefied ambient gas, such as helium or argon, using a diffusion pump. The electrical discharge causes the temperature to rise to 6000 °C. This temperature is high enough to cause the carbon in graphite to sublimate. Carbon atoms are expelled from the anode, and plasma is generated when the pressure rises during sublimation. As these atoms get closer to the cathode, a nanotube deposit forms. Single-wall carbon nanotubes are the main by=product of the usage of catalytic metal particles. Without such catalysts, multiwall carbon nanotubes are more likely to form. During the arc discharge, web-like structures grow around the electrodes' cooler regions. Within these structures, bundles of 10–100 single-wall carbon nanotubes are produced. This method typically produces just around 25% pure carbon nanotubes, which is useless. However, the use of a combined nickel–yttrium catalyst has boosted the efficiency and total synthesis of single-wall carbon nanotubes.

Electric Arc Discharge in Liquid Media

For the traditional electric arc discharge technique of generating carbon nanotubes and fullerenes, sophisticated gas handling apparatus, a cooling system, a sealed reaction chamber, and several purification procedures are needed. Contrarily, the development of arc plasma in water calls for straightforward operation and apparatus and has increased the uniformity and efficiency of CNT synthesis. This method may be used to create encapsulates, nanotubes, and carbon onions. A schematic representation of an arc discharge in a liquid medium is shown in Fig. 1.12. The electrodes

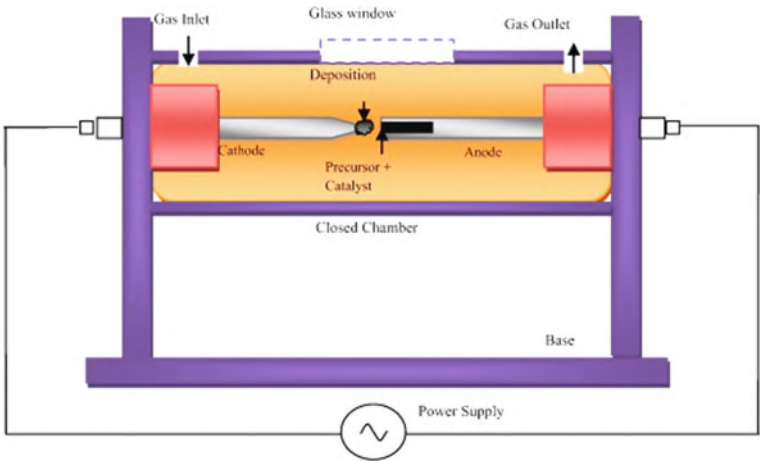

Fig. 1.11 Schematic diagram for electric arc discharge method

are constructed of graphite, and there are typically 1–2 mm between each rod tip. The cathode has a diameter of 12–20 mm, while the anode is 6 mm in diameter. A 5 mm diameter hole was bored at the open end of the anode and filled with a combination of graphite and metallic catalyst powder. The two electrodes are placed in an exposed tank that may either be filled with liquid nitrogen or deionized water. The two electrodes are driven by a direct current source and are initially in contact with one another. The arc discharge is started when the mobile anode progressively separates from the cathode. The arc gap is maintained at a one millimetre spacing. Under these circumstances, the carbon material that sublimated at the anode was deposited as a hard crust at the cathode. The applied voltage determines the growth rate. A steady temperature of around 250 °C is the ideal thermal setting for the arc discharge method of synthesising CNTs in liquid. Recently, NaCl solution has been used as a liquid medium to create carbon nanotubes.

Chemical Vapour Deposition (CVD)

For more than two decades, chemical vapour deposition of hydrocarbons on a metal catalyst has been utilized to make diverse carbon materials such as carbon fibres and filaments. It is a versatile technology for producing large quantities of defect-free CNTs at low temperatures. A metal catalyst is used to achieve thermal breakdown of a hydrocarbon vapour in this procedure. As a result, it is sometimes called heat CVD or catalytic CVD.

Figure 1.13 shows a schematic diagram of the CVD setup. A substrate material, such as quartz or alumina, is cleaned well before being placed in a tube furnace for catalyst deposition. A porous substrate is commonly employed because it speeds

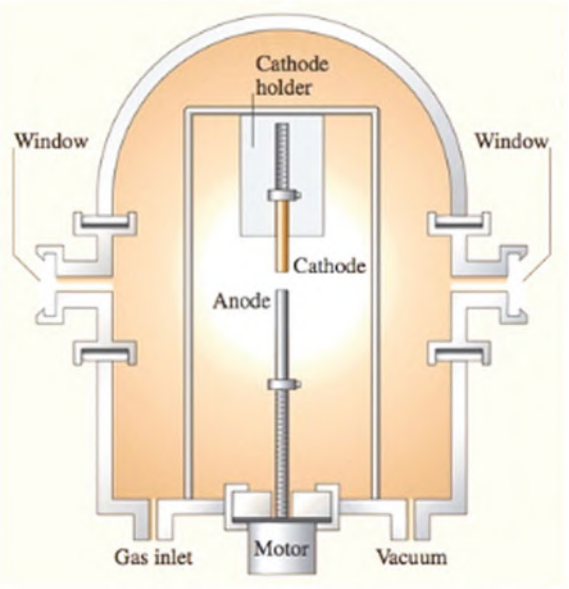

Fig. 1.12 Electric arc discharge method in deionized water

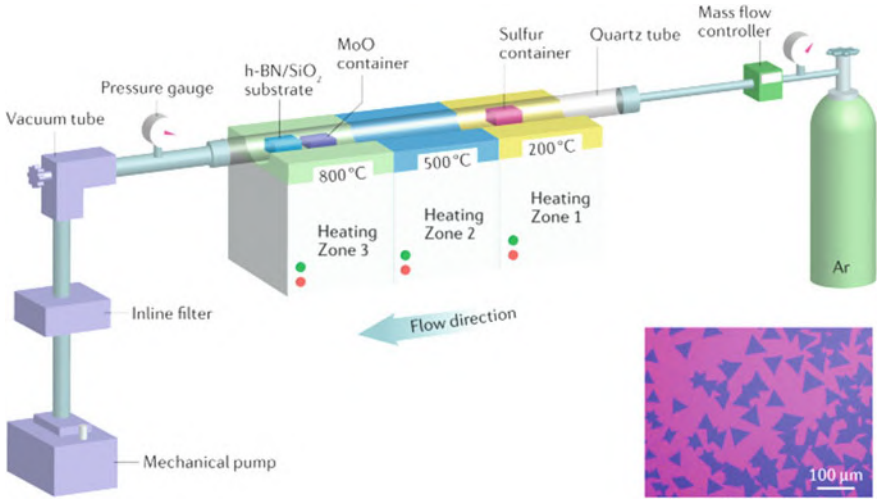

Fig. 1.13 Chemical vapour deposition

up the growth of carbon nanotubes. Thermal evaporation deposits a catalyst, such as iron or nickel, on the substrate's surface. The furnace is kept at a temperature of between 600 and 1200 °C. A hydrocarbon vapour (acetylene, ethylene, carbon monoxide, etc.) is passed through the furnace during the process. When it comes to liquid hydrocarbons (benzene, alcohol, etc.), in a flask, the liquid is heated, and an inert gas is purged through it, carrying the hydrocarbon entering the reaction zone with vapours. If a solid hydrocarbon is to be employed as a CNT precursor, it can be stored in the reaction tube's low-temperature zone. Volatile materials (camphor, naphthalene, etc.) go from solid to vapour quickly and perform CVD while passing over the high-temperature catalyst.

Carbon dissociates from these precursor molecules and diffuses into the catalyst at these high temperatures. CNTs form on the catalyst in the reactor and are collected after the system is cooled to room temperature.

The CVD approach based on the substrate bound catalyst has two primary mechanisms for the development of nanotubes.

- **Model of tip growth (Top carbon diffusion)**: The generation of carbon species occurs when the carbon source decomposes on the exposed surface of the metal catalyst. They dissolve in the catalyst and diffuse through it, eventually precipitating as nanotubes at the end. The catalytic particle is always on top of the nanotube as it grows.
- **Base growth model (bottom carbon diffusion)**: The catalyst remains on the substrate in this scenario. The carbon species dissolve in the catalyst and diffuse through it, eventually precipitating as nanotubes on top of the metal particle (Fig. 1.14).

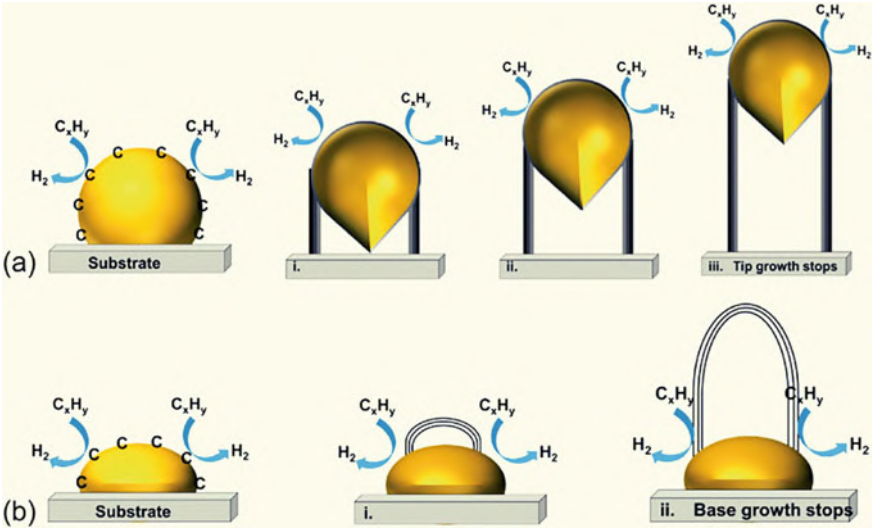

Fig. 1.14 Tip growth and base growth model for growth of carbon nanotubes

The size of the catalyst particle determines whether SWNTs or MWNTs form. SWNTs form when the particle size is a few nanometres, while MWNTs form when the particle size is bigger.

CVD is a simple and cost-effective technology for manufacturing CNTs at low temperature and ambient pressure as compared to arc discharge and laser ablation. Arc- and laser-grown CNTs outperform CVD-grown CNTs in terms of crystalline (although CVD-grown MWCNTs possess inferior crystalline, the crystalline of SWCNTs grown by CVD is close to that grown by arc or laser methods). CVD, on the other hand, outperforms the arc and laser processes in terms of yield and purity. CVD is the only option when it comes to structural control or CNT architecture. CVD is versatile in that it allows for the capture of a large amount of hydrocarbons in any state (solid, liquid, or gas), the use of a variety of substrates, and the growth of CNTs in a variety of forms, including powder, thin or thick films, aligned or entangled, straight or coiled nanotubes, or a desired architecture of nanotubes on predefined sites of a patterned substrate. It also allows for more precise control over the growth parameters.

Properties of Carbon Nanotubes

Electrical Properties

Carbon nanotubes' electrical characteristics are determined by how the hexagons are oriented along the tube's axis. The amount of twist in the pattern of carbon atoms around the perimeter of a nanotube can be used to classify it into several kinds (C). Armchair, zig-zag, and chiral are the three potential orientations. Electrical characteristics of carbon nanotubes with hexagons oriented parallel to the nanotube axis are similar to metals. There will be a current flow when a voltage is put between the two ends of an armchair nanotube. In fact, an armchair carbon nanotube is a greater conductor than copper, which is commonly used in electrical wire, or any other metal. The electrical characteristics of the next two potential hexagon orientations in carbon nanotubes are similar to semiconductors. A zig-zag configuration is one in which the hexagons are aligned in a circle around the nanotube. Chiral nanotubes have a twist to them so that the hexagons do not form a line. When extra energy in the form of light or an electric field is provided to release electrons from carbon atoms, these two topologies of nanotubes will only carry electric current (Fig. 1.15).

The diameter and helicity of a carbon nanotube determine its electrical characteristics. A seamless wrapping of a graphene sheet into a cylinder along the (n, m) roll-up vector is known as a SWCNT. The (n, m) indices characterize the SWNT radius and chirality in detail, as well as its electronic structure unambiguously.

The chiral vector (n, m), where n and m are integers, can be used to characterize the many types of nanotubes. The diagram in Fig. 1.16 shows the chiral vector. The chiral angle, θ is given by $0 \leq |\theta| \leq 30°$. Consider a graphene layer in which each carbon atom in a hexagon is assigned a number. All carbon atoms with the same number in a graphene sheet are referred to as comparable carbons. The two

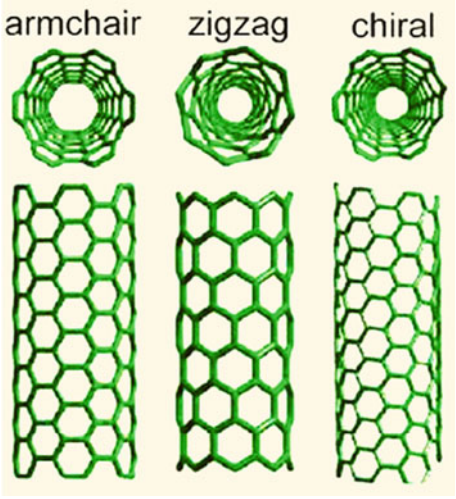

Fig. 1.15 Types of carbon nanotubes

vectors a_1 and a_2 connect the carbon at the origin to analogous carbon atoms in the surrounding area. These vectors are referred to as a_1 and a_2 since they are not perpendicular to each other. The number of comparable carbons required in each direction to return to the origin carbon atom must be counted in order to name a nanotube. The number of equivalent carbons in the a_1 direction is denoted by the letter n, whereas the number of analogous carbons in the a_2 direction is denoted by the letter m. The set of coordinates represents the generated vector (n, m).

For example: A (3, 0) nanotube ($n = 3$ and $m = 0$) can be obtained by starting from the origin andmoving along three analogous carbons (n) in the $a1$ direction. If the graphene sheet is rolled up so that the two points (origin and $n = 3$) are superimposed on each other, then it is possible to obtain $a(3, 0)$ carbon nanotube.

A (3, 3) nanotube ($n = 3$, $m = 3$) can be obtained by starting at the origin and moving along threeanalogous carbon in the $a1$ direction and then three analogous

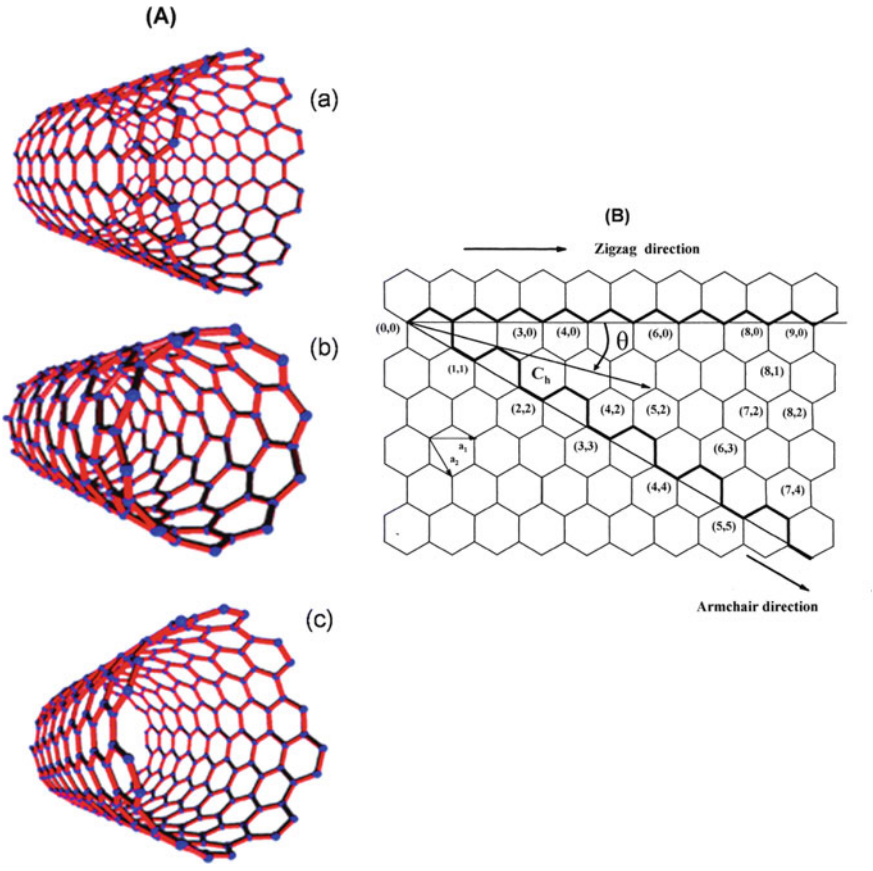

Fig. 1.16 Structural representation of metallic and semiconducting carbon nanotubes

carbons in the $a2$ direction. When these two points (origin and $n = 3$, $m = 3$) are superimposed on each other, $a(3, 3)$ can be obtained.

The values of n and m determine the chirality, or "twist" of the nanotube. The chirality in turn affects the conductance of the nanotube, its density, its lattice structure, and other properties. Hence, based on the type of carbon nanotube, it is possible to determine whether it is metallic or semiconducting. All armchair carbon nanotubes are of the type (n, n) because of their symmetry and are metallic. The chiral angel of armchair tubes is $\theta = 30°$. Zig-zag nanotubes are of the type $(n, 0)$ with a chiral angle of 0°. They show metallic properties if $n - m = 3i$, where i is an integer, whereas if $n–m \neq 3i$, they are semiconducting. For chiral carbon nanotubes, the chiral angle is $0 < \theta < 30°$. Carbon nanotubes can carry approximately 1000 times the current of copper.

Mechanics

Tensile strength is a measurement of how much force an object can withstand before breaking. Carbon nanotubes are one of the strongest materials accessible, with Young's modulus and tensile strength defining its mechanical qualities.

Carbon nanotubes have a tensile strength that is 100 times stronger than steel of the same diameter. There are two factors that contribute to this strength. The interconnecting carbon-to-carbon covalent bonds offer the initial source of strength. The second is that each carbon nanotube is made up of a single big molecule. This implies it lacks the weak points found in other materials, such as the borders between crystalline grains in steel.

CNTs are projected to have stiffness similar to graphite, which has an in-plane modulus of 1.06 TPa due to its carbon–carbon sp^2 bonding. Single-wall CNTS have modulus values ranging from 0.32 to 1.47 TPa and tensile strengths ranging from 10 to 52 GPa, whereas multiwall CNTS have modulus values ranging from 0.27 to 0.95 TPa and tensile strengths ranging from 11 to 63 GPa. It has five times the Young's modulus of steel.

Carbon nanotubes are also light, with a density ranging from 1.3 to 1.4 g/cm^3 depending on the kind. It is a quarter the weight of steel.

Nanotubes are both strong and flexible. Using atomic force microscopes, researchers were able to physically push nanotubes around and measure their elastic properties. When a nanotube is twisted or compressed, the bonds in the atomic lattice do not break, according to tests done using transmission electron microscopes.

Carbon nanotubes also transport heat and cold extremely efficiently (they have a high thermal conductivity); some researchers estimate that their thermal conductivity will be more than ten times that of silver. While metals use electron movement to conduct heat, carbon nanotubes use the vibration of the covalent bonds that keep the carbon atoms together to carry heat; the atoms themselves are wiggling around and sending heat through the material. The carbon bond's rigidity aids in the transmission of vibrations throughout the nanotube, resulting in excellent heat conductivity.

Applications of Carbon Nanotubes

- Carbon nanotubes' characteristics have prompted researchers and businesses to contemplate employing them in a variety of applications.
- CNTs can be used as catalyst supports because they have large surface areas, good chemical stability, and controlled surface chemistry.
- Hydrogen storage: Carbon nanotubes have recently been proposed as a hydrogen storage material for hydrogen–oxygen fuel cells.
- AFM probe tips: "Probes" are used to characterize the surface of a material. CNTs are commonly utilized in the production of AFM (atomic force microscope) probes.
- Drug delivery: Because CNTs can easily adapt to their surroundings and penetrate the nuclei of cells, they can be employed as drug carriers.
- Actuator/Artificial muscles: An actuator is a motion-inducing device. Electrical energy is transformed to mechanical energy in a carbon nanotube actuator, causing the nanotubes to move.
- Chemical sensors/Biosensors: Sensors are devices that detect changes in physical and chemical quantities. Pressure, temperature, gas, optical, mass, position, stress, strain, chemical, and biological sensors all use carbon nanotubes as sensing materials.
- CNTs are a suitable field emitter because of their high current density, low turn-on and operating voltage, and stable, long-lived behaviour.
- Touch screens: CNT films as thin as 10 or 20 nm are transparent to visible light and can conduct enough electricity to be helpful in a variety of applications such as thin-film solar cells, organic LEDs, and touch screens.
- Structural and mechanical applications: Carbon nanotubes (CNTs) have excellent mechanical qualities such as stiffness, toughness, and strength. These qualities allow for the creation of extremely strong, lightweight materials that can be used in construction, structural engineering, and aerospace applications.
- Aerospace components: Carbon nanotubes have high fatigue strength over a long period of time, allowing them to be used as aircraft components.

1.12 Nanometal Oxides

Nanometal oxides possess unique characteristics due to their large surface area to volume ratio and unusual catalytic activity, electronic properties, optical properties, and antimicrobial activity. Different types of nanoparticles can be synthesized using various methods. Metal oxides are crystalline solids that contain a metal cation and an oxide anion. They typically react with water to form bases or with acids to form salts. Metal oxides/mixed metal oxides have wide applications as catalyst, adsorbents, superconductors, semiconductors, ceramics, antifungal agents and also have spacious applications in medicines. This review article is focused on their applications as photocatalyst in various organic reactions. In technological applications, metal oxide nanoparticles are used in the fabrication of microelectronic circuits,

sensors, piezoelectric devices, fuel cells, coatings for the passivation of surfaces against corrosion, and as catalysts.

1.13 Band Gap Energy

It is the range of energy values that are prohibited to electrons in the material. This energy difference exists between the valence band and conduction band of a solid material (such as an insulator or semiconductor). A band gap is the amount of energy needed for electrons and holes to move from the valence band to the conduction band. Wide band gap semiconductors are defined as having a big value. a band gap in a material's range of energy levels where electrons are not possible. We may learn more about a material's electrical activity by looking at its band gap, both in terms of its size and presence or absence. In the semiconductors, conductors, and electrical insulators. Therefore, compared to other semiconductor devices, wide band gap devices are suitable at shorter wavelengths. Since the electrons aren't always in the conduction band, a band gap avoids short circuits. A solid may have some conductivity if it has a strong enough flow of electrons from the valence to conduction bands, which is made possible by a tiny band gap. Because of how they transfer charges, metal oxide semiconductors are a special type of materials. They set themselves apart from normal covalent semiconductors, where a large amount of charge carrier transport is caused by the interaction between the metal and oxide orbitals. The least amount of energy needed to liberate an electron from its bound state and into a condition where it may conduct electricity is known as a semiconductor's band gap. A "band diagram" is a representation of the band structure of a semiconductor, which displays the energy of the electrons on the *y*-axis.

1.14 DFT Calculations on Nanometal Oxides

Metal oxides that exhibit a high optical transmittance and in addition are highly electrically conductive are referred to as transparent conductive oxides (TCO). They can also be described as wide band gap oxide semiconductors. Examples of the material class TiO_2, PbO, SiO_2, TiO_2-SiO_2. Since the band gaps of these materials lie in the ultraviolet wavelength region they do not absorb visible light as a consequence, they appear transport to the human eye. If such an oxide is doped with a sufficient amount of suitable ions, high electrical conductivities can be achieved. TCOs are of major technical importance since thin films exhibiting a high electoral conductivity and optical transmittance are needed in for instance, solar cells, flat panel displays, and electrochromic devices. TCO films are commonly produced via vacuum-based gas phase methods, such as magnetron sputtering or chemical vapour deposition. Due to the high crystalline and compactness of the resulting thin films, excellent conductivities can be achieved. There has been increasing interest in the synthesis and study

of inorganic nanostructures in recent years for their widely varying properties and potential applications. Metal oxide nanostructures with well controllable size and shape have received increasing attention in current material synthesis and device fabrication. In recent years, considerable interest has been focused on metal oxide nanoparticles that are extensively used in a number of applications due to their possession of enthralling electrical, optically catalytic, and magnetic properties. Among metal oxides, titanium dioxide, lead oxide, and silicon dioxide nanoparticles have been of great interest due to their potential applications in many important fields of science and technology such as gas sensors, solar cells, field emitters, piezoelectric nanogenerators, light emitting diode, excellent photocatalyst and nanooptoelectronic devices. TiO_2, PbO, SiO_2, TiO_2-SiO_2 nanoparticles are fundamental building blocks in photocatalysis. Their theoretical description is indeed relevant and requires the size of the model to be as realistic as possible, for direct comparison with experimental samples. TiO_2, PbO, SiO_2, TiO_2-SiO_2 nanoparticles are most typically obtained from sol–gel synthesis. Several studies have proven that shape and size can be successfully tailored by controlling the conditions of preparation and by using ad hoc surface chemistry. The minimum energy shape was predicted by the construction, for dimensions below 10 nm, to be a decahedron in the anatase phase, exposing mainly and small facets. However, growth determining factors are pH and particle density. An excessive dilution may cause a partial dissolution of titanium, lead, and silicon nanocrystals leading to the formation of spherical nanoparticles. Those, analogously to nanotubes and nanorods, are characterized by a high curvature profile and, thus, expected to be more reactive towards molecular adsorption. The majority of the computational first-principles studies are devoted to bulk or surface slabs of anatase, TiO_2, PbO, SiO_2, TiO_2-SiO_2. Few works have dealt with the decahedral faceted nanoparticles but none with spherical ones. Modelling nanoparticles of realistic size (few nanometres) by first-principles calculations is very demanding and a global optimization is hardly feasible. Ours is a multistep/scale approach. The propose first to apply a less expensive but still rather accurate method based on density functional theory (DFT), to perform a global structure optimization search of the nanoparticles further DFT relaxation to determine structural and electronic properties with first-principles level accuracy. For the latter, we use hybrid functionals since they are known to better describe electronic structure details of TiO_2, PbO, SiO_2, TiO_2-SiO_2 materials. DFT has been demonstrated to be a powerful tool for the quantum mechanics study of many systems involving TiO_2, PbO, SiO_2, TiO_2-SiO_2. The method retains most of the physics of standard DFT at an extremely reduced computational cost. We would like to describe the interaction of such nanoparticles with light and their photoactivation producing energy carriers (exactions) and charge carriers (electrons and holes). The aim is to improve the general understanding of the processes at the basis of light energy conversion into chemical species with intrinsic redox potential that are those triggering the redox reaction at the oxide surface. It is generally accepted that water, as the surrounding environment where titanium dioxide, lead oxide, silicon dioxide nanoparticle work in photocatalytic processes, plays an active role. It is, therefore, fundamental to describe accurately the dynamical water layers arrangement on the surface and how water molecules may

enter the photoactivated reaction chain. In the following, we will present a critical review of our work, relative to the topics highlighted, and as discussed above in the section, we present the computational methodology; in the describe how to obtain realistic spherical nanoparticles models in discuss the description of the photoexcitation processes and, in a analyse how the water environment can be modelled with sufficient accuracy. Semiconductor metal oxides thin films have been the subject of too much investigation in the last decade, thanks to the possibility of applications in advanced fields such as optoelectronic, catalysis, sensing and solar cells. The film scan be built of as metal oxide or be mounted by layers of different oxides and grown according to distinct geometries and crystallographic directions. In the case of combination of different materials, the superposition can affect the electronic structure and the surface properties of each one, resulting in a high performance composite for a specific application. Of course, the properties of the system will depend on the individual materials used for mounting the film and can be remarkable unique the individual properties of the components. Some of these systems have been the subject of a series of experimental and theoretical studies performed in our group, as it has been reported in the last few years, and new ones continue to be looked for. In the present work, the scrutiny is upon the TiO_2, PbO, SiO_2, TiO_2-SiO_2 rutile system. Although these oxides share a common crystalline structure (rutile), which facilitates the mounting, they have tremendously different electric properties. Typically displays degenerate *n*-type conductivity assigned to oxygen vacancies, and although opaque (into its low band gap) it can potentially become a transparent conducting oxide (TCO), as it has already been observed with other materials. This result is achieved with the blue shift of the optical band gap, according to the Moss-Burstein effect. The optical transparency is guaranteed in the transitions from the bottom filled conduction band states to the next highest conduction band lie above the threshold for visible light absorption. Computational modelling and simulation have proved to be useful tools to assist experimental indings and and develop new materials with specific or poorly studied properties. Some of these techniques have been used in our group to study the most diverse systems. In a recent study, theoretical investigations of surface and electronic structures of TiO_2 and PbO films coated with SiO_2 have been performed through density functional theory (DFT) calculations, using the B3LYP hybrid density functional with the approaching to describe the long-range weak interactions. At work now, the study is being extended to SiO_2 thin films coated with SiO_2 (TiO_2-SiO_2), both in the tetragonal rutile phase. As far as we know, this is the first time this system is being investigated. Bulk of both neat TiO_2, PbO, and SiO_2 and surfaces of neat TiO_2, PbO have also been simulated for comparison. In the terms of optimized geometric parameters, band structure, density of states (DOS), distribution of charge density, and surfaces order stability. Titanium dioxide (TiO_2), lead oxide (PbO), and silicon dioxide (SiO_2) are the archetypal water splitting photocatalyst and semiconductor material for dye-sensitized solar cells. In its use as a photocatalyst, absorption of light excites electrons from the valence band of the material to the conduction band, which leaves holes in the former and results in the creation of excited electron—hole pairs (excitons). These excitons can then, either directly or after having been ionized into “free” electrons and holes, reduce

protons to hydrogen and oxidize water to oxygen. The excitons can, however, also annihilate, i.e. excited electrons and holes recombine, or become trapped. Similar processes take place in dye-sensitized solar cells, where electrons are excited from the highest occupied molecular orbital to the lowest unoccupied molecular orbital of the dye and subsequently transferred to the semiconductor (i.e. titanium dioxide, lead oxide, silicon dioxide), while the formed holes react with a redox mediator in solution. Overall, the physics and chemistry involved in those processes are often complicated, with the quantum efficiency—the fraction of photons absorbed resulting in the desired process taking place—depending strongly on the material properties. Recent studies, for example, show that photocatalytic activity does not only depend on the material's composition (e.g. doping level) but that both particle size and shape can play a pivotal role in controlling the fate of excitons in TiO_2, PbO, SiO_2, TiO_2-SiO_2. Hence, it is crucial to properly understand the behaviour of both excitons and free charge carriers (free electrons, holes) in titanium dioxide, lead oxide, silicon dioxide. This is hard to achieve by experiment alone, for instance, because of the transient nature of excitons and the complex structures of samples. Computational chemistry can thus make a potentially significant contribution to our understanding of these systems. For the potential of computational chemistry to be realized, however, one should be able to make relatively accurate predictions of not only the optical absorption spectra, which is routinely done but also the reduction potentials of the free charge carriers and excitons as well as the energetics and the structural distortion associated with trapped excitons. Such properties require the calculation of not only vertical excited state energies but also the energies and geometries of relaxed excited states. The method of choice for calculating such properties is a combination of density functional theory (DFT), for ground state energies and structures, and density functional theory (DFT), for their excited state counterparts. Alternative approaches exist in the form of quantum chemical wave function or Green's function-based methods. Such alternatives have advantages in terms of reliability and inherent accuracy but unfortunately lack currently the desired scaling with system size and the ease of use of DFT. This is especially true when studying the nanostructured materials relevant to applications in photocatalysis and dye-sensitized solar cells, where one has to be able to calculate the properties of systems composed of tens to hundreds of atoms. In this article, we extend our previous work by exploring the effect of the choice of XC potential on the nature of the lowest singlet excited state (S1) minima found. We explore the S1 potential energy surface in the downhill direction, as determined from the DFT analytical gradients, in order to find the S1 minima in the so-called Franck–Condon region and, subsequently, characterize these minima in terms of their photoluminescence (PL) energy and Stokes' shift. In some cases, we will also find what appears to be conical intersections (CXs), where the ground and excited state potential energy surfaces touch, and the PL energy goes to zero. We limit ourselves to calculations using B3LYP. For the smaller (TiO_2, PbO, SiO_2, TiO_2-SiO_2) particle, we are also able to compare the predictions of DFT with that of equation-of-motion CC theory with singles and doubles. Using this approach, we will show here that B3LYP a make very similar predictions regarding the geometries and

properties of the S1 minima of titanium dioxide, lead oxide, silicon dioxide nanoparticles, which, moreover in the case of agrees (TiO_2, PbO, SiO_2, TiO_2-SiO_2) with results obtained using DFT, whereas employing B3LYP yields drastically different results. While the particles used in this study are by necessity smaller than those studied experimentally, we believe that the methodological issues discussed here are independent of size range. Titanium dioxide (TiO_2), lead oxide (PbO), silicon dioxide (SiO_2) nanostructures have attracted great interest in the past few decades due to their low cost, environmental compatibility, and experimentally proven potential for photocatalytic and photovoltaic applications. In particular, the use of such nanostructures as heterogeneous catalysts for the photocatalytic splitting of water to produce renewable hydrogen and in dye-sensitized solar cells has been the subject of intense research. Recent studies suggest that the size and the shape of (TiO_2, PbO, SiO_2, TiO_2-SiO_2) nanostructures directly influence their performance in these applications and hence must have a clear effect on the microscopic electron−hole pair production, recombination, separation, and diffusion rates. To understand the physics and chemistry underlying the application of nano metaloxides in photocatalysis and photovoltaics from a theoretical point of view TiO_2, PbO, SiO_2, TiO_2-SiO_2 and extended systems have been computationally studied using a variety of theoaratical methods. Most of these studies employ either ground state density functional theory (DFT). In the former case, optical excitations are generally assumed to map onto excitations from occupied to unoccupied Kohn−Sham orbitals, which is theoretically somewhat difficult to justify. Alternatively, for the lowest triplet excited state, the excitation is modelled as a state obtained self-consistently by using in approach. DFT, in contrast, is a genuine excited state method that can be used for any number of excitations of any multiplicity. However, just like DFT in the case of the ground state, DFT suffers from the fact that the results are, to a smaller or larger degree, dependent on the exchange–correlation (XC) potential used. However, the poor scaling of such methods with the number of electrons in the system means that they can only be used for very small nanoclusters containing merely a few transition metal atoms. For example, the largest system studied to date for TiO_2, PbO, SiO_2, TiO_2-SiO_2 using correlated wave function methods is the (TiO_2, PbO, SiO_2, TiO_2-SiO_2). In this paper, we will demonstrate that, for most of the TiO_2, PbO, SiO_2, TiO_2-SiO_2 nanoparticles, DFT with all the tested XC potentials and the calculations give qualitatively similar results. Moreover, we will show that DFT calculations, using the B3LYP and XC potential, give the best quantitative fit to the excitation energies. Importantly, however, we will also show that for an important subset of structures, DFT can give qualitatively different results depending on the XC potential used and that, in this case, only B3LYP calculations yield results that are qualitatively consistent with those obtained using DFT theory. We will demonstrate that the discrepancies for these structures arise from a particular combination of defects, excitation involving which are poorly described by B3LYP. Finally, we demonstrate that these defects react exothermically with water to form hydroxyl groups and show that for hydrated TiO_2, PbO, SiO_2 and TiO_2-SiO_2 nanoparticles the qualitative discrepancies between the different methods, observed for naked particles, disappear to calculated using the same DFT setup (B3LYP level) to verify that

the optimized structures correspond to proper minima on the ground state potential energy surface. The nanosized particles possess astonishing physical and chemical properties and have a number of fascinating potential applications in a wide range of industrial sectors such as electronics, magnetic and optoelectronics, biomedical, pharmaceutical, cosmetics, energy, environmental, catalytic, space technology, and many others. The unusual properties of nanoparticles such as hardness, rigidity, high yield strength, flexibility, ductility are attributable to their high surface-to-volume ratio, the quantum size effect, and macroquantum tunnelling effect that are related to their nanosize. Indeed, the properties of nanoparticles may differ significantly from those observed for fine particles or bulk materials having the same chemical composition. Moreover, some physicochemical properties of nanoparticles can be altered with their varying size. For instance, by decreasing the size, particles change the colour, semiconducting materials exhibit metallic properties, and nonmagnetic particles become magnetic. Therefore, the understanding of the size-sensitive properties of engineering nanoparticles is essential from the scientific and technological viewpoint. It is even more important to be able efficiently model/predict such properties. Unfortunately, detailed analysis of the available databases reveals lack or/and inconsistent data describing physicochemical properties of the nanoparticles in relation to the size variations. Obtaining systematic data that reflect the change of the properties along with changing size requires very time-consuming procedures and generates high costs of the experimental research. Moreover, because of the difference in behaviour between nanoparticles and bulk chemicals, the characterization of bulk materials cannot be directly extrapolated to nanomaterials. Those knowledge gaps could be bridged by employing a computational approach, such as the combination of quantum chemical approaches and quantitative structure-properties relationship (QSPR) methods. This provides an efficient alternative to the empirical studies. However, because the properties of nanomaterials vary with size of a particle, the existing "traditional" methodology and descriptors are insufficient to express the unique physical and chemical properties of nanoparticles. The authors of current study previously successfully applied various novel approaches to study properties of nanoparticles by computational methods, including solubility of fullerenes, solubility of carbon nanotubes in water. Young's modulus and cytotoxicity of small nanosized metal oxide particles (10–100 Å) are evaluated by various nonempirical computational chemistry methods. Thus, it is necessary to maximally simplify the molecular models used for geometry optimization and calculation of the molecular properties, reflecting variability of the nanoparticles structures. Fortunately, recent contributions highlight that the most significant size-dependent changes of some physicochemical properties of the nanoparticles are observed below about 5 nm, whereas the changes for the sizes of nanomaterials between 15 and 90 nm can be neglected. The main objective of the present study is to investigate, how the molecular properties of nanometre-sized metal oxides change with the increasing size of the particle going from molecular clusters to the bulk form. Moreover, we have hypothesized that, for some properties, the extensive calculations for the whole structure can be replaced by calculations performed only for a representative fragment of the nanoparticle. The empirical methods the calculations have been performed

at the semi-empirical level of the theory with use of the efficient parameterized model to method recently parameterized for the considered elements and implemented in the Gaussian software package. We have calculated, for various sizes of molecular clusters, the following molecular properties heat of formation, dipole moment, total energy, electronic energy, the total solvent accessible surface area of the cluster, energy of the highest occupied molecular orbital (HOMO), energy of the lowest unoccupied molecular orbital (LUMO), band gap energy, chemical hardness, chemical softness, electrophilicity, and molecular weight of nanometre metal oxides. Future technologies depend on new materials with tailored, enhanced, and novel functionalities. Strongly correlated materials exhibit rich physics that offers unique opportunities in this regard, particularly in their magnetic, optical, and transport properties. While progress in computational materials design has greatly accelerated the process of identifying and realizing materials with moderate correlations, significant challenges remain for the quantitative, and in some cases, even qualitative, computational prediction of the properties of interest of strongly correlated materials. Furthermore, accurate computation of excited state properties even in moderately correlated materials is beyond the scope of density functional theory (DFT), and in strongly correlated materials, it is well known that DFT can even fail correctly to predict whether a system is a metal or an insulator. The existing materials databases constructed in the spirit of the Materials are built almost exclusively by DFT engines and are thus very often making incorrect predictions in correlated materials. There is thus a longstanding interest in developing the hybrid functional approaches, referred to as "beyond-DFT" methods, to treat strongly correlated and excited state properties. In strongly correlated materials, one reason for the failure of DFT is the delocalization or self-interaction error, which can be partially fixed by adding a method in the DFT approach. This method recovers the insulating state in many materials that are incorrectly predicted to be metallic in DFT. Moreover, DFT method give quite accurate results for structural parameters in most materials. However, unique determination of an appropriate value of the more general quantitative calculations has proved surprisingly problematic. Hybrid functionals, which also correct most of the self-interaction error by incorporating a certain fraction of exact exchange, significantly improve the descriptions of many systems. The beyond-DFT methods vary greatly in their suitability for different classes of correlated materials. In addition, they are considerably more computationally intensive than DFT. Especially in the context of high throughput studies, this means that there is a pressing need for a systematic way to choose, for any given material, the computational method that will give physically accurate results without unnecessary computation. Development of this capability requires that the performance of various beyond-DFT methods be systematically and uniformly tested on a diverse training set of strongly correlated materials that are experimentally well characterized. In this paper, we systematically and uniformly test various beyond-DFT methods on the set of metal oxides as TiO_2, PbO, SiO_2, TiO_2-SiO_2 allowing a head-to-head comparison between the various methods with experimental photoemission and inverse photoemission measurements. The methods included in the study are generalized gradient approximation with the hybrid functional with B3LYP and LANL2DZ in method to in the

addition, optical properties are computed with B3LYP and LANL2DZ compared with the available experiments. We expect to expand the training set of materials dramatically in future work, with the eventual goal of constructing a database in which a chosen set of DFT methods are systematically applied to an increasingly wide range of materials. Such a database holds great promise to enhance the power of computational materials design and discovery. Electron transfer (ET) processes at semiconductor surfaces constitute the basis for some technological applications including solar cells. In particular, solar cells of a type are based on transition metal complexes or dye molecules adsorbed on a nanocrystalline semiconductor material, typically titanium dioxide, lead oxide, silicon dioxide. In these cells, the key process is the charge injection from the adsorbate to the semiconductor. Thus, for a dye-sensitized solar cell using TiO_2, PbO, SiO_2, TiO_2-SiO_2, upon absorbing visible light, the dye molecules are excited from their ground state (with energy located in the TiO_2, PbO, SiO_2, TiO_2-SiO_2 band gap) to an excited state resonant with the TiO_2, PbO, SiO_2, TiO_2-SiO_2 conduction band. In particular, this process can follow two different mechanisms classified as DFT methods. In the first case, there is a photoexcitation to a dye excited state and then an electron transfer to the semiconductor. In this direct mechanism in which the electron injection occurs in one step from the dye ground state to the semiconductor conduction band. These cells present high photon to electron energy conversion yields; however, competing mechanisms reduce the efficiency of the process many different photosensitizers are known and some of them have been investigated widely. However, major effort is still invested in both developing new ones and finding optimal working conditions to improve the photon to current conversion efficiencies. Two representative organic sensitizers through mechanisms are alizarin and catechol, respectively. Both dyes have extensively been studied by experimental and theoretical methods, since they have simple molecular structures, low cost of fabrication and high photon to current conversion efficiencies. In a previous work, we tested the computational methodology on metal oxides. Theoretical methods constitute a complementary approach to understand the electronic processes that take place in the devices. The structure of the adsorbed on extended anatase TiO_2, PbO, SiO_2, TiO_2-SiO_2 surfaces has been investigated by using plane-wave DFT methods. The same conclusions are drawn from DFT calculations on the adsorbed on small hydrogen-terminated TiO_2, PbO, SiO_2, TiO_2-SiO_2 anatase clusters. In clusters with an oxygen vacancy, twice-deprotonated catechol adsorbs on it forming a bidentate structure, whereas in stoichiometric clusters, all adsorption modes are similar in energy. In a more recent work based on the molecular dynamic's simulations, it was observed that the singly charged anion do not chemical adsorb on different TiO_2, PbO, SiO_2, TiO_2-SiO_2 surfaces. Additionally, a combined study theoretical DFT calculations has also shown that the monodentate configuration on the rutile surface is easily transformable into the mononuclear bidentate configuration, and only the latter introduces states in the TiO_2, PbO, SiO_2, TiO_2-SiO_2 band gap a more recent study on the rutile surface has demonstrated that on the clean surface, the monodentate configuration is more favourable than the molecular adsorption, while the bidentate configuration is only favoured at an oxygen defect. In order to model, the electronic spectrum of density functional theory (DFT) has

been used. This method provides an improved treatment of the electron correlation effects relative to other methods like to metal oxides. Nevertheless, calculations with conventional DFT implementation are computationally rather expensive, and therefore they are limited to relatively small systems. They also calculated the spectrum of adsorbed catechol by using a minimal model, which included the molecule bound to a single TiO_2, PbO, SiO_2, TiO_2-SiO_2 atom and a set of water and hydroxyl ligands. Their results and another work showed qualitatively the main features of the theoretical spectra, and the effect of the binding to the surface, but they do not compare well with the experimental spectra in terms of absolute energies or relative intensities. Other theoretical studies have focused on simulating the electron injection dynamics of the on TiO_2, PbO, SiO_2, TiO_2-SiO_2. We report on density functional theory (DFT) calculations on the B3LYP method, TiO_2, PbO, SiO_2, TiO_2-SiO_2 clusters. Our main aim is to simulate the optical spectra of these systems by using two different DFT methods to compare them with the theoretical spectra and analyse the origin of the emerging band gap in a mechanism. We also investigate the effect of the adsorption mode on the spectra. Given the high computational cost of these sort of calculations, we use a set of clusters with different sizes intending to find the minimal size required to reproduce the main features of the spectra. The geometries are optimized in the electronic ground state for both free species and different dye–cluster models. The optical spectra are simulated for each structure using conventional (frequency domain) and real-time TD-DFT. In a previous work, this strategy was described in detail and applied to the study of DFT supported on TiO_2, PbO, SiO_2, TiO_2-SiO_2 nanoclusters. There are some advantages associated with the real-time DFT formulation; all the possible excitations are generated at the same time; the implementation is relatively simple; and although the computational cost is not cheap for small systems, it becomes competitive with traditional methods as the system size increases. However, the main disadvantage is that it is not possible to characterize the nature of the different transitions because the implementation of the method is based on electron density, and it does not provide any information about wave functions. For this reason, the combination with conventional DFT helps in that characterization. Because of the reduction of the computational cost, it is possible to tackle extended systems more comparable with experiments and thus to explore the influence of the model size on the results.

Bibliography

1. http://cdn.intechopen.com/pdfs-wm/37900.pdf
2. http://education.mrsec.wisc.edu/documents/usingVectors-_answers.pdf
3. http://myukk.xsrv.jp/free_journal/download.php?fn=NDFCT511_full.pdf
4. http://www.researchgate.net/profile/Yoshinori_Ando/publication/42804843Chemical_Vapor_Deposition_of_Carbon_Nanotubes_A_Review_on_Growth_Mechanism_and_Mass_Production/links/0fcfd50809726e590a000000.p
5. http://www.understandingnano.com/electrical-properties-carbon-nanotubes.html
6. http://www.understandingnano.com/nanotubes-carbon-properties.html

7. Ahmed, J., N. Alhokbany, T. Ahamad, and S.M. Alshehri. 2022. Investigation of enhanced electro-catalytic HER/OER performances of copper tungsten oxide @ reduced graphene oxide nanocomposites in alkaline and acidic media. *New Journal of Chemistry* 46 (3): 1267–1272.
8. Balasubramaniam, S., A. Mohanty, S.K. Balasingam, S.J. Kim, and A. Ramadoss. 2020. Comprehensive insight into the mechanism, material selection and performance evaluation of supercapatteries. *Nano-Micro Letters* 12 (1): 1–46.
9. Chen, Y., T. Liu, L. Zhang, and J. Yu. 2019. N-doped graphene framework supported nickel cobalt oxide as supercapacitor electrode with enhanced performance. *Applied Surface Science* 484: 135–143.
10. De, B., T. Kuila, N.H. Kim, and J.H. Lee. 2017. Carbon dot stabilized copper sulphide nanoparticles decorated graphene oxide hydrogel for high performance asymmetric supercapacitor. *Carbon* 122: 247–257.
11. Esposito, S. 2019. "Traditional" sol-gel chemistry as a powerful tool for the preparation of supported metal and metal oxide catalysts. *Materials* 12 (4): 668.
12. Ezeigwe, E.R., P.S. Khiew, C.W. Siong, and M.T. Tan. 2017. Synthesis of $NiMoO_4$ nanorods on graphene and superior electrochemical performance of the resulting ternary based composites. *Ceramics International* 43 (16): 13772–13780.
13. Guldi, Dirk M., and Nazario Martin. Carbon nanotubes and related structures–Synthesis, characterization, functionalization and applications. Wiley-VCH Verlag GmbH&Co.KGaA.
14. Jeyaranjan, A., T.S. Sakthivel, M. Molinari, D.C. Sayle, and S. Seal. 2018. Morphology and crystal planes effects on supercapacitance of CeO_2 nanostructures: Electrochemical and molecular dynamics studies. *Particle and Particle Systems Characterization* 35 (10): 1800176.
15. Kathalingam, A., S. Ramesh, A. Sivasamy, H.S. Kim, and H.S. Kim. 2019. Supercapacitor performance of MnO_2/$NiCo_2O_4$@ N-MWCNT hybrid nanocomposite electrodes. *Journal of Sol-Gel Science and Technology* 91 (1): 154–164.
16. Kaur, J., K. Anand, K. Anand, and R.C. Singh. 2018. WO_3 nanolamellae/reduced graphene oxide nanocomposites for highly sensitive and selective acetone sensing. *Journal of Materials Science* 53 (18): 12894–12907.
17. Kumar, R., R.K. Singh, A.R. Vaz, R. Savu, and S.A. Moshkalev. 2017. Self-assembled and one-step synthesis of interconnected 3D network of Fe_3O_4/reduced graphene oxide nanosheets hybrid for high-performance supercapacitor electrode. *ACS Applied Materials and Interfaces* 9 (10): 8880–8890.
18. Lee, M., S.K. Balasingam, H.Y. Jeong, W.G. Hong, H.B.R. Lee, B.H. Kim, and Y. Jun. 2015. One-step hydrothermal synthesis of graphene decorated V_2O_5 nanobelts for enhanced electrochemical energy storage. *Scientific Reports* 5 (1): 1–8.
19. Li, M., G. Sun, P. Yin, C. Ruan, and K. Ai. 2013. Controlling the formation of rodlike V_2O_5 nanocrystals on reduced graphene oxide for high-performance supercapacitors. *ACS Applied Materials and Interfaces* 5 (21): 11462–11470.
20. Liang, L., Y. Xu, X. Wang, C. Wang, M. Zhou, Q. Fu, M. Wu, and Y. Lei. 2015. Intertwined $Cu_3V_2O_7(OH)_2{\cdot}2H_2O$ nanowires/carbon fibers composite: A new anode with high rate capability for sodium-ion batteries. *Journal of Power Sources* 294: 193–200.
21. Liu, G., Y. Zhou, C. Zou, X. Zhu, and Y. Guo. 2018. Heat-pulse assisted NH_3 gas sensing based on cuprous oxide nanoparticles anchored on reduced graphene oxide nanosheets. *Journal of Materials Science: Materials in Electronics* 29 (4): 3317–3325.
22. Loiseauetal, A. 2006. Understanding carbon nanotubes. Lecture Notes in Physics, 677. Berlin: Springer. https://doi.org/10.1007/b10971390.

Chapter 2
Theoretical Aspects of Nanometal Oxides

2.1 Introduction

In forecasting the properties of metal oxides, DFT modelling plays a distinctive function. The effect of nanometal oxides MOs such as CuO, OCu, ZnO, and OZn on biopolymers such as cellulose, chitosan, and sodium alginate was investigated. As a result, a model structure of two-unit organic polymers cellulose, chitosan, and sodium alginate is proposed, together with micro-MOs such as CuO, OCu, ZnO, and OZn. This effect was investigated using density functional theory (DFT) at B3LYP/LANL2DZ. The calculated HOMO–LUMO band gap energy (ΔE) and Total dipole moment (TDM) showed that nano-MOs influenced cellulose and chitosan, with TDM increasing and ΔE decreasing, while sodium alginate had a minor change with no effect. The electrostatic potential (ESP) of cellulose and chitosan was also calculated.

2.2 Band Gap Energy and Photocatalysis

Polyaniline is a conducting polymer, which means it can conduct electricity. It has a strong electrochemical activity, making it ideal for use as a subsequent electrode material in supercapacitors. It is thought to be one of the most promising materials for energy storage. These uses stem from the structure's controllability, as well as other benefits such as low cost and environmental stability. The capacitive behaviour of polyaniline has been linked by some researchers to the reversible electrochemical doping–dedoping process. This advantage is responsible for the phenomena of charge storage and subsequent release. Polyaniline in the electrolyte undergoes ion transfer from solution to the polymer backbone and vice versa as a result of the oxidation/reduction process. High electrochemical stability was observed when carbon nanomaterials such as carbon nanotubes (CNTs) interacted with polyaniline,

B. Karthikeyan et al., *Nano Metal Oxides*,
https://doi.org/10.1007/978-981-19-9444-9_2

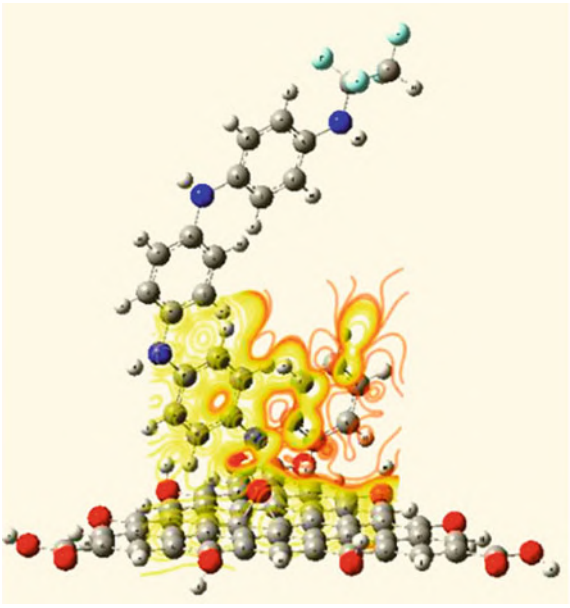

Fig. 2.1 Metal cluster organic ligand interaction

according to the findings. Carbon nanomaterials, such as carbon nanotubes (CNTs), activated carbon (AC), and graphene, are presently considered promising materials because of their conductivity, physicochemical stability, and excellent and long-life cycle. Graphene is more easily handled and made than carbon nanotubes (Fig. 2.1).

To figure out where the HER activity of g-C_3N_4@FeO comes from, DFT calculations are used. Although the FeO nanoparticles and g-C_3N_4 used in the calculations are significantly smaller than the FeO nanoparticles and g-C_3N_4 observed experimentally, this simplistic shape may already represent the crucial influence on the electronic structure, as demonstrated below. The rectangular lattice of the supercell g-C_3N_4 repeats four-unit cells of the bare tube in the *c* direction, while the vacuum thicknesses in the a and b directions are equal (Figs. 2.2 and 2.3).

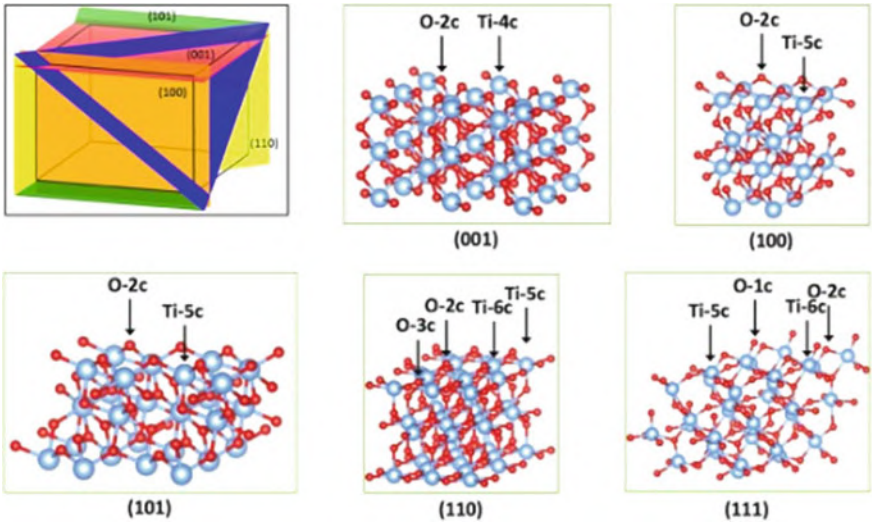

Fig. 2.2 Modelling rutile TiO_2 nanorod growth preferences: a density functional theory study

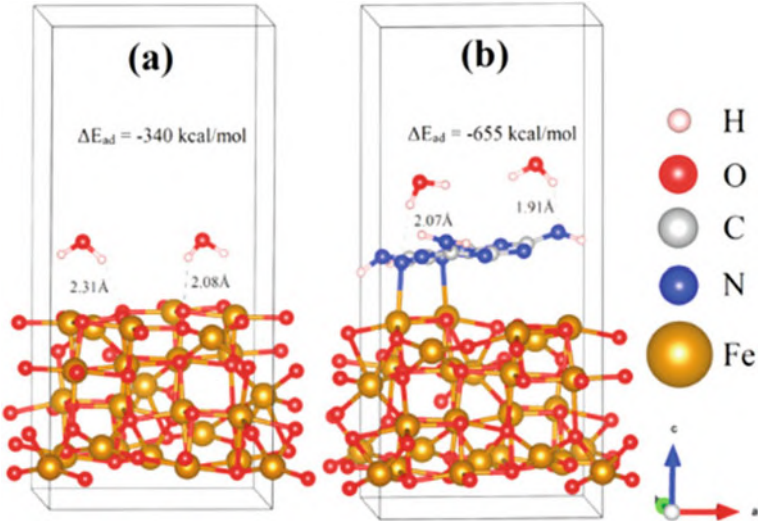

Fig. 2.3 Magical nanoclusters

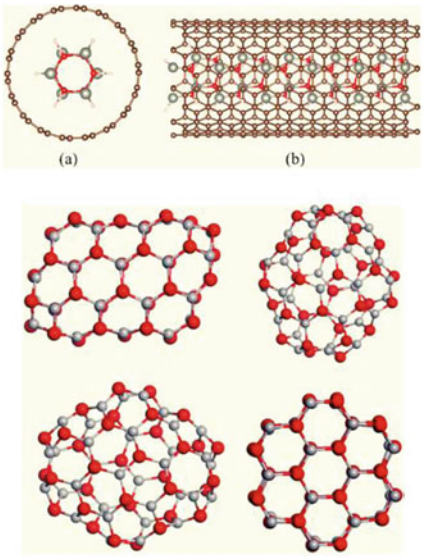

Theory of density functional density

The structural and electrical properties of nanoclusters (ZnO) in various geometric configurations ($n = 34, 60$) were investigated. The basic features of the band structure were explored, and an optimization (relaxation) of structure geometry was done for each cluster. It was discovered that fullerene-like hollow structures that satisfy the rule of six isolated quadrangles are the most stable for (ZnO) 34 nanoclusters. Different forms of isomers, including hollow structures and sodalite-like structures comprised of (ZnO) 12 nanoclusters, were studied for the (ZnO) 60 nanoclusters. The sodality-type structure, formed of seven (ZnO) 12 clusters with shared quadrangle edges, was found to be the most energetically advantageous structure.

We confirmed that the sodalite structure, which is made up of 7 (ZnO) 12 nanoclusters with joint quadrangle edges, is the most stable among the (ZnO) 60 nanoclusters. Previous research found that the (ZnO) 12 cage-like structure (truncated octahedron) was extremely stable when compared to other small (ZnO) n, implying that it might be employed as a building block for ZnO nanostructures. Figure 2.4 shows the values for HOMO and LUMO for sodalite, as well as the other (ZnO) 60 structural isomers. For each (ZnO) 34 nanocluster, partial densities of states from the contributions of distinct orbital components for the valence band (left) and conduction band (right) are shown in Fig. 2.5. Graphs I, III, and V show the *s*, *p*, and *d* states of Zn atoms, respectively; graphs II, IV, and V show the *s*, *p*, and *d* states of Zn atoms.

Between 7.0 and 4.0 eV, each cluster's valence band is dominated by Zn 3*d* states and O 2*p* states. O 2*p* states, Zn 3*d* states, and, on a smaller scale, Zn 3*p* and 3*s* states make up the bands between 4.0 and 0 eV. Between 1 and 5 eV, however, the conduction band is dominated by Zn 4*s* and O 2*p* and O 2*s* states. Figure 2.6 depicts partial densities of states for the valence band (left) and conduction band (right) for each (ZnO) 60 nanocluster based on the contributions of distinct orbital components

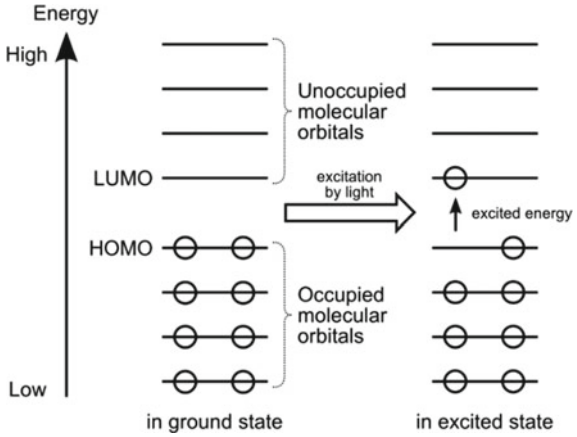

Fig. 2.4 Molecular orbital diagram of representative materials

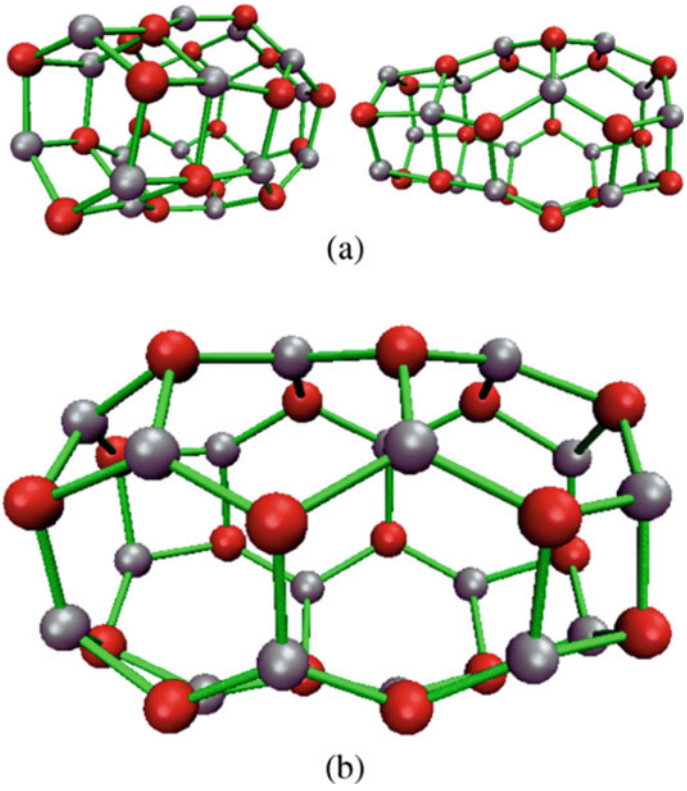

Fig. 2.5 ZnO nanocluster models

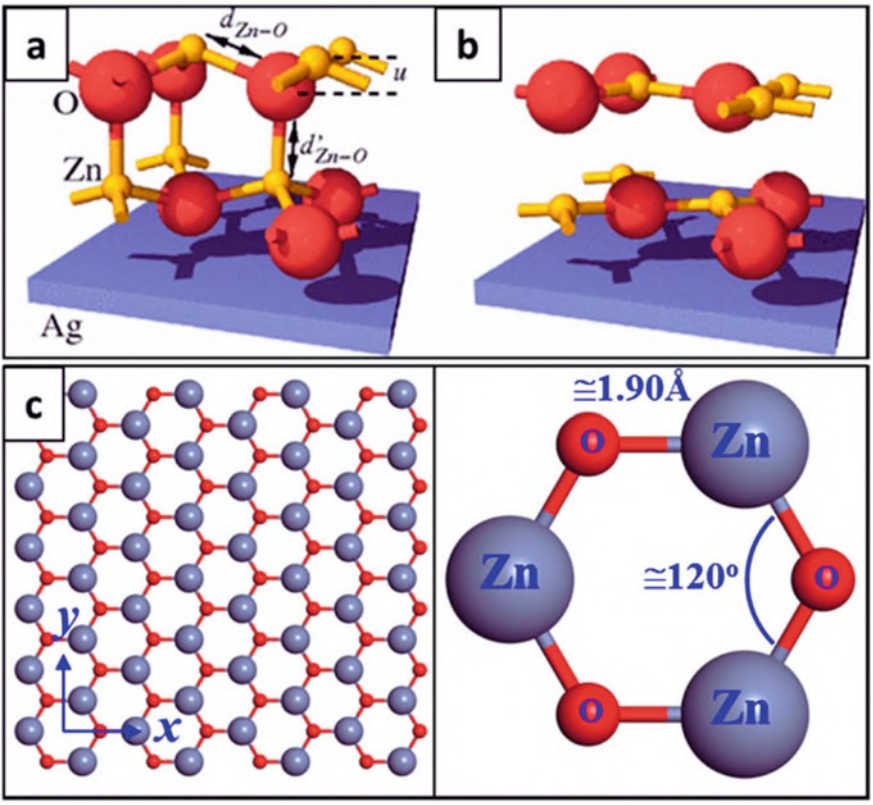

Fig. 2.6 Partial densities of state

(right). The *s*, *p*, and *d* states of Zn atoms are depicted in graphs I, III, and V, while the *s* and *p* states of O atoms are depicted in graphs II, IV, and VI. Each cluster's valence band between 7.0 and 4.0 eV, like in the case of (ZnO) 34 nanoclusters, is made up of Zn 3*d* states and O 2*p* levels. Between 4.0 and 0 eV, O 2*p* states, Zn 3*d* states, and, on a smaller scale, Zn 3*p* and 3*s* states predominate. Between 1 and 5 would be the conduction band.

2.3 Insights into the Electrical and Optical Characteristics of the ZnO @ CNT Core from a First-Principles Perspective

One-dimensional (1D) nanostructures, such as nanowires, nanobelts, and nanotubes, have gained a lot of attention in recent years because of their superior characteristics, wide range of potential applications, and different capabilities. Core @ shell

structures, on the other hand, have variable surface characteristics and improved electrical, optical, and catalytic performance, making them popular in a variety of electronic and photonic device applications. Since Suenaga et al. discovered the coaxial structure in 1997, several efforts have been made to synthesize 1D core @ shell nanostructures. Guo et al., for example, demonstrated new electrical and optical features of TiO_2-CdS and TiO_2-Au nanotube arrays, which could lead to improved catalytic functionalities. Lou et al. described the utilization of Au@ ZrO_2 nanorattles as a stable catalyst for CO oxidation at high temperatures. The interplay of dielectric resonance and plasmonic bowtie nanoantennas in ZnTe @ZnO core @ shell nanowires was also described by Nie et al., which might considerably improve the efficiency of intermediate band solar cells. Zinc oxide (ZnO) is an II–VI semiconductor with a large band gap (3.37 eV), a high exciton binding energy (60 meV), and good thermal stability. ZnO has been shown to be a potential nanomaterial for a wide range of technical applications, such as photodetectors, solar cells, photonic crystals, transparent conducting oxides, and so on.

The significance of materials has driven research into the creation of ZnO micro/nanostructures. Metal organic chemical vapour deposition (MOCVD), catalytic growth via vapour–liquid–solid (VLS) epitaxial process, and pulsed laser deposition are the techniques used among them.

Bibliography

1. Wang, G., L. Zhang, and J. Zhang. 2012. A review of electrode materials for electrochemical super capacitors. *Chemical Society Reviews* 41: 797–828. https://doi.org/10.1039/C1CS15060J.
2. Mi, H., J. Zhou, Z. Zhao, C. Yu, X. Wang, and J. Qiu. 2015. Block copolymer–guided fabrication of shuttle–like polyaniline nanoflowers with radiated whiskers for application in super capacitors. *RSC Advances* 5: 1016–1023. https://doi.org/10.1039/C4RA10273H.
3. Chen, W., R.B. Rakhi, and H.N. Alshareef. 2013. Facile synthesis of polyaniline nanotubes using reactive oxide templates for high energy density pseudo capacitors. *Journal of Materials Chemistry A* 1: 3315–3324. https://doi.org/10.1039/C3TA00499F.
4. Wang, L., Y. Ye, X. Lu, Z. Wen, Z. Li, H. Hou, and Y. Song. 2013. Hierarchical nano composites of polyaniline nanowire arrays on reduced graphene oxide sheets for super capacitors. *Scientific Reports 3*. https://doi.org/10.1038/srep03568.
5. Wang, L., X. Lu, S. Lei, and Y. Song. 2014. Graphene-based polyaniline nano composites: Preparation, properties and applications. *Journal of Materials Chemistry A* 2: 4491–4509. https://doi.org/10.1039/C3TA13462H.
6. Li, Y., X. Zhao, Q. Xu, Q. Zhang, and D. Chen. 2011. Facile preparation and enhanced capacitance of the polyaniline/sodium alginate nano fiber network for super capacitors. *Langmuir* 27: 6458–6463. https://doi.org/10.1021/la2003063.
7. Wang, X., J. Deng, X. Duan, D. Liu, J. Guo, and P. Liu. 2014. Crosslinked polyaniline nano rods with improved electrochemical performance as electrode material for super capacitors. *Journal of Materials Chemistry A* 2: 12323–12329. https://doi.org/10.1039/C4TA02231A.

8. Xie, Y., Y. Liu, Y. Zhao, Y.H. Tsang, S.P. Lau, H. Huang, and Y. Chai. 2014. Stretchable all-solid-state supercapacitor with wavy shaped polyaniline/graphene electrode. *Journal of Materials Chemistry A* 2: 9142–9149. https://doi.org/10.1039/C4TA00734D.
9. Hu, N, L. Zhang, C. Yang, J. Zhao, Z. Yang, H. Wei, H. Liao, Z. Feng, A. Fisher, Y. Zhang, and Z.J. Xu. 2016. Three-dimensional skeleton networks of graphene wrapped polyaniline nanofibers: An excellent structure for high-performance flexible solid-state supercapacitors. *Scientific Reports 6*. https://doi.org/10.1038/srep19777
10. Guo, F., H. Mi, J. Zhou, Z. Zhao, and J. Qiu. 2015. Hybrid pseudo capacitor materials from polyaniline @multi-walled carbon nano tube with ultrafine nano fiber-assembled network shell. *Carbon* 95: 323–329. https://doi.org/10.1016/j.carbon.2015.08.052.
11. Yang, M., B. Cheng, H. Song, and X. Chen. 2010. Preparation and electrochemical performance of polyaniline-based carbon nanotubes as electrode material for super capacitor. *Electrochimica Acta* 55: 7021–7027. https://doi.org/10.1016/j.electacta.2010.06.077.
12. Fan, H., H. Wang, N. Zhao, X. Zhang, and J. Xu. 2012. Hierarchical nano composite of polyaniline nano rods grown on the surface of carbon nanotubes for high-performance super capacitor electrode. *Journal of Materials Chemistry* 22: 2774–2780. https://doi.org/10.1039/C1JM14311E.
13. Kumar, R., E. Joanni, R.K. Singh, D.P. Singh, and S.A. Moshkalev. 2018. Recent advances in the synthesis and modification of carbon-based 2D materials for application in energy conversion and storage. *Progress in Energy and Combustion Science* 67: 115–157. https://doi.org/10.1016/j.pecs.2018.03.001.
14. Kumar, R., J.-H. Oh, H.-J. Kim, J.-H. Jung, C.-H. Jung, W.G. Hong, H.-J. Kim, J.-Y. Park, and I.-K. Oh. 2015. Nano hole-structured and palladium-embedded 3D porous graphene for ultrahigh hydrogen storage and CO oxidation multifunctionalities. *ACS Nano* 9: 7343–7351. https://doi.org/10.1021/acsnano.5b02337.
15. El-Khodary, S.A., G.M. El-Enany, M. El-Okr, and M. Ibrahim. 2014. Preparation and characterization of microwave reduced graphite oxide for high-performance super capacitors. *Electrochimica Acta* 150: 269–278. https://doi.org/10.1016/j.electacta.2014.10.134.
16. Hwang, J.Y., M.F. El-Kady, M. Li, C.W. Lin, M. Kowal, X. Han, and R.B. Kaner. 2017. Boosting the capacitance and voltage of aqueous super capacitors via redox charge contribution from both electrode and electrolyte. *Nano Today* 15: 15–25. https://doi.org/10.1016/j.nantod.2017.06.009.
17. Tiwari, S.K., R.K. Mishra, S.K. Ha, and A. Huczko. 2018. Evolution of graphene oxide and graphene: From imagination to industrialization. *Chem NanoMat* 4: 598–620. https://doi.org/10.1002/cnma.201800089.
18. Hughes, Z.E., and T.R. Walsh. 2015. Computational chemistry for graphene-based energy applications: Progress and challenges. *Nanoscale* 7: 6883–6908. https://doi.org/10.1039/C5NR00690B.
19. Kumar, R., R.K. Singh, D.P. Singh, E. Joanni, R.M. Yadav, and S.A. Moshkalev. 2017. Laser-assisted synthesis, reduction and micro-patterning of graphene: Recent progress and applications. *Coordination Chemistry Reviews* 342: 34–79. https://doi.org/10.1016/j.ccr.2017.03.021.
20. Ates, M., S. Caliskan, and E. Özten. 2018. Supercapacitor study of reduced graphene oxide/Zn nanoparticle/polycarbazole electrode active materials and equivalent circuit models. *Journal of Solid State Electrochemistry* 22: 3261–3271.
21. Li, H., Q. Su, J. Kang, H. Feng, P. Huang, M. Feng, M. Huang, and G. Du. 2018. Fabrication of MoS_2 @ SnO_2-SnS_2 composites and their applications as anodes for lithium ion batteries. *Materials Research Bulletin* 108: 106–112. https://doi.org/10.1016/j.materresbull.2018.08.042.
22. Park, S., K.S. Lee, G. Bozoklu, W. Cai, S.T. Nguyen, and R.S. Ruoff. 2008. Graphene oxide papers modified by divalent ions—Enhancing mechanical properties via chemical cross-linking. *ACS Nano* 2: 572–578. https://doi.org/10.1021/nn700349a.
23. Aghazadeh, M. 2018. One-step electrophoretic/electrochemical synthesis of reduced graphene oxide/manganese oxide (RGO-Mn_3O_4) nanocomposite and study of its capacitive performance. *Analytical and Bioanalytical Electrochemistry* 10: 961–973.

24. Alghunaim, N.S., S.A. El-Khodary, M. Ibrahim, and G.M. El-Enany. 2019. Spectroscopic analyses of iron doped protonated polyaniline/graphene oxide system. *Spectrochimica Acta Part A* 216: 349–358. https://doi.org/10.1016/j.saa.2019.03.053.
25. Bayoumy, A.M., A. Refaat, I.S. Yahia, H.Y. Zahran, H. Elhaes, M.A. Ibrahim, and M. Shkir. 2019. Functionalization of graphene quantum dots (GQDs) with chitosan biopolymer for biophysical applications. *Optical and Quantum Electronics* 52: 1–14. https://doi.org/10.1007/s11082-019-2134-z.
26. Grenni, P., A. Barra Caracciolo, L. Mariani, M. Cardoni, C. Riccucci, H. Elhaes, and M.A. Ibrahim. 2019. Effectiveness of a new green technology for metal removal from contaminated water. *Microchemical Journal* 147: 1010–1020. https://doi.org/10.1016/j.microc.2019.04.026.
27. Fahmy, A, R.M. Khafagy, H. Elhaes, and M.A. Ibrahim. 2020. Molecular properties of polyvinyl alcohol/sodium alginate composite. *Biointerface Research in Applied Chemistry 10*: 4734–4739. https://doi.org/10.33263/BRIAC101.734739.
28. Refaat, A., M.A. Ibrahim, H. Elhaes, R. Badry, H. Ezzat, I.S. Yahia, H.Y. Zahran, and M. Shkir. 2019. Geometrical, vibrational and physical properties of polyvinyl chloride nanocomposites: Molecular modeling approach. *Journal of Theoretical and Computational Chemistry 18*. https://doi.org/10.1142/S0219633619500378
29. Ezzat, H.A., M.A. Hegazy, N.A. Nada, and M.A. Ibrahim. 2019. Effect of nano metal oxides on the electronic properties of cellulose, chitosan and sodium alginate. *Biointerface Research in Applied Chemistry 9*: 4143–4149. https://doi.org/10.33263/BRIAC94.143149.
30. Ibrahim, M., and H. Elhaes. 2005. Computational spectroscopic study of copper, cadmium, lead and zinc interactions in the environment. *International Journal of Environment and Pollution* 23: 417–424. https://doi.org/10.1504/IJEP.2005.007604.
31. Ibrahim, M., and A.A. Mahmoud. 2009. Computational notes on the reactivity of some functional groups. *Journal of Computational and Theoretical Nano science* 6: 1523–1526. https://doi.org/10.1166/jctn.2009.1205.
32. Politzer, P., P.R. Laurence, and K. Jayasuriya. 1985. Molecular electrostatic potentials: An effective tool for the elucidation of biochemical phenomena. *Environmental Health Perspectives* 61: 191–202. https://doi.org/10.1289/ehp.8561191.
33. Ahin, Z.S., H. Şenöz, H. Tezcan, and O. Büyükgüngör. 2015. Synthesis, spectral analysis, structural elucidation and quantum chemical studies of (E)-methyl-4-[(2-phenyl hydrazono)methyl] benzoate. *Spectrochimica Acta Part A* 143: 91–100. https://doi.org/10.1016/j.saa.2015.02.032.
34. Frisch, M.J., et al. 2010. Gaussian09, revisions D. 01 and B. 01; Gaussian, Inc. *Wallingford, CT*.
35. Becke, A.D. 1993. Density-functional thermo chemistry. III. The role of exact exchange. *The Journal of Chemical Physics 98*: 5648–5652. https://doi.org/10.1063/1.464913
36. Lee, C., W. Yang, and R.G. Parr. 1988. Development of the Colle-Salvetti correlation-energy formula into a functional of the electron density. *Physical Review B* 37: 785–789. https://doi.org/10.1103/PhysRevB.37.785.
37. Miehlich, B., A. Savin, H. Stoll, and H. Preuss. 1989. Results obtained with the correlation energy density functionals of becke and Lee, Yang and Parr. *Chemical Physics Letters* 157: 200–206. https://doi.org/10.1016/0009-2614(89)87234-3.
38. Abdelsalam, H., H. Elhaes, and M.A. Ibrahim. 2018. Tuning electronic properties in graphene quantum dots by chemical functionalization: Density functional theory calculations. *Chemical Physics Letters* 695: 138–148. https://doi.org/10.1016/j.cplett.2018.02.015.
39. Badry, R., S. El-Khodary, H. Elhaes, N. Nada, and M. Ibrahim. 2019. On the molecular modeling analyses of sodium carboxymethyl cellulose treated with acetic acid. *Letters in Applied Nano BioScience 8*: 553–557. https://doi.org/10.33263/LIANBS82.553557.
40. Huang, H.M., et al. 2001. Room-temperature ultraviolet nanowire nanolasers. *Science* 292: 1897–1899.
41. Yang, G., et al. 2017. High performance core-shell TiO_2(B)/anatase homojunction nanobelts with active cobalt phosphide cocatalyst for hydrogen production. *Science and Reports* 7: 14594.
42. Agrawal, K.V., S. Shimizu, L.W. Drahushuk, D. Kilcoyne, and M.S. Strano. 2017. Observation of extreme phase transition temperatures of water confined inside isolated carbon nanotubes. *Nature Nanotechnology* 12: 267–273.

43. Duan, X.F., Y. Huang, Y. Cui, J.F. Wang, and C.M. Lieber. 2001. Indium phosphide nanowires as building blocks for nanoscale electronic and optoelectronic devices. *Nature* 409: 66–69.
44. Ribeiro, M.S., A.L. Pascoini, W.G. Knupp, and I. Camps. 2017. Effects of surface functionalization on the electronic and structural properties of carbon nanotubes: A computational approach. *Applied Surface Science* 426: 781–787.
45. Qu, K.G., et al. 2017. Polydopamine-inspired, dual heteroatom-doped carbon nanotubes for highly efficient overall water splitting. *Advanced Energy Materials* 7: 1602068.

Chapter 3
Ceramic Semiconductor Photocatalysts as Therapeutic Agent

Metal oxide coatings have been investigated intensively; in particular, TiO_2-based coatings have sparked a lot of interest due to their photocatalytic capabilities. By combining diverse substrates with TiO_2-based coatings, new materials in the fields of textiles, structures, and plastics with self-cleaning, antibacterial, and self-decontaminating capabilities have been produced. The application of nanostructured coatings on substrates permits the creation of novel materials in which nanoparticle properties are transferred to the surface. Surface functionalization can be used for a variety of applications, including barrier coatings, self-cleaning hydrophobic or photocatalytic coatings, antistatic coatings, and superparamagnetic coatings, all of which have significant technical implications. The ultimate qualities of the material are influenced by the type of support, the nature of the coating, and how they interact. Because of the self-cleaning effect offered by nano-TiO_2 coatings on textile substrates, their application of nano-TiO_2 in textile finishing has been an important topic of research in the last year. In reality, TiO_2 applied to textiles may result in high levels of self-cleaning activity, with the potential to destroy stains, germs, and volatile organic compounds (VOCS) adsorbing on fibres and converting them to CO_2 and H_2O. As a result, a thorough examination of the coating preparation and application process is critical in the production of high-quality and high-performance end products.

Many methods for producing supported TiO_2 films exist, including anodic oxidation sputtering and the sol–gel process; however, sol–gel derived approaches like as dip or spray coating are the most extensively used. Sol–gel synthesis from precursors or colloidal dispersion from commercial powder is described in the mentioned sol–gel methods. In the context of a large-scale application, each of these strategies has some shortcomings. The first is hampered by the complexity and limited reproducibility of wet chemical procedures, while the second is hampered by issues with the stability and transparency of the nanopowder dispersion. The current work addresses these issues by describing a dip-pad-dry-cure process for creating self-cleaning photocatalytic textiles from TiO_2 commercial nanosols with stabilized properties and guaranteed reproducibility. The features and performance of sols used for

B. Karthikeyan et al., *Nano Metal Oxides*,
https://doi.org/10.1007/978-981-19-9444-9_3

synthesis after treatment were compared, and the data gathered was used to conduct a first semi-industrial sampling. UV light stimulation causes TiO_2 to become photocatalytic, resulting in the creation of electron −/ hole + pairs. Free radicals are formed when the liberated electrons react with water and oxygen molecules on the surface. These radicals are highly reactive entities capable of decomposing a wide range of organic stains as well as biological pollutants found in aqueous conditions. The photocatalytic activity of TiO_2 coated materials is governed by the interphase domain, and macroscopic parameters such as surface hydrophilicity have a direct impact on photocatalytic performance.

In order to get the desired control over final qualities, the nanomaterial scientist community is working together to develop novel materials through design and engineering at the nanoscale level. This research is the first attempt to link TiO_2 nanoscale qualities like nanostructure and surface chemistry to macroscale properties like hydrophilicity and functional properties like photocatalytic activity. The hydrophilic behaviour and catalytic performance of TiO_2 coatings supported on various substrates (fabric, glass, and ceramic) were evaluated and compared to the results of physicochemical characterization. Dip coating was used to deposit TiO_2 coatings on glass substrates and ceramic tiles, while a dip-pad-dry-cure process was used to cover fabrics. The ceramic tiles used were unglazed porcelain stoneware and soda-lime flat glass (Fig. 3.1).

The use of acid nanosol (TAC) directly on the skin must be avoided. Because of its low pH and the presence of synthesis by-product (organics, salts), TiO_2's photocatalytic activity is reduced. As a result, the TAC sol was subjected to ultra-filtration prior to usage (TACF). The pH was raised while synthesis by-products were removed by ultra-filtering employing polymeric filters with a pore size of 100 k Dalton, which allow the retention of TiO_2 nanoparticles. The vessel can be replenished with water multiple times to get the desired qualities. Three nanosol samples with varied pH values were generated by varying the washing degree: 3.5, 4.0, and 4.2. (Called TACF3.5, TACF4.0, and TACF4.2 respectively). The commercial sol acidity was also reduced by adding citrate salt (TiO_2: citrate weight ratio 1:1) as an alternative to

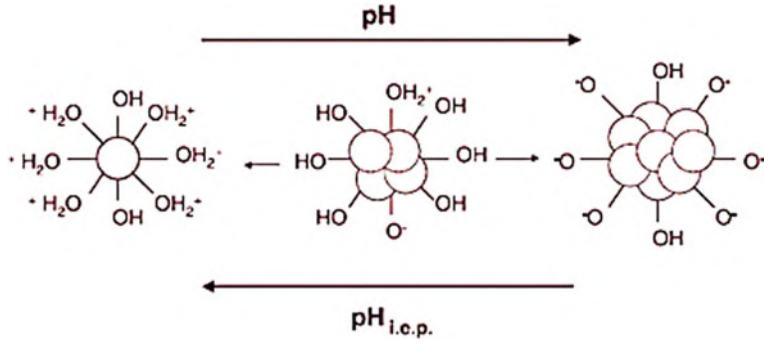

Fig. 3.1 Schematic representation of surface properties of TiO_2 dispersed nanoparticles as a function of pH and agglomeration state

ultra-filtration, resulting in neutralized sample (TN, pH 6). To achieve a solid content of 3 wt%, pristine and modified commercial sols were diluted with distilled water. These sols samples' chemical–physical properties are described (Fig. 3.2).

Metals, nanofibres, and nanotubes are just a few illustrations of nanostructures that have gotten a lot of interest because of their uses in various disciplines. Due to their wide range of applications in photocatalysis, dye-sensitized solar cells, and biomedicine, nanostructured TiO_2 materials are among the most investigated substances in material science. TiO_2 nanotubes (TiO_2NT) have gotten the most attention among nanostructured TiO_2 materials because of their low cost of synthesis, regular and predictable nanoscale geometry, and unique functional properties for biomedical applications. TiO_2NT are now ideal candidates for application in vascular implants, biosensors, and drug delivery systems due to their superior biocompatibility.

Encapsulation of a wide range of medicines into TiO_2NT has been described in recent years, demonstrating the extraordinary characteristics of these materials for drug delivery. In this context, obtaining novel materials capable of encapsulating a wide range of treatments with varied chemical and biological capabilities, with high loading capacities and slow-release rates, is a major issue in the creation of TiO_2NT-based drug delivery systems. These targets can be fulfilled by combining TiO_2NT with biopolymers such as poly (lactic-co-glycolic acid) and chitosan, which

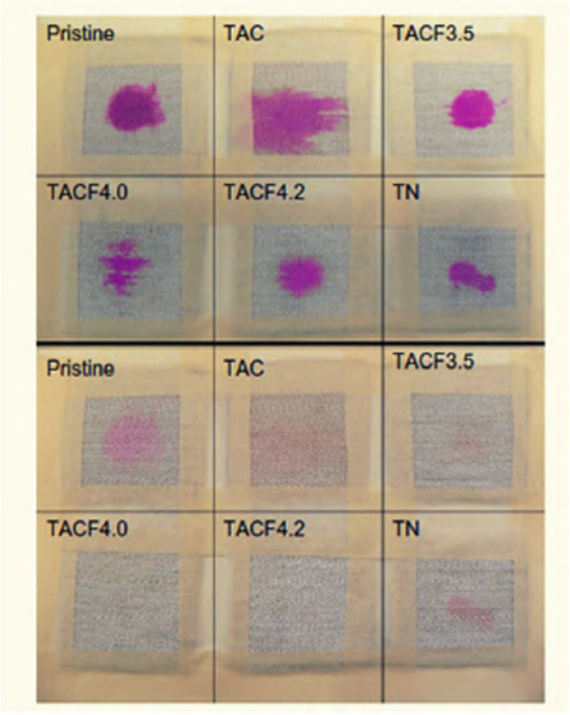

Fig. 3.2 Rhodamine B stains discoloration on the fabric samples under UV irradiation. $T = 0$ (up) $t =$ 30 min (under)

have been successfully used to create polymer-TiO_2NT nanocomposites with encapsulating and controlled release capabilities for pharmaceuticals like lidocaine and indomethacin. In another approximation, polymeric micelles encapsulating pharmaceuticals were encapsulated in TiO_2NT to provide materials with extended delivery of poorly soluble drugs such indomethacin, coumarin 6, and gentamicine, among others. The drug release properties of these nanomaterials have also been altered by surface modification of TiO_2NT.

A typical surface alteration when compared to pristine TiO_2NT, the strategy involves the use of silane coupling agents such as 3-aminopropyltriethoxy saline and 3-mercaptopropyltrimethoxy silane, which have been used to obtain new nanocarriers for enrofloxacin with increased drug loading capacity and long-term sustained release. Surface modification of TiO_2NT with nanostructured polymeric moieties with drug encapsulating capabilities and rich chemical functionality, such as polyamidoamine (PAMAM) dendrimers, is a still unexplored method in this field. PAMAM dendrimers have been used as templates for nanotube synthesis and as surface modifiers for TiO_2 and ZnO nanoparticles in recent years, demonstrating that dendrimer moieties retain their encapsulating properties while also improving the inherent properties of inorganic materials. Nonetheless, the covalent attachment of dendritic moieties to TiO_2NT has yet to be investigated, and it represents a promising prospect for the development of more efficient nanomaterials for drug delivery applications.

Polyamidoamine (PAMAM) dendrimers are monodisperse synthetic polymers with globular-ellipsoidal shape, hyper-branched structure with hydrophobic interior chambers, and multivalent surface functionality. An ethylene diamine core and branched homocentric layers of Amide-amine functionality (called generations) up to the periphery, where surface primary amine groups are placed, and produce PAMAM dendrimers. The polyelectrolyte characteristics of PAMAM dendrimers are due to surface primary amines and interior tertiary amines. Primary amines (pKa 9.4–9.7) are protonated under physiological conditions (pH = 7.4), but tertiary amines (pKa 3–6) stay neutral. Due to their well-documented ability to interact with chemically diverse therapeutics either through physical encapsulation of drug molecules into internal dendrimer cavities or electrostatic interaction with protonated surface amino groups, PAMAM dendrimers have been extensively studied as supramolecular hosts for drug delivery purposes. PAMAM dendrimers have been shown to improve the dissolution rate, water solubility, bioavailability, and stability of therapeutic molecules when used as drug carriers (Fig. 3.3).

Nonetheless, PAMAM dendrimers' cytotoxicity, along with their short half-life in plasma circulation, poses serious constraints to their usage in drug administration. PAMAM dendrimers are frequently partially modified with neutral or anionic groups, such as polyethylene glycol, polypropylene imine, and fatty acids, to circumvent these limitations, which have been shown to successfully minimize dendrimer cytotoxicity (Fig. 3.4).

This report discusses the synthesis of surface-conjugated TiO_2NT with PAMAM dendrimer of the third generation (PAMAM-G3), with the goal of generating a novel nanocarrier material that combines the encapsulating and drug release features of

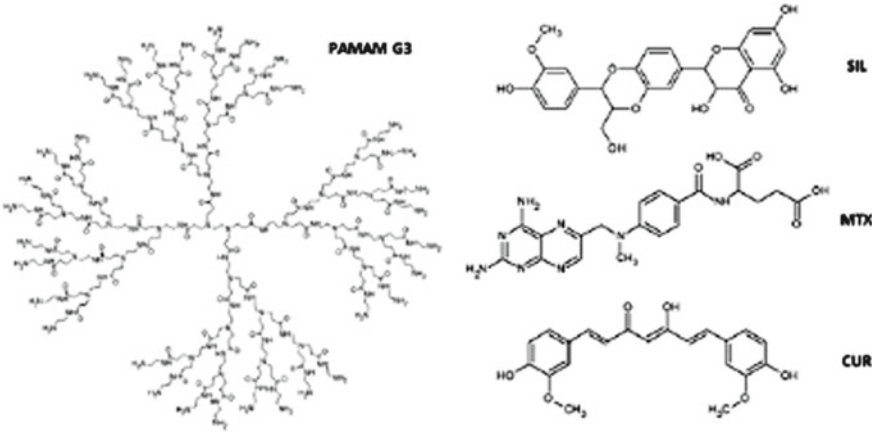

Fig. 3.3 Structure of PAMAM-G3 dendrimer, curcumin (CUR), methotrexate (MTX), and silibinin (SIL)

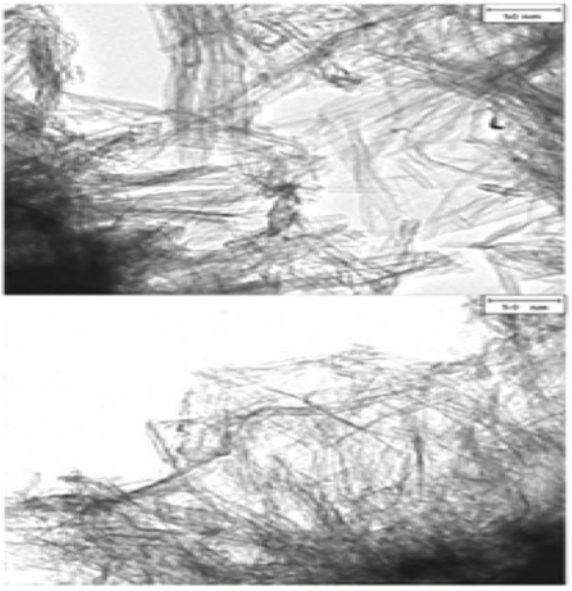

Fig. 3.4 TEM micrograph and size distribution of (up) TiO_2NT and (down) PAMAM-TiO_2NT

both systems. Our primary goal was to develop a versatile platform capable of interacting effectively with a wide range of chemically diverse medications while also being suited for long-term drug release. Curcumin (CUR), methotrexate (MTX), and silibinin (SIL), three well-known medicinal drugs exploited in the treatment of cancer, autoimmune, and liver disorders, were selected as model compounds to

address this issue. The PAMAM modification of TiO_2NT disclosed our findings. When compared to pristine nanotubes, PAMAM-TiO_2NT has a higher drug loading capacity and longer drug release times, highlighting its potential as a novel drug carrier material.

For the treatment of resistant dirty water sources, heterogeneous photocatalytic ozonation stands out. In a short reaction time, the pollutants' degradation rate reaches its maximum, and the biodegradability of the pollutants in the wastewater grows significantly. The intermediate compounds created during the biological treatment procedure inclined to be hazardous and resistant to chemical oxidation treatments that did not include ozone. However, by using photocatalytic ozonation as a potential treatment approach to boost degradability and reduce toxicity, these resistant by-products might be entirely destroyed.

The constant formation of oxidizing species and active radicals both inside the reaction mass and on the surface of the catalyst, which is fed with dissolved ozone, is the basis of the photocatalytic ozonation process. When compared to un-immobilized approaches, the photocatalytic ozonation method avoids the separation expenses of the nanocatalyst from the solution by zapping stable nanocatalysts such as TiO_2NPs on to an appropriate and inexpensive substrate. This is the initial stage that will greatly aid the process's modernization.

The heterogeneous photocatalytic ozonation approach in the vicinity of immobilized nanocatalysts is an especially appealing technology, as it can proceed via both homogeneous and heterogeneous paths. It has been successfully used in the laboratory for the degradation of many pollutants polluted water supplies, including synthetic colours. MBZ is a drug that, despite having a painkilling effect in the human body, can be dangerous if it is not preprocessed before entering the body. High levels of MBZ in effluent will cause an ecological disaster for organisms. Furthermore, it is a benzimidazole-type broad-spectrum anthelminthic drug that is used to treat a variety of parasitic worm infections.

However, due to the complexity of its mechanism, the precise progression via heterogeneous or homogeneous pathways has yet to be investigated. In fact, estimating the concentration of active radicals and oxidant species involved and created in situ inside the reaction fluid and on the surface of the catalyst has some limits. Using a suitable modelling tool to determine the reaction route, illustrate how radicals are distributed inside the reactor and show continuous creation of radicals at the surface and inside the solution under various experimental conditions can assist to elucidate the mechanism of this method. This is the alternative strategy for introducing and transferring the method and its efficacy to industrial wastewater treatment zones (Fig. 3.5).

One of the greatest approaches to avoid the above-mentioned drawbacks is to use modelling and simulation. Computational fluid dynamics (CFD) is a type of numerical modelling that includes equations for the species' momentum, energy, and mass balance. CFD can accurately mimic fluid hydrodynamics and interactions between species at the same time. The Lattice Boltzmann method (LBM), finite volume method (FVM), finite element method (FEM), and finite difference technique are all simulation methodologies (FDM). FVM is the most accurate method,

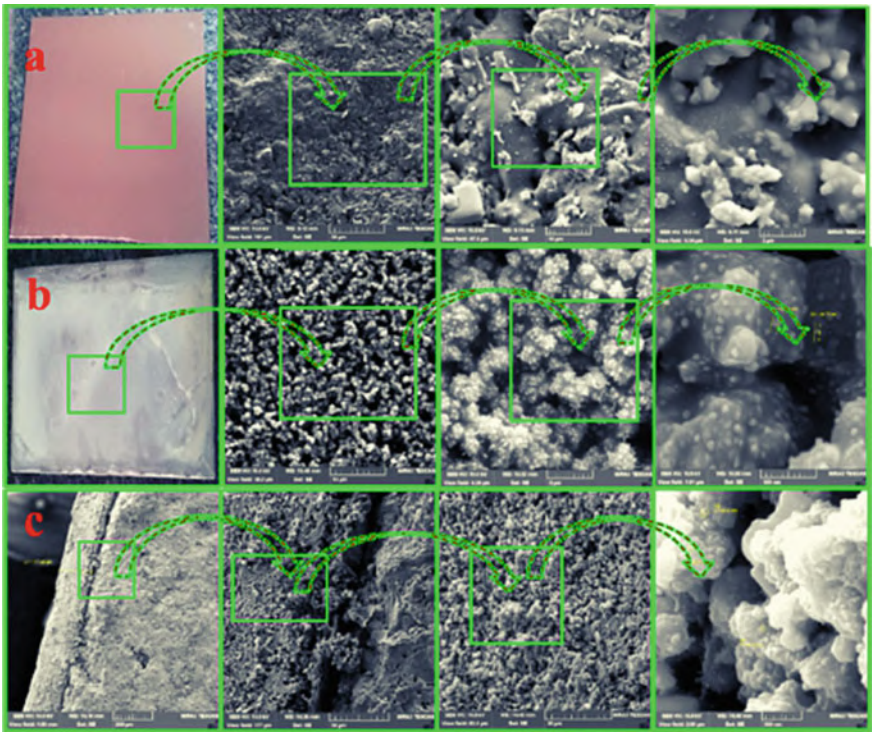

Fig. 3.5 SEM images of **a** uncoated **b** surface coated and **c** wall of the coated surface of the ceramic plates in different magnification

especially for processes that involve species interactions. AOPs have been the subject of a few CFD research. To determine the kinetic parameters, Verbruggen et al. used both analytical mass transfer and the CFD approach. In contrast to the analytical mass transfer approach, they discovered that CFD simulation had a good agreement with the practical data. In a photoreactor, Mohajerani et al. created a CFD model for removing Metronidazole from effluent.

This research proposes using advanced modelling and simulation techniques such as CFD to investigate the heterogeneous photocatalytic ozonation process from new perspectives. TiO_2 NPs were attached to the outer surface of the industrial ceramic panels in the first step of the investigation, providing a modified sol–gel approach with the advantages of low cost and easy operation. The MBZ was degraded in a semi-batch rectangular photocatalytic reactor (containing the four-coated ceramics on the walls).

The deterioration of the MBZ polluted water supply was investigated using experimental factors such as a model MBZ content, ozone inlet flow rate, and time. The heterogeneous photocatalytic ozonation ion process was simulated using the CFD method in the second portion of this work to forecast its progress from two perspectives: hydrodynamic and chemical evaluation in this type of photoreactor.

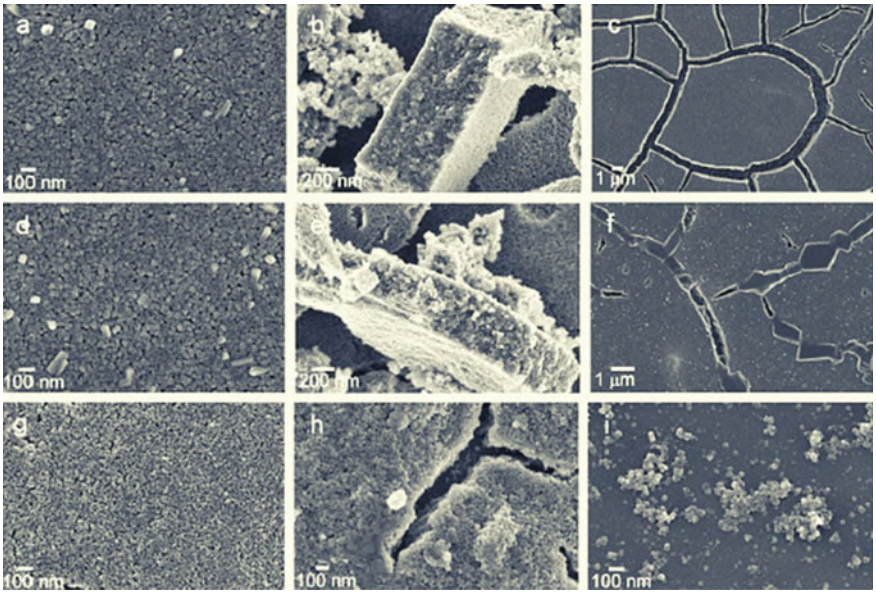

Fig. 3.6 FE-SEM micrographs of TiO_2 film on a ceramic tile fired at 700 °C: **a**–**c** 4.5% of TiO_2, **d**–**f** 1% of TiO_2, **g**–**h** 0.5% of TiO_2, and **i** 0.1% of TiO_2

This modelling method could help with a variety of challenges, such as providing a process mechanism and confirming the efficacy of the catalysts utilized. There are no initiatives about MBZ degradation in a stirred tank photoreactor, according to prior peer-reviewed studies. The goal of this research was to better understand, model, and stimulate the photocatalytic ozonation process using an immobilized nanocatalyst in order to improve its use in pilot and industrial scale for more effective treatment, so MBZ was only used as a model of a persistent pharmaceutical pollutant (Fig. 3.6).

The degradation of organic dyes MB, RB, and CV as model pollutants in an aqueous solution with a TiO_2 photocatalytic surface treated with UV radiation was investigated in this article. The study concentrated on determining factors such as spectra, wavelength, and intensity. The effects of these variables were investigated on laboratory-prepared samples of ceramic tiles coated with commercially available TiO_2 sol.

Coal, oil, and natural gas continue to be the world's most important energy sources. Most fossil fuels are predicted to be depleted in the twenty-first century as a result of continued industrialization. Furthermore, the usage of fossil fuels pollutes the environment significantly. In recent years, increasing levels of serious air and water pollution have posed a direct threat to human life and health. Since then, TiO_2 has been used as a photocatalyst in a wide range of environmental control applications. The potential application range of photocatalysis is also enhanced by extensive research into photocatalyst technology. Photocatalytic disinfection, photocatalytic hydrogen production, photocatalytic reduction of photocatalyst wastewater treatment, and air

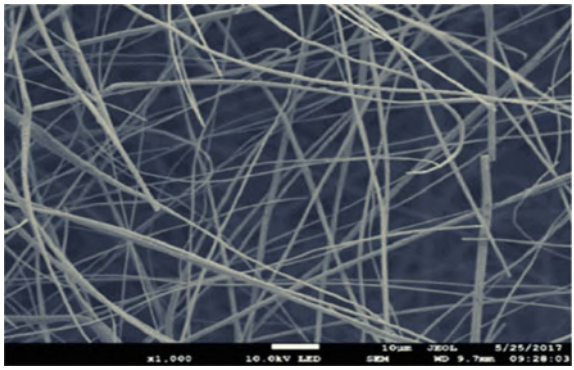

Fig. 3.7 SEM image of TiO_2 nanofibres prepared by electrospinning

purification are the key research directions at present time. However, photocatalytic technology is still in the lab, and there is still a long way to go before it can be used in the real world. With the progress of photocatalytic technology, several outstanding evaluations have been posted (Fig. 3.7).

The majority of existing reviews concentrate on only one or a few features of photocatalyst. We have compiled a list of typical photocatalyst preparation and modification methods in the hopes of assisting researchers in their search for more efficient photocatalysts. Meanwhile, a series of breakthroughs in photocatalyst technology have been examined to help academics better understand the latest photocatalyst research trends. This review article attempts to highlight researchers' efforts to develop optimum photocatalyst using various preparation and modification approaches. This evaluation also encourages the advancement of photocatalytic technology, as well as the industrialization of photocatalytic technology.

Bibliography

1. Costa, Anna Luisa, Simona Ortelli, Magda Blosi, Stefania Albonetti, Angelo Vaccari, Michele Dondi. 2013. *Chemical Engineering Journal 225*: 880–886.
2. AlShehri, S.M., J. Ahmed, A.M. Alzahrani, and T. Ahamad. 2017. Synthesis, characterization, and enhanced photocatalytic properties of $NiWO_4$ nanobricks. *New Journal of Chemistry* 41 (16): 8178–8186.
3. An, L., Q. Ren, W. Li, K. Xu, Y. Cao, T. Ji, R. Zou, Z. Chen, and J. Hu. 2015. Highly ordered mesoporous $NiCo_2O_4$ with superior pseudocapacitance performance for supercapacitors. *Journal of Materials Chemistry A* 3 (21): 11503–11510.
4. Torres, Cecilia, C., Cristian H. Campos, Carola Diáz, Verónica A. Jiménez, Felipe Vidal, Leonardo Guzmán, and Joel B. Alderete. 2016. *Materials Science and Engineering C 65*: 164–171.
5. Chaudhari, S., D. Bhattacharjya, and J.S. Yu. 2015. Facile synthesis of hexagonal $NiCo_2O_4$ nanoplates as high-performance anode material for Li-Ion batteries. *Bulletin of the Korean Chemical Society* 36 (9): 2330–2336.
6. Chen, Y., T. Liu, L. Zhang, and J. Yu. 2019. N-doped graphene framework supported nickel cobalt oxide as supercapacitor electrode with enhanced performance. *Applied Surface Science* 484: 135–143.

7. Khataee, Alireza, Mahdi Ebrahimi Farshchi, Mehrangiz Fathinia, and Hassan Aghdasinia. 2020. *Process Safety and Environmental Protection 141*: 37–48.
8. Petrovic, Vladimira, Vilma Ducman, and Sreco D. Skapin. 2012. *Ceramics International 38*: 1611–1616.
9. Zhang, Fubao, Xianming Wang, Haonan Liu, Chunli Liu, Yong Wan, Yunze Long, and Zhongyu Cai. 2019. *Applied Sciences* 9: 2489.
10. Emiru, T.F., and D.W. Ayele. 2017. Controlled synthesis, characterization and reduction of graphene oxide: A convenient method for large scale production. *Egyptian Journal of Basic and Applied Sciences* 4 (1): 74–79.
11. Esposito, S. 2019. "Traditional" sol-gel chemistry as a powerful tool for the preparation of supported metal and metal oxide catalysts. *Materials* 12 (4): 668.
12. Foo, C.Y., A. Sumboja, D.J.H. Tan, J. Wang, and P.S. Lee. 2014. Flexible and highly scalable V_2O_5-rGO electrodes in an organic electrolyte for supercapacitor devices. *Advanced Energy Materials* 4 (12): 1400236.
13. Fu, M., Z. Zhu, W. Chen, H. Yu, and Q. Liu. 2020. Microwave-assisted synthesis of MoS_2/graphene composites for supercapacitors. *Journal of Materials Science* 55 (34): 16385–16393.
14. Govindarajan, D., V. Uma Shankar, and R. Gopalakrishnan. 2019. Supercapacitor behavior and characterization of rGO anchored V_2O_5 nanorods. *Journal of Materials Science: Materials in Electronics* 30 (17): 16142–16155.
15. Guan, X.H., X. Lan, X. Lv, L. Yang, and G.S. Wang. 2018. Synthesis of NiMoSO/rGO composites based on $NiMoO_4$ and reduced graphene with high-performance electrochemical electrodes. *Chemistry Select* 3 (24): 6719–6728.
16. Hassan, D., S. El-Safty, K.A. Khalil, M. Dewidar, and G. Abu El-magd. 2016. Carbon supported engineering $NiCo_2O_4$ hybrid nanofibers with enhanced electrocatalytic activity for oxygen reduction reaction. *Materials* 9 (9): 759.
17. He, G., L. Wang, H. Chen, X. Sun, and X. Wang. 2013. Preparation and performance of $NiCo_2O_4$nanowires-loaded graphene as supercapacitor material. *Materials Letters* 98: 164–167.
18. Hekmat, F., Y. Tutel, and H.E. Unalan. 2020. Wearable supercapacitors based on nickel tungstate decorated commercial cotton fabrics. *International Journal of Energy Research* 44 (9): 7603–7616.
19. Kamalam, M.B.R., B.K. Balachander, and K. Sethuraman. 2016. Solvothermal synthesis and characterization of reduced graphene oxide/Vanadium pentoxide hybrid nanostructures. *Materials Today: Proceedings* 3 (6): 2132–2140.
20. Karmakar, A., and S.K. Srivastava. 2019. In situ fabricated nickel vanadate/N-doped reduced graphene oxide hybrid as an advanced electrocatalyst in alkaline hydrogen evolution reaction. *Journal of Materials Chemistry A* 7 (25): 15054–15061.

Part II
Metal Oxides Used as a Protective Materials

Chapter 4
Metal Oxides as Protective Materials-Boon in Pandemic (Antimicrobial Surface Coatings)

Microbial cross-contamination from food contact and non-food contact surfaces is a primary source of food-borne illness. Contaminated surfaces are one of the top five risk factors contributing to food-borne outbreaks, according to the US Food and Drug Administration (FDA). In a food production, processing, and preparation environment, food contact and non-food contact surfaces such as equipment surfaces, knives, utensils, cutting boards, work tables, conveyor belts, packaging materials, product tote boxes, and floor drains are common sources of microbial cross-contamination. Several studies have shown that bacteria on food processing facility surfaces are a main source of product contamination, leading to food degradation, and disease transmission. Furthermore, food residues that collect on inert surfaces contribute to the creation of mature biofilms, which are difficult to remove using standard sanitation measures. Several food-borne diseases and outbreaks have been linked to surface contamination, colonization, and subsequent biofilm formation.

Several food-borne epidemics are thought to have been caused by improper washing and disinfection of pathogen-infested equipment and surfaces. Several multistate food-borne outbreaks in the United States, including ice cream premix contaminated with *Salmonella enteritidis*, peanut butter contaminated with Salmonella Tennessee, and cantaloupes contaminated with *Listeria monocytogenes*, have been linked to contaminated equipment surfaces or unsanitary processing, packaging, transportation, and preparation conditions. It reveals that both food contact and non-food contact surfaces have a high potential of microbial cross-contamination, which can seriously harm consumers' health. In a food processing facility, cleaning, sanitation, and disinfection of surfaces is standard procedure.

For this goal, a variety of physical and chemical processes have been used, including high-pressure water cleaning, irradiation, ozonation, fumigation, and the use of alkaline detergents, chlorinated compounds, quaternary ammonium compounds, iodophors, and a variety of other disinfectants. Chemical disinfectants are used to disinfect contaminated surfaces in the majority of cases, although they may not be suitable as agents to prevent future contamination of surfaces. Chemical disinfectants are also difficult to use and can be caustic at times. Furthermore,

B. Karthikeyan et al., *Nano Metal Oxides*,
https://doi.org/10.1007/978-981-19-9444-9_4

there is mounting evidence that chemical disinfectants produce harmful disinfection by-products.

Nanotechnologies can be used across the food supply chain, from production through processing, to ensure the safety of the product, packaging, transportation, storage, and delivery. Nanotechnology's potential benefits in the food industry have been extensively researched. Surface modification using antimicrobial compounds is one interesting area of application that has gained a lot of attention in recent years. Antimicrobial compounds-containing materials have been introduced into the food industry as a new concept to improve cleanliness. Many applications in the food sector, such as food processing and storage, could benefit from the introduction of a safe, cost-effective, and broad range of long-lasting nanosize biocides into polymers, paints, or working surfaces. Several materials having antimicrobial activity were previously available on the market, including kitchen utensils, chopping boards; counter surfaces, storage containers, freezers, conveyor belts, and packaging films. Antimicrobial nanoparticles such as silver ions and triclosan, as well as organic and inorganic antimicrobial nanoparticles, are widely used to generate antimicrobial functional materials. When utilized in a food processing setting, however, these chemicals frequently failed to provide a broad spectrum of antibacterial action and to maintain that activity for long periods of time. Advanced oxidation techniques employing photocatalytic metal oxide nanoparticles (NPs) have showed tremendous potential as non-targeted disinfectants against a variety of bacteria and chemical pollutants in this setting.

There has been a surge in interest in using photocatalytic disinfection techniques to improve food safety and quality during the last decade. Titanium dioxide (TiO_2), zinc oxide (ZnO), tungsten oxide (WO_3), and iron oxide (Fe_2O_3) are all semiconductor metal oxide NPs that have been demonstrated to have antibacterial activity in light-catalysed chemical processes without producing any toxic by-products. The background, progress and promise of heterogeneous photocatalytic disinfection technology to ensure microbiological food safety are addressed in this section.

4.1 Semiconductor Photocatalysts

Antimicrobial agents used in the food business are categorized as (i) organic or (ii) inorganic based on their chemical composition. Organic antibacterial compounds have several drawbacks, including limited heat resistance, high decomposability, and a short half-life. Because of their capacity to survive harsh processing conditions and increased mechanical and chemical stability at high temperatures and pressures, inorganic antimicrobial agents have grown in importance. Furthermore, their antibacterial activity is highly non-specific, making resistance development difficult for microbes. As a result, inorganic NPs have gotten a lot of attention and can be found in a lot of antibacterial products.

A number of inorganic NPs are now being investigated for their antibacterial effects. Inorganic NPs (gold, silver, and platinum) and magnetic NPs (iron, cobalt,

and nickel) are divided into three categories: (i) semiconductor NPs (titanium, zinc, and tungsten oxides); (ii) engineered carbon NPs (carbon nanotubes (CNTs), C60, and C70 fullerenes); and (iii) engineered carbon NPs (carbon nanotubes (CNTs), C60 Because of their unique photocatalytic capabilities, semiconductor metal oxides are particularly appealing. As a result, they're also called semiconductor photocatalysts.

In the presence of a certain range of radiation, photocatalytic processes take place on the semiconductor's surface. Typical photocatalysts include oxide semiconducting materials (such as TiO_2, ZnO, CuO, MgO, SnO_2, WO_3, SiO_2, Fe_2O_3, and Nb_2O_3), metal hybrid nanocomposites (CdS and ZnS), and doped structures (such as Ag/TiO_2, TiO_2/CuO, TiO_2/Pt, Au/TiO_2, Fe_2O_3/TiO_2, and N-, C S doped TiO_2.

4.2 Working Principle of Semiconductor Photocatalysis

Due to their distinctive electrical configuration (such as a filled valence band and an empty conduction band) and the creation of electron–hole pairs, semiconductor metal oxides participate in light-catalysed redox processes. The quantity of light energy necessary to create these electron–hole pairs, on the other hand, is dependent on the size of the band gap (Eg), which is unique to each semiconductor. As a result, each photocatalyst corresponds to a range of light wavelengths where electron–hole pairs can be produced through energy absorption and photoactivation. When a photon with an energy of h meets or surpasses the semiconductor's band gap energy (Eg), an electron (ecb−) is promoted from the valence band (VB) into the conduction band (CB), leaving a hole (hvb+) behind, according to Hoffmann and others. CB electrons and VB holes in the excited state can recombine in pico seconds and release the input energy as heat, become stuck in meta-stable surface states, or react with electron donors and electron acceptors adsorbed on the semiconductor surface (Fig. 4.1).

4.3 The Band Gap of the Anatase Form of TiO_2

Approximately 3.2 eV, which means that photocatalysis can be initiated by photons that can exert energy of 3.2 eV. It implies a light having a wavelength of below 385 nm required for the anatase form of TiO_2 which falls in the near-UV spectrum or UVA range. The photo-generated electron (e^-) − hole (h^+) pairs on the surface of TiO_2 can react with surface-bound electron acceptors or donors such as molecular O_2, H_2O, and other organic compounds to initiate redox reactions. This process results in the generation of reactive oxygen species (ROS) such as hydroxyl (OH), superoxide (O_2^-) radicals, and hydrogen peroxide (H_2O_2) in various chain reactions. The generated ROS can be used to totally mineralize organic molecules, such as bacterial cells, and convert them to CO_2 and H_2O. The capacity of a semiconductor to undergo photocatalytic redox reactions is determined by the semiconductor's band

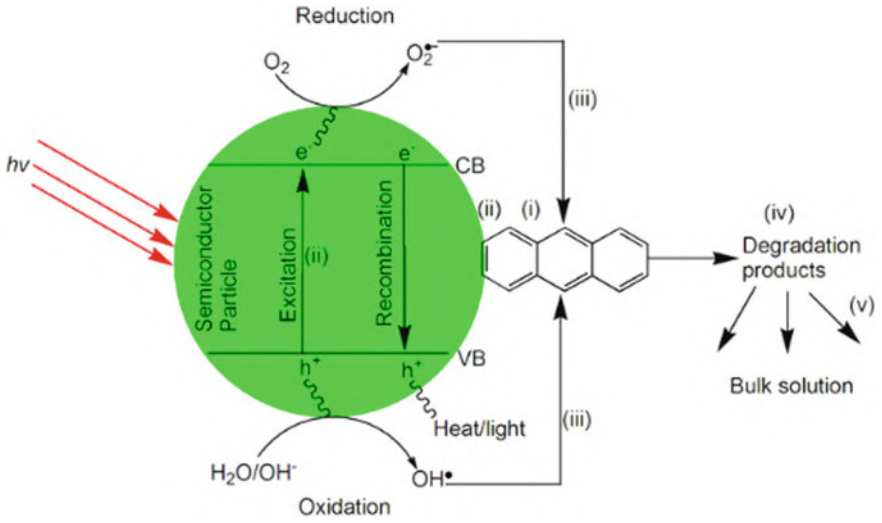

Fig. 4.1 Mechanism for semiconductor photocatalysis

energy positions and the acceptor species' redox potentials. It means that the recombination rate of e^-h^+ pairs must be avoided for more efficient photocatalysis (Figs. 4.2 and 4.3; Table 4.1).

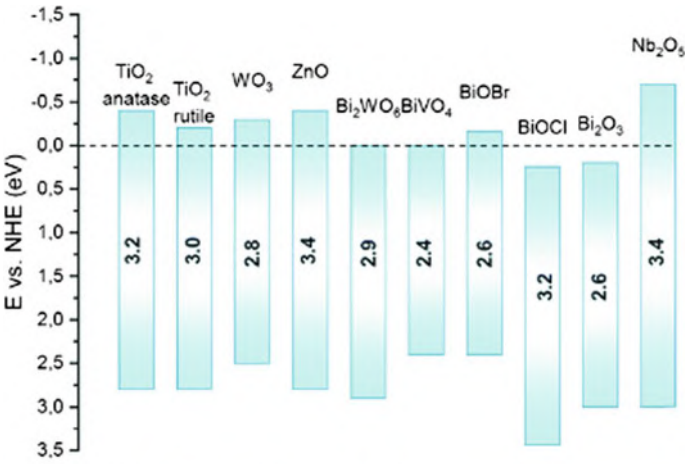

Color	Wavelength (nm)	Band gaps (eV)	MOS
Blue	450<λ<500	2.48<E_g<2.76	BiOBr, $BiVO_4$, Bi_2O_3
Violet	400<λ<450	2.76<E_g<3.10	TiO_2 rutile, WO_3, Bi_2WO_6
Ultraviolet	λ<400	3.1<E_g	TiO_2 anatase, ZnO, BiOCl, Nb_2O_5

Fig. 4.2 Band gap energies for various metal oxides

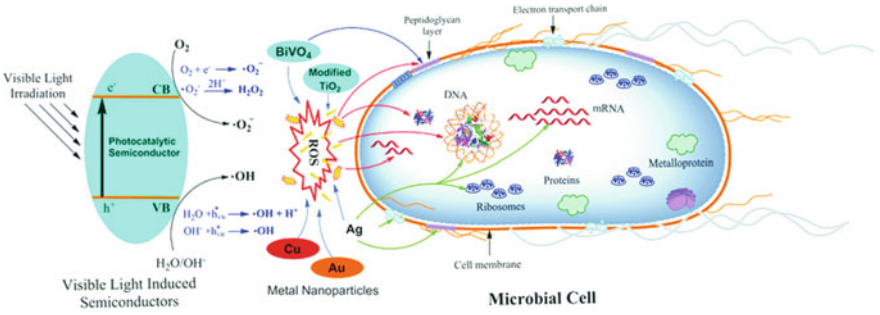

Fig. 4.3 Various mechanisms of antimicrobial activity of the metal nanoparticles

Table 4.1 List of common semiconductor photocatalysts and their band gap energies

Photocatalyst	Bandgap (eV)	Spectral	Region pros and cons
SnO_2	3.8	UV (326 nm)	
TiO_2 [anatase]	3.24	UV (383 nm)	Stable, corrosion-resistant,
$SrTiO_2$	3.2	UV (387 nm)	Large band gap
ZnO	3.2	UV (387 nm)	Large band gap
Degussa P25	3.14	UV (395 nm)	Large band gap, high
TiO_2 (rutile)	3.02	Visible (411 nm)	Stable, less photoactive
WO_3	2.8	Visible (443 nm)	Photo corrode
Cd S	2.4	Visible (517 nm)	Photo corrode, unstable
Fe_2O_3	2.3	Visible (539 nm)	Photo corrode
Cu_2O	2.2 V	Visible (564 nm)	Unstable
MoS_2	1.8 V	(689 nm)	Ultra-visible
Cd Se	1.7	(729 nm)	Photo corrode, unstable

4.4 Photocatalysts Made of Semiconductors Have the Following Properties

Titanium dioxide:

The anatase and rutile forms of TiO_2 were discovered to have the highest photocatalytic activity of the three. Due to its unique electrical arrangement, photo-stability, chemical inertness, commercial availability, low cost, and lack of toxicity, TiO_2 has been identified as one of the most promising photocatalysts. Anatase, rutile, and brookite are the three most common polymorphs of TiO_2. The energy band gap for anatase is 3.2 eV, with an excitation light wavelength in the near-UV or UVA range (385 nm), whereas the band gap for rutile is 3.02 eV, with an excitation wavelength that extends into the visible light range (410 nm). However, due to the combined effect of its larger surface absorptive capacity and high rate of trapping,

anatase is thought to be the most photoactive. Because the structure of an anatase is less vulnerable to recombination processes, the excited state has a longer lifespan. Rutile, on the other hand, is prone to recombination of electron–hole pairs. Anatase–rutile or brookite-anatase mixes were found to be more active than anatase alone in several investigations. Degussa P25, a commercial mixed phase TiO_2 with anatase and rutile weight ratios of roughly 3:1, was shown to have outstanding photocatalytic capabilities.

As a result, it is used as a benchmark for comparing photocatalytic activity of different NPs. P25 photocatalytic reactions have been documented in over 1000 papers, making it the most extensively studied photocatalyst to date. Several research projects are currently underway to narrow TiO_2's band gap into the visible light area. Excellent reviews of the synthesis, characteristics, concepts, and applications of TiO_2 photocatalysts have been written by Linsebigler and others, as well as Chen and Mao.

Since the discovery of TiO_2's photocatalytic water-splitting, it has been used in a variety of additional applications, including soil, air, and water purification. TiO_2 can breakdown and mineralize a wide range of contaminants in the environment, including organic and inorganic pollutants, carbon dioxide, and simple inorganic anions. Furthermore, when exposed to UV radiation, a TiO_2-coated surface becomes hyper hydrophilic due to the development of meta-stable hydroxyl groups, resulting in the formation of a thin liquid layer with a narrow contact angle. This feature is reversible and is dependent on the quantity of light exposure. TiO_2's photo-induced self-cleaning characteristic has been widely exploited in a variety of applications.

Zinc oxide:

Emami-Karvani and Chehrazi both observed similar findings. In comparison to CuO and Fe_2O_3 NPs, Azam and colleagues (2012) discovered that ZnO has the strongest bactericidal activity against Gram-negative (*Escherichia coli* and *Pseudomonas aeruginosa*) and Gram-positive (*Staphylococcus aureus* and *Bacillus subtilis*) bacteria. Though the actual mechanism of ZnO's antibacterial activity is unknown, breakdown of the cell membrane caused by oxidative stress caused by ROS and accumulation of NPs on the bacterial cell surface caused by electrostatic forces are thought to be probable explanations. For photocatalytic applications, zinc oxide (ZnO) is frequently suggested as a substitute for TiO_2. It has band gap energy of 3.2 eV, which is similar to TiO_2, and as a result, photoactivation requires UVA light. Furthermore, it is one of five zinc compounds currently recognized as safe (GRAS) by the US Food and Drug Administration (21CFR182.8991). Due to its UV absorption efficiency and visible light transparency, ZnO NPs are widely employed in sunscreens, coatings, and paints. Furthermore, ZnO NPs have been found to have a stronger antibacterial effect on Gram-positive (*S. aureus*) bacteria than Gram-negative (*E. coli* and *P. aeruginosa*) bacteria, with the bactericidal activity increasing as particle size decreased.

ZnO treatment caused morphological alterations, membrane leakage, and a 52-fold increase in oxidative stress gene expression in *Campylobacter jejuni*, according to Xie and colleagues. A more extensive evaluation of the antibacterial activity and toxicity mechanisms of ZnO NPs was published by Sirelkhatim and colleagues. ZnO

was shown to be among the top total ROS generators, second only to TiO_2, in a study by Li and colleagues on seven distinct types of metal oxides (TiO_2, CeO_2, ZnO, CuO, SiO_2, Al_2O_3, and Fe_2O_3) and their propensity to create ROS for antibacterial activity.

Copper oxide:

Copper oxide (CuO) is a *p*-type semiconductor, which means its band structure has a higher concentration of holes than electrons. It possesses a 1.2 eV band gap, which makes it ideal for photocatalytic applications. Copper has been utilized in antibacterial applications for a long time. Although there is more agreement on CuO's antibacterial activity, which is attributed to the release of Cu^{2+} ions, the actual mechanism of action remains unknown. CuO was shown to be the most hazardous against *E. coli*, *B. subtilis*, and *S. aureus* in a study by Baek and An on the antibacterial activity of various NPs, followed by ZnO, NiO, and Sb_2O_3.

CuO has chemical and physical properties that are relatively stable, and it can be easily combined with polymers. CuO NPs have been studied for their antibacterial properties when embedded in a variety of polymer substrates. In comparison to Cu ion release killing ability against MRSA strains, NP contact-killing ability was shown to be weaker in their studies. It shows that, in addition to photocatalytic processes, a release of Cu ions into the nearby environment is required for maximum antibacterial activity of CuO.

4.5 Surface Coatings of Semiconductor Metal Oxide

Possibilities for application in the field of food safety entail:

Although semiconductor NPs' photocatalytic properties have been extensively used in a variety of applications, including optics, electronics, photovoltaics, solar cells, cosmetics, and environmental clean-up, their use in the food sector is relatively new, and most research in this area is still in its infancy. The application of semiconductor photocatalysis in the domains of food safety and quality has received a lot of attention in the recent decade.

Treatment of water and waste water:

Metal oxides' photocatalytic characteristics have long been used to provide clean water that is free of microbiological and chemical pollutants. Under solar/visible/UV light illuminations, composite materials such as Ag NP-incorporated and TiO_2-modified nylon 6, CuO/ZnO deposited glass membrane, and TiO_2-deposited polymers were investigated for their prospective applications in water treatment. In addition, unlike traditional chlorination treatments, innovative photocatalyst coated materials have the distinct advantage of preventing the generation of disinfection by-products. Several outstanding assessments of semiconductor photocatalysis for water

disinfection developments and potential implications are available. Organic contaminants such imazalil, thiabendazole, and acetamiprid detected in agro-food processing waste were found to be degraded by a biomass reactor immobilized with TiO_2. The influence of various factors on photocatalysis to digest pesticides and phenolic pollutants reported on the positive effects of TiO_2 photocatalysis on changing the physicochemical properties of wash waters from various fresh-cut vegetables and subsequent microbial reductions in the wash water. Another study used a COD-based model to estimate TiO_2 photocatalytic disinfection efficacy in the presence of produce and meat wash solutions. These researches indicate how semiconductor photocatalysis could be used to treat and recycle agro-food waste water.

Surface coatings for food contact and non-food contact:

To prevent microbial growth and multiplication, coatings containing metal or metal oxide NPs were developed for both food contact and non-food contact surfaces. TiO_2 coatings on stainless steel and glass substrates inhibited the growth and survival of plank tonic *E. coli* O157: H7 cells and *L. monocytogenes* biofilms, respectively. In addition, TiO_2-coated SS was discovered to inactivate a variety of viruses. On SS food contact surfaces, mechanical and photocatalytic disinfection capabilities of TiO_2, Ag-doped TiO_2, and/or Mo-doped TiO_2 coatings were tested for 3–5 months at numerous beer brewing businesses' canning and bottle-filling lines. *Escherichia coli* 0157: H7 was found to be reduced on food processing surfaces covered with copper cast alloys. The presence of organic matter in the form of meat residues, on the other hand, was discovered to be a limiting factor in achieving the requisite growth inhibition. Antiviral effects of TiO_2 thin film coatings on glass against influenza virus have been reported. At only 0.01 mW/cm^2 UVA intensity, they saw a reduction of roughly 4 log viral reductions. They also discovered that viral inactivation kinetics was linked to exposure time, UV intensity, and virus suspension concentrations of bovine serum albumin.

Metal oxides' photo-induced super-hydrophilic nature aids cleaning operations in the food sector. This characteristic is important for preventing bacterial adhesion when the surface qualities change. The nature of *E. coli* cell adhesion on carbon nanotube-filled polytetrafluoroethylene and TiO_2-coated SS surfaces, for example, was investigated under various fluid flow conditions. At various flow conditions, they observed a 60–80% reduction in bacterial adherence on these surfaces. They also discovered that these coatings might be used on the surface of a parallel-plate unit to limit the danger of cross-contamination between liquid food and biofilms, which can be a severe issue in ready-to-eat (RTE) food. In addition, introducing photocatalyst NPs like TiO_2, ZnO, Cu, and other metallic NPs into paints and lacquers has been shown to improve mechanical, rheological, self-cleaning, super-hydrophilic, and disinfection capabilities. These new paints and lacquers as coatings provide a great way to prevent bacterial multiplication and growth on non-food contact surfaces.

Metal oxides are used into food packaging materials in the following ways:

Metal oxides stand out among them because they provide stable antibacterial action (through the generation of ROS) without releasing the NP into the food matrix or the environment. Because of their improved functions, such as better mechanical strength, barrier, and antibacterial capabilities, food packaging films supplemented with nanomaterials such as chitosan, cellulose, metal ions (Ag, Cu, Au, and Pt), and metal oxides (TiO_2, ZnO, and MgO) are becoming more popular. During in vitro storage investigations involving cut lettuce, apples, tomatoes, and lemons, as well as fresh pears, TiO_2-incorporated polypropylene and/or polyethylene films were found to have photocatalytic antibacterial and antifungal effects. Due to the suppression of lactic acid bacteria and coli forms, short-ripened cheese placed in a composite (PE/PS/HDPE + $CaCO_3$ + TiO_2) food tray was shown to retain the desired cheese structure better. The quality characteristics of Chinese jujube packaged and stored in TiO_2-incorporated polyethylene film, as well as Chinese bayberries packaged in Ag-TiO_2 composite packaging with hot air treatment, were found to improve over time and control the growth of green mould and ethylene production, respectively.

Similarly, it was discovered that cut Fuji apples stored in a ZnO-incorporated packaging material retained more quality features including ascorbic acid, polyphenols, and had lower numbers of spoiling microbes. In another study, they had to use ZnO NPs to reduce the number of *L. monocytogenes*, *S. enteritidis*, and *E. coli* O157: H7 bacteria in suspension. When integrated in polystyrene, however, the same ZnO NPs showed no antibacterial action. To show considerable antibacterial activity, the NPs must either contact or penetrate bacterial cells, according to their findings (Tables 4.2 and 4.3).

Table 4.2 Metal oxide coatings are commonly developed using the following techniques

Method	Brief description	Reference
Sputter deposition	In a vacuum chamber an ionizing plasma sputters the target and the ionized atoms will be deposited on the substrate	Basnet and others
Atomic layer deposition	TiO_2 precursor solutions will be deposited on a substrate using a carrier gas at specific temperature and pressure conditions in a reactor	Visai and others
Chemical vapour deposition	A thin film of metal oxide will be formed on a heated substrate from a gaseous phase in a closed chamber	Visai and others
Sol–gel synthesis	A wet chemical method involving hydrolysis and condensation of metallo-organic alkoxide precursors to form a gel followed bydip/spin/spray coating or screen printing	Visai and others
Coating with binders	An organic/inorganic binder and a suitable solvent will be used to prepare a suspension of NPs for coating on a substrate	Yemmireddy and others
Melt-blending	Polymer pellets will be mixed with NPs and processed through a film extruder under controlled conditions	Threepopnatkul and others
Plasma-spraying	An electric arc is used that melts and sprays powdered materials into a solid surface	Ctibor and others
Anodic oxidation	An electrical field-driven metal and oxygen ion diffusion leads to formation of an oxide film at the anodic surface	Visai and others
Electrophoretic	Movement of charged particles in suspension in deposition the presence of an appropriate electric field result in formation result in formation of a coating on the charged substrate	Visai and others

Table 4.3 Examination of photocatalytic semiconducting materials using ISO and JIS standard test methods

ISO method	JIS method	Purpose
ISO 22197:2007	JIS R 1701: 2016	Test methods for air-purification performance of semiconductor photocatalytic material
ISO 27447:2009	JIS R 1702:2012	Test method for antibacterial activity of semiconducting photocatalytic materials
ISO 27448:2009	JIS R 1703-1:2014	Test method for self-cleaning performance semiconducting photocatalytic materials-measurement of water contact angle
ISO 10678:2010	JIS R 1703-2:2014	Determination of photocatalytic activity of surfaces in aqueous medium by degradation of methylene blue
ISO 10678:2010	JIS R 1703-2:2014	Determination of photocatalytic activity of surfaces in aqueous medium by degradation of methylene blue
ISO 10676:2010	JIS R 1704:2007	Test method for water purification performance of by forming ability of oxygen
ISO 10677:2011	JIS R1709:2007	Ultraviolet light source for testing semiconducting photocatalytic materials
ISO 14605:2013	JIS R 1750:2012	Light source for testing semiconducting photocatalytic materials used under indoor light environment
ISO 13125:2013	JIS R 1705:2008	Test method for antifungal activity of semiconducting photocatalytic materials
ISO 17094:2014	JIS R 1752:2013	Test method for antibacterial activity of semiconducting photocatalytic materials under indoor lighting environment
ISO 18071:2016	JIS R 1756:2013	Determination of antiviral activity of semiconducting photocatalytic materials under indoor light environment-test method using bacteriophage Q-beta

Bibliography

1. Adams, L.K., D.Y. Lyon, and P.J.J. Alvarez. 2006. Comparative eco-toxicity of nanoscale TiO_2, SiO_2, and ZnO *water suspensions*. *Water Research* 40 (19): 3527–3532.
2. Ahmed, S., M.G. Rasul, R. Brown, and M.A. Hashib. 2011. Influence of parameters on the heterogeneous photocatalytic degradation of pesticides and phenoliccontaminants in wastewater: A short review. *Journal of Environmental Management* 92: 311–330.
3. Appiagyei, A.B., J.O. Bonsu, and J.I. Han. 2021. Robust structural stability and performance-enhanced asymmetric supercapacitors based on $CuMoO_4/ZnMoO_4$ nanoflowers prepared via a simple and low-energy precipitation route. *Journal of Materials Science: Materials in Electronics* 32 (5): 6668–6681.
4. Arasi, S.E., R. Ranjithkumar, P. Devendran, M. Krishnakumar, and A. Arivarasan. 2020. Electrochemical evaluation of binary $Ni_2V_2O_7$ nanorods as pseudocapacitor electrode material. *Ceramics International* 46 (14): 22709–22717.
5. Arshadi Rastabi, S., R. Sarraf Mamoory, N. Blomquist, M. Phadatare, and H. Olin. 2020. Synthesis of a $NiMoO_4$/3D-rGO nanocomposite via starch medium precipitation method for supercapacitor performance. *Batteries* 6 (1): 5.

6. Basnet, P., G.K. Larsen, R.P. Jadeja, Y.C. Hung, and Y. Zhao. 2013. Alpha-Fe_2O_3 nanocolumns and nanorods fabricated by electron beam evaporation for visible light photocatalytic and antimicrobial applications. *ACS Applied Materials and Interface* 5 (6): 2085–2095.
7. Bekbolet, M., and C.V. Araz. 1996. Inactivation of Escherichia coli by photocatalytic oxidation. *Chemosphere* 32 (5): 959–965.
8. Bonetta, S., F. Motta, A. Strini, and E. Carraro. 2013. Photocatalytic bacterial inactivation by TiO_2-coated surfaces. *AMB Express* 3 (1): 59.
9. Bower, C.K., J. McGuire, and M.A. Daeschel. 1996. The adhesion and detachment of bacteria and spores on food-contact surfaces. *Trends in Food Science & Technology* 7 (5): 152–157.
10. Brody, A.L. 2006. Nano and food packaging technologies converge. *Food Technology* 60 (3): 92–94.
11. Caballero, L., K.A. Whitehead, N.S. Allen, and J. Verran. 2010. Photo inactivation ofEscherichia coli on acrylic paint formulations using fluorescent light. *Dyes Pigments* 86 (1): 56–60.
12. Balamuralitharan, B., S.N. Karthick, S.K. Balasingam, K.V. Hemalatha, S. Selvam, J.A. Raj, K. Prabakar, Y. Jun, and H.J. Kim. 2017. Hybrid reduced graphene oxide/manganese diselenide cubes: A new electrode material for supercapacitors. *Energy Technology* 5 (11): 1953–1962.
13. Balasubramaniam, S., A. Mohanty, S.K. Balasingam, S.J. Kim, and A. Ramadoss. 2020. Comprehensive insight into the mechanism, material selection and performance evaluation of supercapatteries. *Nano-Micro Letters* 12 (1): 1–46.
14. Saravanan, R., E. Sacari, F. Gracia, M.M. Khan, E. Mosquera, and V.K. Gupta. 2016. *Journal of Molecular Liquids.* 53 (1): 1–10.
15. Chaudhari, S., D. Bhattacharjya, and J.S. Yu. 2015. Facile synthesis of hexagonal $NiCo_2O_4$ nanoplates as high-performance anode material for Li-Ion batteries. *Bulletin of the Korean Chemical Society* 36 (9): 2330–2336.
16. Chen, Y., T. Liu, L. Zhang, and J. Yu. 2019. N-doped graphene framework supported nickel cobalt oxide as supercapacitor electrode with enhanced performance. *Applied Surface Science* 484: 135–143.
17. Das, A.K., N.H. Kim, S.H. Lee, Y. Sohn, and J.H. Lee. 2018. Facile synthesis of $CuCo_2O_4$ composite octahedrons for high performance supercapacitor application. *Composites Part B: Engineering* 150: 269–276.
18. De Moura, A.P., L.H. de Oliveira, I.L. Rosa, C.S. Xavier, P.N. Lisboa-Filho, M.S. Li, F.A. La Porta, E. Longo, and J.A. Varela. 2015. Structural, optical, and magnetic properties of $NiMoO_4$ nanorods prepared by microwave sintering. *The Scientific World Journal*.
19. De, B., T. Kuila, N.H. Kim, and J.H. Lee. 2017. Carbon dot stabilized copper sulphide nanoparticles decorated graphene oxide hydrogel for high performance asymmetric supercapacitor. *Carbon* 122: 247–257.
20. Dong, Y., S. Li, K. Zhao, C. Han, W. Chen, B. Wang, L. Wang, B. Xu, Q. Wei, L. Zhang, and X. Xu. 2015. Hierarchical zigzag $Na_{1.25}V_3O_8$ nanowires with topotactically encoded superior performance for sodium-ion battery cathodes. *Energy and Environmental Science*, *8*(4): 1267–1275.

Part III
Smart Material Finding Their Way in a New Class of Sensors

Chapter 5
New Class of Sensors: Smart Materials Finds Their Way

Various innovative optical fibres or wave guides have been extensively investigated in recent years for their ultra-high sensitivity and super continuous optical light source. A variety of photonic modulation and integrated all optical sensing devices have been developed, combining the unique properties of optical fibres, such as low transmission and antielectromagnetic interference, to provide a possible technical path for the integration of planar and fibre wave guides. Many intelligent and high-performance optical wave guide devices or fibre sensors have been developed as a result of the development of novel smart materials, nanoprocessing technologies, and optical spectra analysis techniques. Smart polymer, metal, metal oxides, and semiconductor material have been used to either fabricate the optical fibre sensor or as the sensitive material to effectively improve the sensitivity and selection performance. Microfibre, nanofibre, micro/nanostructure on fibre tip, multimode interference fibre structure, and in line optical fibre structure are some of the fibre structures that have been modified to achieve this enhancement.

All optical chips have been developed using optical fibre sensors coupled with microfluidic devices and planar photonic structures at the micro/nanoscale, resulting in high-speed acquisition, transmission, and processing of sensing signals. Optical fibres sensors will be a good choice for use in wearable or implantable devices because they are enclosed in flexible material. The creation of several outstanding integrated optical sensors has resulted from combining superior features of micro/nanofibre with innovative nanomaterials (high specific surface area and catalytic activity) employed in the sensors.

The adaptable design and precise control of optical micro/nanofibre and micro/nanostructure are critical components in the development of photonic devices and innovative sensors, often known as "labs on fibre." In the work Optical fibre integrated functional micro/nanostructure induced by two photon polymerizations; Dr. Liao et al. reviewed and addressed the research development in optical integrated micro/nanostructure induced by two photon polymerizations during the last 10 years.

The end face of the optical fibre has been fabricated by laser micro machining focussed ion—beam milling and nanoimprint technologies with combination of two

B. Karthikeyan et al., *Nano Metal Oxides*,
https://doi.org/10.1007/978-981-19-9444-9_5

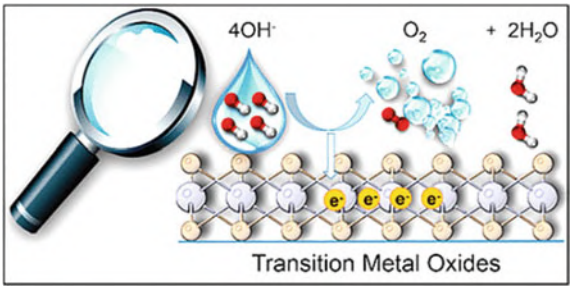

Fig. 5.1 Metal oxides reaction with water

photon polymerization technology, new processing material or methods, and new functional structure have been contributing to the development of new nanophotonic device such as "lab on fibre." For sensing, a variety of optical structures are built and used, relying on the effective interaction of information between the optical signal and the measured environment. On the one hand, this process can be completed by restricting the amount of gas or liquid in the optical fluid channel, such as in a photonic crystal fibre (Fig. 5.1).

On the other hand, the optical signal leaks to the exterior of the fibre, requiring alternative fibre structures composited by dislocation fusion, micro/nanoiberulite mode interference, end reflection, and other techniques to be measured. Traditional biochemical sensor detection is complicated, involving sample collection and long-term laboratory detection, making it challenging to perform quick detection in situ. The latest optical fibres sensors to determine the metal ion liquid based on innovative fluorescent materials such as organic dyes, protein, bacterial, and oligo deoxyribo nucleotide or conventional inorganic Quantum dots have been developed for metal ion detection based on fluorescent material. Carbon dots and semiconductors. This article focuses on semiconducting devices that use quasi-one-dimensional nanostructures like nanowires and nanobelts. Similarly, we limit ourselves to two device designs that are related: conductometric elements and field-effect transistors.

There are also a few concerns with real-world sensors and sensor arrays discussed. The evolution of gas sensors is similar to that of microelectronics in that the architecture of sensing elements is influenced by planar electronics design trends, and one of the field's major goals is to design nanosensors that can be easily integrated with modern electronic fabrication technologies. The proposed sensors offer a potential method for detecting metal ions in environmental water samples. More work is needed, however, on fibre structure design, sensing system reform, quantitative method reconstruction, and fluorescent materials immobilization.

Currently, the pricey super continuous laser source has a high power and is frequently made up of several broad spectrum light sources. It's exclusively utilized in space optical systems, and it's tough to integrate with optical wave guides or fibre optic systems. In his study on a chip broad band mid-infrared super continuum generation based on a highly non-linear chalcogenide glass wave guide, Prof. Zing Zang proposed on a chip mid-infrared super continuum generation with the ultra-wide spectral range 3–12 μm. The wave guide on chips has a similar structure to

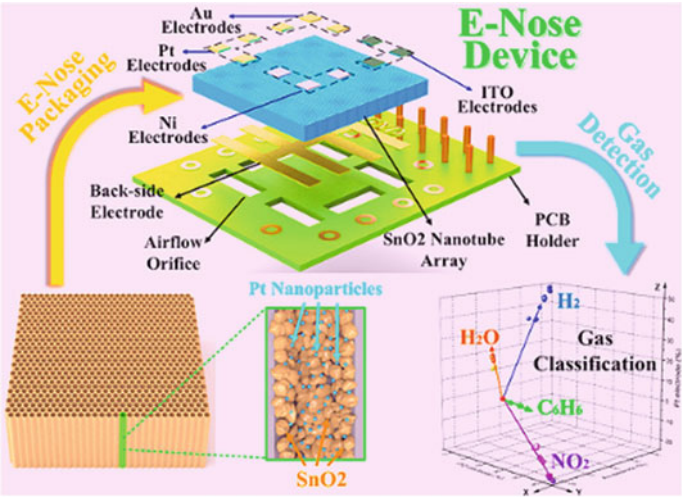

Fig. 5.2 Electronic nose made of nanowires

an optical fibre, with a fibre core and fibre cladding. By optimizing the non-linear coefficient and dispersion profile, the numerical model was developed and proved with dispersive wave generation. The fabrication method was also created with the goal of precisely controlling the dispersion property.

The current goal, for example, is to replace the large arrays of macroscopic individual gas sensors used for multicomponent analysis for many years, each with its own electrodes, filters, heating elements, and temperature detection, with an "electronic nose" encapsulated in a single device that integrates the sensing and signal processing functions in one chip (Fig. 5.2).

Pattern recognition, similar to odour identification by highly evolved creatures, is used to perform multicomponent gas analysis with these instruments. One can imagine a powerful device that can detect minute quantities (ultimately one molecule) of an explosive, biohazard, toxin, or environmentally sensitive substance against a complex and changing background, then signal an alert or take "intelligent" action by increasing the sensitivity, selectivity, number of sensing elements, and the power of the pattern recognition algorithms. However, despite the loss of active area and the greater proximity of surrounding individual sensing elements when individual components are downsized, this necessitates an increase in the sensitivity and selectivity of active sensor elements. Recent advances in materials science, as well as a slew of new sensing paradigms arising from nanoscience and technology, notably bottom-up fabrication, give reason to be confident that these objectives can be met.

Metal oxides have a diverse set of electrical, chemical, and physical properties that are frequently influenced by their chemical environment. Metal oxides have been extensively investigated as a result of these features, and most commercial sensors are based on correctly organized and doped oxides. Nonetheless, much new science is yet to be discovered, and novel production procedures based on nanoscience and

technology are still being investigated in this class of materials. Traditional sensor fabrication methods rely on the semiconducting, ionic conducting, photo conducting, piezoelectric, pyroelectric, and luminescence properties of metal oxide in the form of single crystals, thin and thick films, ceramics, and powders for a variety of detection and transduction principles. Chemical and biological sensors with nanostructured metal oxides, particularly metal oxide nanowires, benefit from a thorough understanding of their macroscopic counterparts' physical and chemical properties. This article focuses on semiconducting devices that use quasi-one-dimensional nanostructures like nanowires and nanobelts. Similarly, we limit ourselves to two device designs that are related: conductometric elements and field-effect transistors. There are also a few concerns with real-world sensors and sensor arrays discussed.

Using so-called bottom-up synthetic techniques, several quasi-one-dimensional oxide nanostructures with relevant characteristics, compositions, and morphologies have recently been produced. Top-down technologies could not have readily or affordably produced several of these structures. Figure 5.3 roughly summarizes a few kinds of these novel nanostructures with potential as sensing devices. Xia et al. and others have evaluated these advancements in oxide one-dimensional nanostructure production and characterization. Much research has also been done on the use of carbon nanotubes as sensors, either singly or in arrays. The enormous progress made to date in understanding the electrical properties of carbon nanotubes, their reactivity towards gases, photochemical properties, junction effects, and performance when designed as transistors undoubtedly informs the study of all quasi-one-dimensional systems. We owe a significant debt of gratitude to the literature for establishing and clarifying many of the key problems about quasi-one-dimensional nanostructures.

5.1 Semiconducting Metal Oxides

Bulk semiconducting oxides' characteristics have been extensively explored and reported. Those of quasi-one-dimensional oxide nanostructures (i.e. systems with diameters less than 100 nm), on the other hand, are likely to have unique properties for the following reasons.

A high surface-to-volume ratio indicates that a big percentage of the atoms (or molecules) in such systems are surface atoms capable of participating in surface processes. Over a wide temperature and doping range, the Debye length D (a measure of field penetration into the bulk) of most semiconducting oxide nanowires is comparable to their radius, causing their electronic characteristics to be highly impacted by processes near their surface. As a result, one might imagine instances where a nanowire's conductivity changes from completely nonconductive to highly conductive only according to the chemistry occurring at its surface.

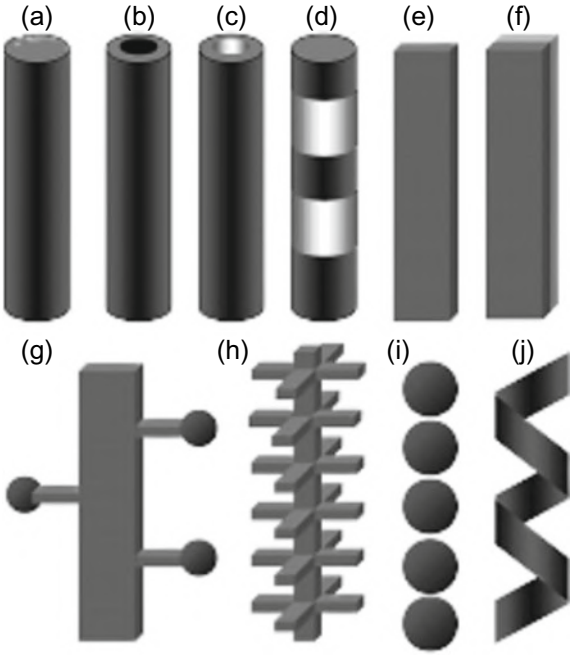

Fig. 5.3 A Schematic summary of the kinds of quasi-one-dimensional metal oxides nanostructure already reported **a** nanowire and nanorods; **b** core–shell structure with metallic inner core, semiconductor, or metal oxides; **c** nanotubules/nanopipes and hollow nanorods; **d** heterostructure; **e** nanobelts/nanoribbons; **f** nanotaps; **g** dendrites; **h** hierarchical nanostructures; **I** nanisphere assembly; **J** nanosprings

5.2 Sensors-Based Metal Oxides

Better sensitivity and selectivity may result as a result of this. Sensors based on individual metal oxides-based nanowires, for example, have been reported to have sensitivity up to 105 times higher than equivalent solid film devices. On a 3-m-long gadget, the signal-to-noise ratio implies that 103 molecules can be reliably detected. The adsorption of as little as 10 molecules may theoretically be detected by shortening the conductive channel length to 30 nm. When compared to electron-to-hole recombination periods (109–108 s), the average time it takes photo-excited carriers to diffuse from the interior of an oxide nanowire to its surface (1012–1010 s) is considerably reduced.

This means that on nanowires, surface photo induced redox reactions (Fig. 5.3) with quantum yields close to unity are common (assuming reactants reach the surfaces rapidly enough and interfacial charge transfer rates are not limiting). Another option is provided by the rapid diffusion of electrons and holes to the surface of a nanostructure. The adsorption-desorption kinetics, which are temperature dependent, determine the recovery and response times of conductometric sensors. Even at ambient temperature, the enhanced electron and hole diffusion rate to the surface of the nanorode allows the analyte to be rapidly photo-desorbed from the surface (a few seconds).

5.3 Metal Oxide Nanowires Semiconductors

Semiconducting oxide nanowires are typically better defined stoichiometrically and have a higher level of crystallinity than the multigranular oxides currently utilized in sensors, thereby lowering the instability associated with percolation or hopping conduction. Nanowires can be easily configured as field-effect transistors (FETs) and may interact with existing devices and production techniques (Fig. 5.4).

The position of the Fermi level within the band gap of the nanowire might be altered and thus utilized to adjust and control surface processes electronically when configured as a three-terminal FET. Finally, as the diameter of the nanowire is lowered or its material properties are modified in either a radial or axial direction. So the commencement of a more significant quantum effect can be expected (2).

The reversible interaction of the gas with the material's surface has been demonstrated by numerous researchers to be a feature of conductometric semiconducting metal oxide gas sensors. Many elements, both internal and external, can influence this response, including natural qualities of base materials, surface areas and microstructure of sensing layers, surface additives, temperature and humidity, and so on. Many studies regarding metal oxide gas sensors have been published in recent years. Sensitivity has been garnering increasing attention as one of the critical aspects of gas sensors, and great effort has been made to improve gas sensor sensitivity. There is currently no standard specification for gas sensor sensitivity. For reducing gases, sensitivity (S) is commonly expressed as Ra/Rg, and for oxidizing gases, as Rg/Ra, where Ra denotes the resistance of gas sensors in the reference gas (usually air) and Rg denotes the resistance in the reference gas including target gases. Ra and Rg have a strong link to the surface reaction(s) that are taking place. Although there are many reviews in this sector, we are unaware of any specific reviews on the elements that influence sensitivity. As a result, the focus of this study has been on a quick overview of the effect of surface reaction variables on sensitivity.

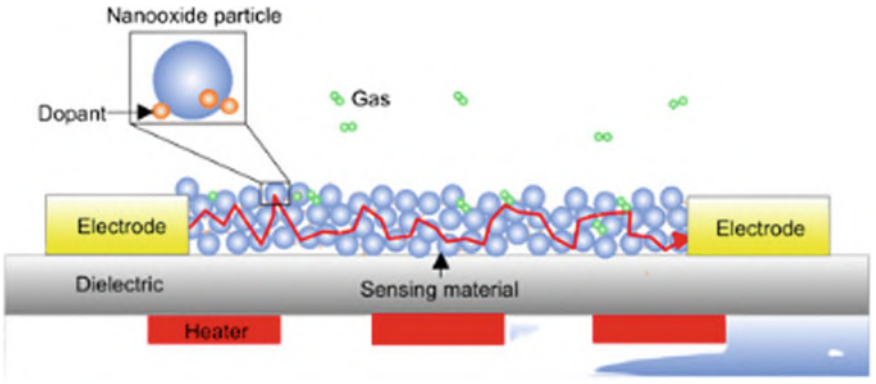

Fig. 5.4 An overview of some of the electrical, chemical, and optical processes that occur on metal oxides that can benefit from nanometer-scale size reduction

1. **Metal oxides for Gas Detection**:

Many metal oxides can be used to conduct measurements to identify flammable, reducing, or oxidizing gases. The conductivity of the following oxides shows a gas response: Cr_2O_3, Mn_2O_3, Co_3O_4, NiO, CuO, SrO, In_2O_3, WO_3, TiO_2, V_2O_3, Fe_2O_3, GeO_2, Nb_2O_5, MoO_3, Ta_2O_5, La_2O_3, CeO_2, Nd_2O_3. Cr_2O_3, Mn_2O_3, Co_3O_4, NiO, CuO, SrO, In_2O_3, WO_3, TiO_2, V_2O_3, Fe_2O_3, GeO_2, N. The electrical structure of metal oxides used in gas sensors can be established. Because metal oxides have such a diverse spectrum of electronic structures, they were separated into two categories:

Oxides of transition metals (Fe_2O_3, NiO, Cr_2O_3, etc.)

Non-transition metal oxides, which include (a) pre-transition metal oxides (Al_2O_3, for example) and (b) post-transition metal oxides (Al_2O_3, for example) (ZnO, SnO_2, etc.).

Because of their huge band gaps, pre-transition metal oxides (MgO, etc.) are considered to be rather inert. It is difficult to create electrons or holes. Due to the challenges in measuring electrical conductivity, they are rarely used as gas sensor materials. Because the energy difference between a cationic *dn* configuration and either a $dn + 1$ or $dn1$ configuration is often rather tiny, transition metal oxides act differently. They can take on many shapes in a variety of oxides. As a result, they are more environmentally sensitive than pre-transition metal oxides.

Structure instability and non-optimality of other critical parameters for conductometric gas sensors, on the other hand, limit their applicability. Only transition metal oxides with electrical configurations of $d0$ and $d10$ find real-world use as gas sensors. Binary transition metal oxides such as TiO_2, V_2O_5, and WO_3 have the $d0$ configuration. Post-transition metal oxides, such as ZnO and SnO_2, have the $d10$ configuration (Table 5.1).

2. **Mechanism of detection**:

Given the many influences on metal oxide gas sensing capabilities, the sensing mechanism of a metal oxide gas sensor must be revealed. The exact underlying mechanisms that create a gas reaction are still debated; however a change in conductivity is caused by electron trapping at adsorbed molecules and band bending induced by these charged molecules. In comparison to a flat band condition, the negative charge trapped in these oxygen species induces upward band bending and hence lower conductivity. When O_2 molecules are adsorbed on the surface of metal oxides, as shown in Fig. 5.5, they take electrons from the conduction band Ec and trap them as ions at the surface. The band bending is reduced and can be reversed by reacting these oxygen species with reducing gases or by competitive adsorption and replacement of the adsorbed oxygen by other molecules, resulting in enhanced conductivity.

At operating temperatures of 300–450 °C, O is thought to be dominant. Most metal oxide gas sensors work at this temperature. Figure 5.5 depicts the structure and band model of the conductive mechanism after exposure to a reference gas containing or

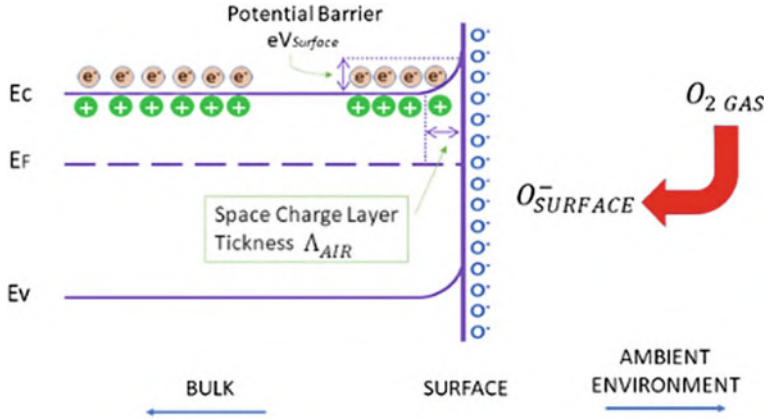

Fig. 5.5 Band bending after charged species chemisorption is depicted in this diagram (here the ion sorption of oxygen)

Table 5.1 Metal oxides and applications of various field

ZrO_2—mixed metal oxide nanoparticles	Synthetic method	Application	Inference
ZrO_2/ZnO	Sol–gel	Optical uses	Bashir et al.
Al_2O_3/ZrO_2	Sol–gel	Catalytic uses	Angel et al.
ZrO_2/CeO_2	Sol–gel Co-precipitation	Photocatalytic uses	Rossignov et al.
CeO_2/ZrO_2	Sol–gel	Catalytic uses	Thammachart et al.
ZrO_2/CeO_2	Co-precipitation	Thermal application	Arcent'ev et al.
MgO/ZrO_2	Co-precipitation	Antibacterial uses	Kumar et al.
$CeO_2/Sc_2O_3/ZrO_2$	Co-precipitation	Fuel cells	Liu et al.
ZrO_2/graphene oxide	Wet chemical method	Electrochemical agent	Mudila et al.

excluding CO. CO is oxidized by O^- and released electrons to the bulk materials when gas sensors are exposed to the reference gas with CO. The thickness of the space-charge layer reduces as the number of surface O^- decreases.

The energy of the conduction band, valence band, and Fermi level are denoted by the letters EC, EV, and EF, respectively, whereas Air signifies the thickness of the space-charge layer and surface denotes the potential barrier. The donor sites are denoted by +, and the conducting electrons are represented by e^-.

The Schottky barrier between two grains is then decreased, allowing electrons to easily conduct between sensing layers via different grains. Figure 5.4 mechanism, on the other hand, is only applicable to *n*-type semiconducting metal oxides with depletion zones smaller than grain size (Fig. 5.6).

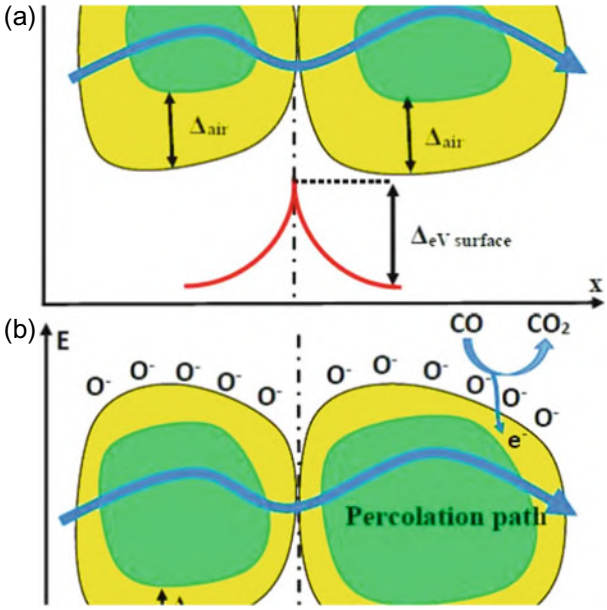

Fig. 5.6 Conductive mechanism structural and band models after exposure to reference gas. **a** With or **b** without carbon monoxide

5.4 Factors That Influence Sensitivity

5.4.1 Chemical Composition

At high temperatures, semiconducting metal oxides have been widely studied for the detection of simple gases. For gas sensor applications, there are numerous material properties to consider, such as adsorption ability, catalytic activity, sensitivity, thermodynamic stability, and so on. Although many different metal oxide materials appear to be beneficial in some of these qualities, only a few are adequate for all needs. In the light of this, recent research has focussed on composite materials such as SnO_2-ZnO, Fe_2O_3-ZnO, ZnO-CuO, and others. Aside from binary oxides, there are numerous ternary, quaternary, and complex metal oxides that are relevant to the uses stated. The interaction of metal oxides with other components, such as organic and carbon nanotubes, has also been extensively studied. To demonstrate the impact of chemical composition, we use composite metal oxides as an example.

When evaluated under identical experimental settings, the composite ZnO-SnO_2 sensors had much better sensitivity than sensors made entirely of tin dioxide or zinc oxide. Sensors based on the two components mixed together are more sensitive than sensors based on the two components separately, implying that the two components have a synergistic impact. The synergistic effect's exact mechanism is uncertain, however de Lacy Costello and colleagues have proposed one possibility.

They propose that butanol is more successfully dehydrogenated to butanal by tin dioxide, but that tin dioxide is rather unsuccessful in the catalytic breakdown of butanal, using SnO_2-ZnO binary oxides as an example.

Zinc oxide, on the other hand, catalyses the decomposition of butanal quite effectively. Butanol would be successfully dehydrogenated and then butanal would be catalysed by a combination of the two components. The catalysis results achieved when the composite was used back up this theory. This theory implies that not all components perform better than the sum of their parts. The performance of gas sensors will be improved only when the catalytic actions of the components complement each other. When compared to single oxide sensors, composites of tin dioxide/zinc oxide and tin dioxide/indium oxide have higher sensitivity, as demonstrated in Fig. 5.7. When compared directly to identical single oxide sensors, composite sensors made up of mixes of zinc oxide and indium oxide exhibit a loss in sensitivity.

Metal oxides are becoming more popular as active materials in applications like sensors. Recent advancements in the preparation of metal oxide materials open up new possibilities for their integration into devices with new capabilities, such as wearable/flexible devices, smart textiles for everyday well-being and health monitoring, or innovative sensing architectures like work function, surface ionization, magnetic, self-heating, and Schottky-based devices. The author's perspective on advancements and challenges in the field of metal oxide nanowire chemical sensors is presented in this article. Metal oxides will be used in composite gas sensors.

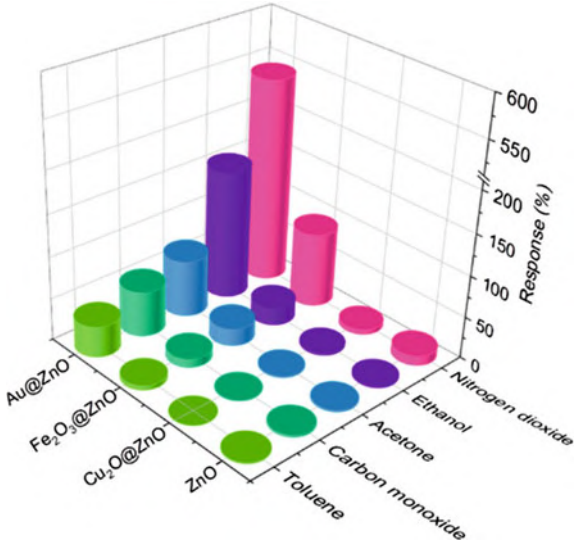

Fig. 5.7 The response of single oxide and composite sensors to 5 ppm ethanol vapours at 100% RH

Bibliography

1. Li, Jin, Duk-Yong Choi, and Mateusz Smietana (eds.). 2021. *Novel Smart Material for Optical Fiber Sensor Development*. https://doi.org/10.3389/fmats.2021.671086.
2. Kolmakov, Andrei, and Martin Moskovits. 2004. Chemical sensing and catalysis by one-dimentional metal-oxide nanostructures. *Annual Review of Material 34*: 151–180.
3. Wang, Chengxiang, Longwei Yin, Luyuan Zhang, Dong Xiang, and Rui Gao. 2010. *Metal Oxide Gas Sensors: Sensitivity and Influencing Factors, Sensors 10*.
4. Lu, X.F., X.Y. Chen, W. Zhou, Y.X. Tong, and G.R. Li. 2015. α-Fe_2O_3@PANI core–shell nanowire arrays as negative electrodes for asymmetric supercapacitors. *ACS Applied Materials and Interfaces* 7 (27): 14843–14850.
5. Machale, A.R., S.A. Phaltane, H.D. Shelke, and L.D. Kadam. 2021. Facile hydrothermal synthesis of Cu_2SnS_3 nanoparticles for photocatalytic dye degredation of mythelene blue. *Materials Today: Proceedings* 43: 2768–2773.
6. Mani, S., V. Vediyappan, S.M. Chen, R. Madhu, V. Pitchaimani, J.Y. Chang, and S.B. Liu. 2016. Hydrothermal synthesis of $NiWO_4$ crystals for high performance non-enzymatic glucose biosensors. *Scientific Reports* 6 (1): 1–8.
7. Mohamed, S.G., I. Hussain, M.S. Sayed, and J.J. Shim. 2020. One-step development of octahedron-like $CuCo_2O_4$@Carbon fibers for high-performance supercapacitors electrodes. *Journal of Alloys and Compounds* 842: 155639.
8. Naderi, H.R., M.R. Ganjali, and A.S. Dezfuli. 2018. High-performance supercapacitor based on reduced graphene oxide decorated with europium oxide nanoparticles. *Journal of Materials Science: Materials in Electronics* 29 (4): 3035–3044.
9. Oh, S.W., Z.D. Huang, B. Zhang, Y. Yu, Y.B. He, and J.K. Kim. 2012. Low temperature synthesis of graphene-wrapped $LiFePO_4$ nanorod cathodes by the polyol method. *Journal of Materials Chemistry* 22 (33): 17215–17221.
10. Palani, S., M. Venkatachalam, R. Palanisamy, U.S. Veerasamy, and K. Kuppusamy. 2021. High performance electrochemical investigations of SnS_2 hierarchichal nanostructures via surfactant-free solvothermal method. *Materials Today: Proceedings* 47: 47–51.
11. Petcharoen, K., and A. Sirivat. 2012. Synthesis and characterization of magnetite nanoparticles via the chemical co-precipitation method. *Materials Science and Engineering: B* 177 (5): 421–427.
12. Kong, L., et al. 2017. Macroscopic bioinspired graphene sponge modified with *in-situ* grown carbon nanowires and its electromagnetic properties. *Carbon* 111: 94–102.
13. Qian, H.S., et al. 2006. Synthesis of uniform Te @carbon-rich composite nano cables with photoluminescence properties and carbonaceous nano fibers by the hydrothermal carbonization of glucose. *Chemistry of Materials* 18: 2102–2108.
14. Caruso, F. 2001. Nano engineering of particle surfaces. *Advanced Materials* 13: 11–22.
15. Iijima, S. 1991. Helical microtubules of graphitic carbon. *Nature* 354: 56–58.
16. Guo, Y.G., J.S. Hu, H.P. Liang, L.J. Wan, and C.L. Bai. 2005. TiO2-based composite nanotubes arrays prepared via layer-by-layer assembly. *Advanced Functional Materials* 15: 196–202.
17. Lou, X.W., L.A. Archer, and Z.C. Yang. 2008. Hollow micro-/nanostructures: Synthesis and applications. *Advanced Materials* 20: 3987–4019.
18. Nie, K.Y., et al. 2017. Extreme absorption enhancement in Zn Te:O/ZnO intermediate band core-shell nanowires by interplay of dielectric resonance and plasmonic bowtie nano antennas. *Science and Reports* 7: 7503.
19. Li, C., et al. 2013. Zno electron field emitters on three-dimensional patterned carbon nano tube framework. *ACS Applied Materials & Interfaces* 5: 9194–9198.
20. Saito, N., et al. 2002. Low-temperature fabrication of light-emitting zinc oxide micropatterns using self-assembled monolayers. *Advanced Materials* 14: 418–421.
21. Pan, Z.W., Z.R. Dai, and Z.L. Wang. 2001. Nano belts of semiconducting oxides. *Science* 291: 1947–1949.
22. Pan, Z., et al. 2009. Zinc oxide microtowers by vapor phase homoepitaxial regrowth. *Advanced Materials* 21: 890–896.

23. Chu, S., et al. 2011. Electrically pumped waveguide lasing from ZnO nanowires. *Nature Nanotechnology* 6: 506–510.
24. Yang, J.C., et al. 2015. GaN-Based LEDs with Al-doped ZnO transparent conductive layer grown by metal organic chemical vapor deposition: Ultralow forward voltage and highly uniformity. *IEEE Electron Device Letters* 36: 372–374.
25. Huang, H., et al. 2001. Catalytic growth of zinc oxide nanowires by vapor transport. *Advanced Materials* 13: 113–116.

Chapter 6
Biological Interactions of Metal Oxides—An Insight

Metal oxide (MO)-based bioinorganic structures such as ZnO, TiO_2, SiO_2, and GeO_2 have significantly increased. Besides traditional approaches, the synthesis, shaping, structural patterning, and post-processing chemical functionalization of the surface of the material are inspired by strategies that mimic processes in nature. This is particularly of concern to bridge between technologies in vitro and biotechnologies in vivo. Further, besides the potential practical technological efficiency and advantages such materials might exhibit, we have to consider the wider long-term implications of material stability and toxicity. This chapter is to present a critical review of recent advances in the chemistry and engineering of MO-based biocomposites, highlighting the role of interactions at the interface and the techniques by which these can be studied. The challenges hamper progress in research and extrapolate to developing and promising directions including additive manufacturing and synthetic biology that could benefit from a molecular-level understanding of interactions (Fig. 6.1).

6.1 Introduction

Nanometal oxide or nanoceramics play a vital role in not only electronic or photo semiconductors but recently so many reviews and research articles are come out on the different uses of metal oxides. The band gap energy of the metal oxides shows the electronic use whereas the nanosize and cytotoxicity play the therapeutic applications. In this chapter, it is summarized the new insights of the interaction cytotoxicity and biointerface is explained in different subheadings. ZnO nanomaterial results are explained and finally, the various metal oxides are given with the new results in the context of nanometal oxide biological interactions.

Synthesis an Example

Literature reported many methods to synthesis nanometal oxide to put it in a nutshell here copper oxide nanoparticles have taken as example the synthetic methods are

B. Karthikeyan et al., *Nano Metal Oxides*,
https://doi.org/10.1007/978-981-19-9444-9_6

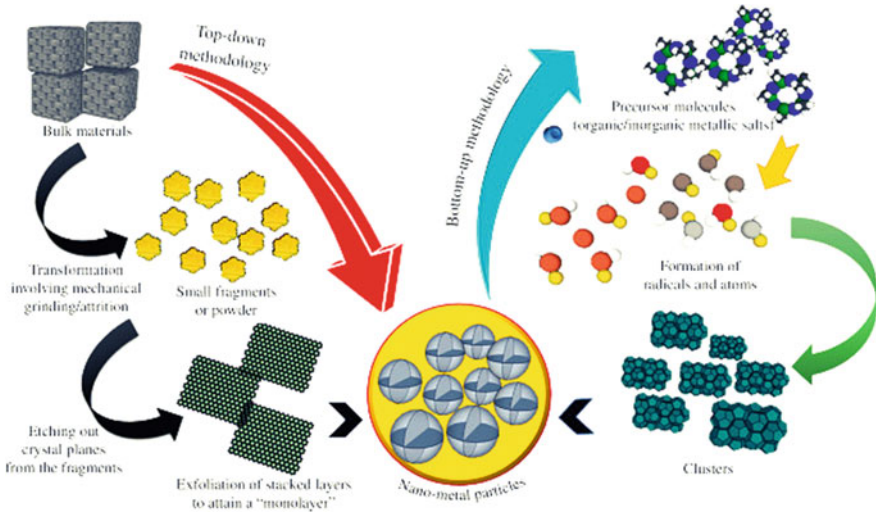

Fig. 6.1 Applications of nanometal oxides

given in Fig. 6.2. In the selected schemes mediated synthesis is widely discussed in the context of its biomedical applications and here as this chapter aims for the biological interactions of the metal oxides with the biological structures. Its cytotoxicity and its various applications will be discussed in detail (Fig. 6.3).

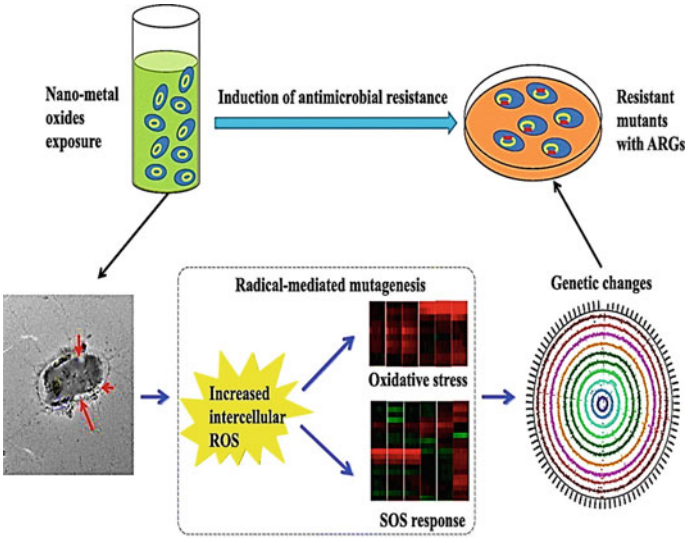

Fig. 6.2 Nanometal oxide biological interactions

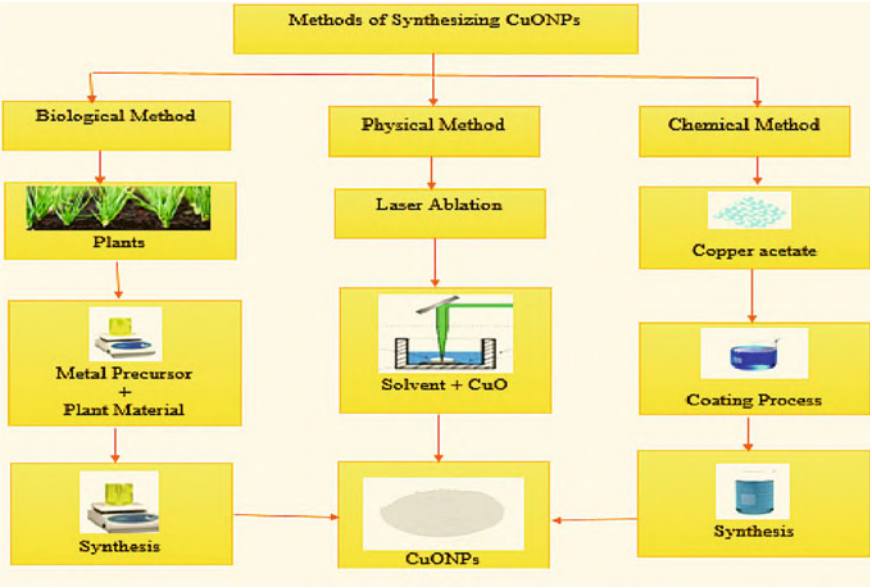

Fig. 6.3 Methods of synthesis of CuONPs

The biological approach of nanoparticles synthesis encompasses the utilization of organisms (bacteria yeast and fungi) and extract from various parts of the plant as reducing agents of the metal ions. The biosynthesis of CuONPs using the following bacteria *Phormidium cyanobacterium*, *Morganella morganii*, *Serratia* sp., and *Escherichia coli* had been reported. Despite the eco-friendly advantage of synthesizing nanoparticles from microorganisms, the following are their limitations; toxicity of some bacterial, difficulties in isolation, and incubation process. Nevertheless, plants remain the only ideal potential for metal and metal oxide nanoparticles; this plausibility is attributed to rapid reaction rate with low energy, the occurrence of several biomolecules, cost-effectiveness, good stability, absence of hazardous chemicals, safe and easy operation procedures [8]. Biomolecules found in plant extracts function as both reducing and stabilizing agents during the synthesis of CuONPs and other metal nanoparticles. Biomolecules such as flavonoids, proteins, tannins, phenols, and terpenoids have been reported as good reducing and stabilizing agents for CuONPs synthesis. Examples of plants that have been used for the synthesis of CuONPs are listed in the same report.

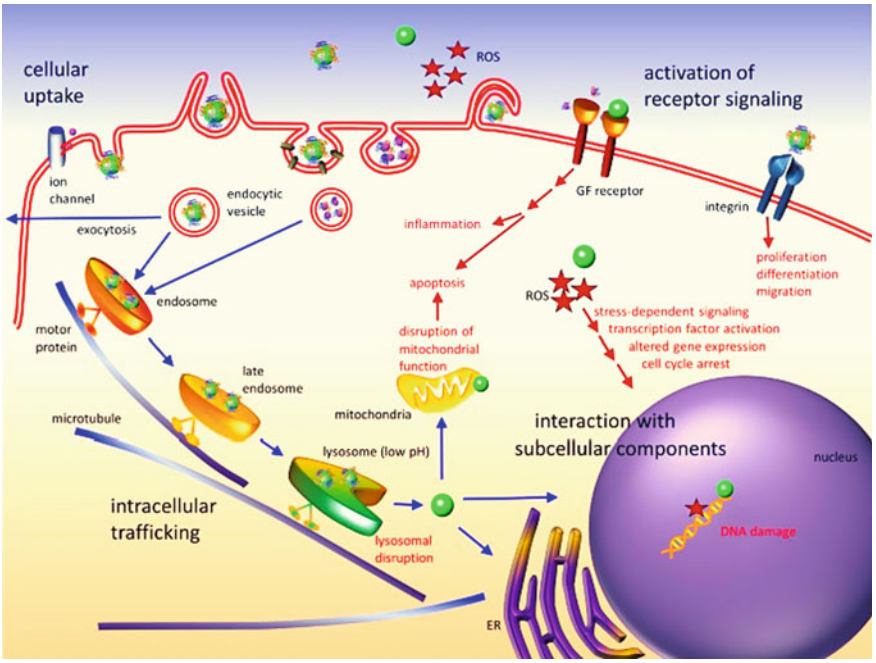

Fig. 6.4 Interaction of metal oxides with the cell membrane

6.2 Mechanism of Interaction

The interaction of metal oxides with the cell membrane is discussed in detail recently oxidative stress is the actual mechanism of the interruption. Damage to the cell membrane by electrostatic interaction is discussed (Figs. 6.4, 6.5 and 6.6).

6.3 TiO_2 Metal Oxide Nanoparticles Well Studied

In the past decade, there has been a rapid growth in publications regarding the safety of TiO_2. TiO_2 particles were originally considered to possess low toxicity, but this general consensus was contested after lung tumours were discovered in rats exposed for two years to high concentrations of fine TiO_2 particles. This revelation caused The International Agency for Research on Cancer to swiftly class TiO_2 as a Group 2B carcinogen (possibly carcinogenic to humans); however, this move has since been questioned as it emerged that the observed tumorigenic effect may have been attributed to lung overload instead of the specific carcinogenicity of fine TiO_2. Further studies have shown that NPs of TiO_2 possess physiochemical properties that affect

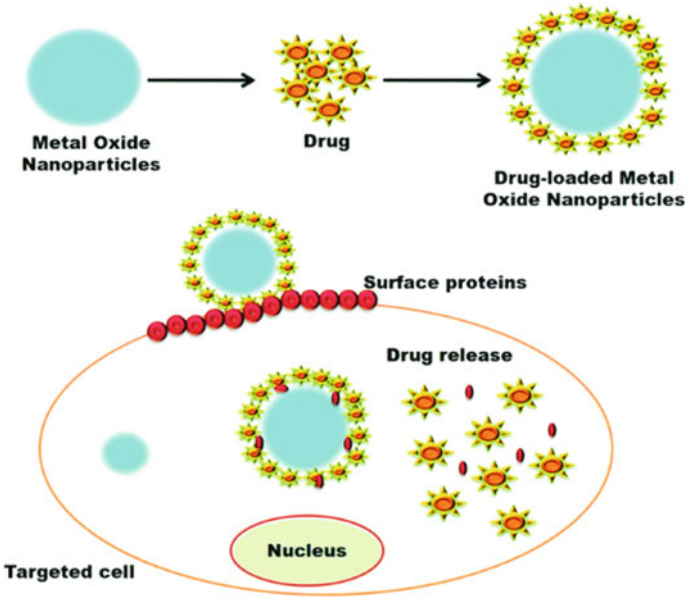

Fig. 6.5 Interaction of metal oxides nanoparticles with the cell membrane

their biological behaviour, and thus potentially these nanoscopic particles offer a greater safety concern compared to larger particles.

Since interest in this material has grown significantly over recent years, the research community has begun to realize what was once regarded as a benign material with low toxicity may not be the case with many credible sources of information highlighting potential toxicity. Today, articles connected with the safety of TiO_2 particles are frequently published, as many research groups explore this important topic. The exposure to TiO_2 NPs can be in the form of aerosols, suspensions, or emulsions. To exert toxicity, titania must be able to enter the organism, via inhalation or ingestion. Once in the organism, it has been shown how NPs can migrate and accumulate in other organs, although these studies were carried out on mice and rat models and at concentrations much higher than those encountered in the workplace or daily life. As nanosized TiO_2 is thought to exert greater toxicity due to the increased surface area, the presence of biomolecules on the TiO_2 surface will increase particle size and potentially reduce toxicity. The use of thin films of good mechanical quality should highly reduce the risk of exposure. Though there is no definitive answer on the topic of the long-term safety of particles at this time, future research into this area may ultimately provide answers to this question. The toxicity of TiO_2 nanoparticles has the potential to be harnessed for the good by the photo induced toxicity of TiO_2 being exploited for medical and clinical purposes.

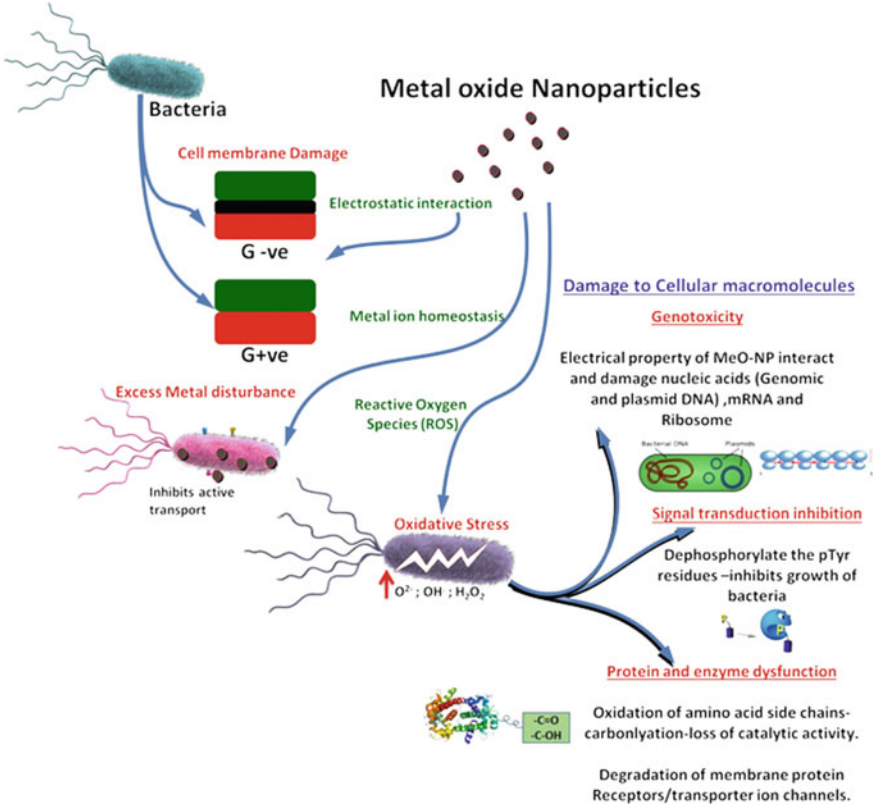

Fig. 6.6 Metal oxide nanoparticles with Bactria's

6.4 Sensing Studies Through Interaction

While DNA/graphene oxide (GO) conjugates have been widely used for DNA detection, they suffer from non-specific DNA displacement by proteins, making their application in biological samples difficult. To find new materials tightly adsorbing DNA but not proteins, we screened seven metal oxide nanoparticles, all interacting with the phosphate backbone of DNA; while DNA uses its nucleobases to interact with GO. In this regard, DNA is a Janus polymer orthogonally adsorbing GO and metal oxides. The DNA adsorption affinity ranks CoO > NiO > Cr_2O_3 > Fe_2O_3 > Fe_3O_4 > TiO_2 > CeO_2 based on a phosphate displacement assay. Among them, CoO is nearly fully resistant to protein displacement, while NiO has the best limit of detection of 0.24 nM DNA. This study provides fundamental insights into the biointerface chemistry of DNA and reveals new materials useful for bioanalytical chemistry, DNA separation, and DNA-directed assembly.

6.5 Mixed Metal Oxide Nanoparticles Cell Interaction

Understanding the mechanisms involved in the interaction of metal oxide nanoparticles with mammalian cells is required for any safe practical application. Presently, we lack knowledge about the general mechanism by which these nanoparticles bind and interact with eukaryotic cells. Similar to antibacterial activity, the cytotoxicity of metal oxide nanoparticles is also dependent on their physicochemical characteristics. Metal oxide nanoparticles of similar size but of different compositions usually show varying cytotoxic effects. For instance, when toxicities of CuO, TiO_2, ZnO, $CuZnFe_2O_4$, Fe_3O_4, and Fe_2O_3 were compared in vitro using human alveolar epithelial cells A549, CuO was shown to induce a high percentage of cell death together with DNA damage, while TiO_2 could only trigger DNA damage. Interestingly, pure Fe_3O_4 and Fe_2O_3 were almost harmless while mixed $CuZnFe_2O_4$ nanoparticles strongly damaged DNA. Such results strongly suggest that metal oxide nanoparticles of different compositions interact with living cells through different mechanisms—some of which are schematically presented in Fig. 6.4. Lai et al. have shown that ZnO nanoparticles are the most, TiO_2 nanoparticles the second most, and MgO nanoparticles the least effective in induction of human cell death. A study of 19 different metal oxide nanoparticles suggested that the most important factor that determines their toxicity is the inherent toxicity of the metal ions released.

Another recent study of 11 types of metal oxide nanoparticles of similar sizes (< 20 nm diameter) suggested that differences in their Stankic et al. J Nanobiotechnol (2016) 14:73 Page 14 of 20 toxicities might be explained by two principal aspects: release of metal ions, which is observed as the main mechanism for ZnO and CuO, and induction of ROS generation, observed for Mn_3O_4 and Co_3O_4. Interestingly, all nanoparticles tested in this study were shown to be internalized by A549 cells. This suggests that ROS formation and metal-ion release may be triggered from internalized nanoparticles within cells. Presently, the surface coating of metal oxide nanoparticles is employed to modify their toxicity. Nevertheless, the same coating may enhance or reduce the toxic effects depending on their initial surface properties. This was shown for different crystals of nano-ZnO stabilized with trichloro-dodecyl silane. Probably, the final toxicity reflects physicochemical modifications obtained upon coatings such as changes in particle aggregation state, dissolution, zeta potential, and ion and free radical releasing to a solution. Thus, the primary determinant of particle toxicity seems to be its starting surface property and not the coating. Furthermore, the same nanomaterial may show different reactivity, and consequently, toxicity in different media. For instance, the toxicity of nano-ZnO comes partially from the released Zn^{2+}-ions into aqueous biological media. It was shown that its toxicity can be lowered using a medium containing phosphate ions. Indeed, the formation of Zn-phosphate inactivates the hazardous Zn^{2+}-ions.

Similarly a metal-ion chelator diethylene triamine pentaacetic acid can be used to decrease the toxicity of metal oxide nanoparticles. Although mild detergents used to prevent nanoparticle aggregation are supposed to be interactive, they may additionally alter the toxicity of a given nanoparticle. Finally, the toxicity can also be

reduced by doping metal oxide nanoparticles with other metal ions. For instance, nano-ZnO released toxic Zn^{2+}-ions and generated ROS causing mitochondria perturbations, cell inflammation and induced cytotoxicity in treated lungs and embryos. All these pro-oxidative and pro-inflammatory effects were reduced by iron doping of nano-ZnO. A uniform distribution of Fe atoms throughout the ZnO crystal structure enhanced the crystal stability in an aqueous solution and reduced the dissolution of doped nanoparticles in biological media. Nano-ZnO was more effective in inducing cellular death than nano-MgO but, surprisingly, mixed nano-ZnMgO nanoparticles, containing less than 5% of zinc were inoffensive to mammalian cells, thus, behaving safely as a pure nano-MgO. Penetration of metal oxide nanoparticles in eukaryotic cells may be prevented by particles binding to specific nalized nanoparticles that are degraded in cellular endosomes or liposomes and then metabolized. Consequently, such metal oxide nanoparticles are considered safe as they neither affect cell viability nor induce apoptosis.

The specific features of nanoparticle interaction with cells depend on the surface energy of the particles, which may be modulated by synthesis procedure or functionalization of their surfaces. The practical application of metal oxide nanoparticles as bactericidal agents is, thus, possible at certain conditions and particle concentrations at which there is low or no toxicity against mammalian cells, as demonstrated for ZnO, Fe_2O_3, or Ag_2O_3. The application of metal oxide nanoparticles as new antibacterial agents strikingly depends on their cytotoxic nature. Meanwhile, it is important to mark that many studies dealing with cytotoxicity of metal oxide nanoparticles are being done with nanoparticles of not well characterized physicochemical properties. Also, the standardized testing procedure for toxicity assessment of nanoparticles is lacking. This implies that our understanding of cytotoxic mechanisms is incomplete and non-uniform. Taking into account that metal oxide nanoparticles are a class of nanomaterials with the highest global annual production, we expect that progress in addressing their cytotoxicity will be made rapidly.

6.6 Applications

In biomedical applications, anatase was shown to be a better osteoconductive polymorph than rutile and brookite. It was recently reported that a layer of 3D rutile nanorods on titanium improves osseointegration and bone formation capacity. Anatase NPs produced from the TiBALDH precursor and using the patented "Captigel" method have been used to support the growth of beneficial rhizobacteria in the colonization of the roots of oilseed rape. The charges on the nanoparticles allow the formation of inner-sphere complexes with phospholipids, thus titania NPs were able to assist bacterial growth via the formation of clusters (Fig. 6.6), resulting in increased bacteria adhesion at the plant root and associated protection against fungal pathogens. Anatase TiO_2 surface selectivity for laevo-serine (L-Ser) has been investigated in detail by the DFTB-D method to design bacteria-friendly anodes for unmediated benthic microbial fuel cells (MFCs), Fig. 6.8. This paper is interesting in

that it uses a theoretical approach to characterize the energetic aspects of adsorption to support the design of an anode with a specific application.

In a highly cited paper with implications for the development of advanced tissue engineering, arginine−glycine−aspartic acid peptide (RGD) was immobilized via simple physical adsorption to TiO_2 nanodot films to produce an efficient light-induced cell detachment method for cell harvesting, Fig. 6.7. We conclude this section with some examples of advanced functional materials prepared by a biomimetic approach. Figure 6.8 shows how the templating effect of self-assembling diphenylalanine in combination with atomic layer deposition can form highly entangled hollow TiO_2 nanoribbons with potential applications in photochemistry and optoelectronics. An interesting cyto compatible process for cell surface deposition of anatase thin films on chlorella cells was achieved using the peptide sequence (RKK) 4D8 and TiBALDH. This process retains cell viability and metabolic activity and increased their tolerance to thermal stress. Finally, we mention the biomimetic layer-by-layer (BioLBL) approach developed by Sano and colleagues. This research is important as it shows a successful example of how a biomimetic approach can assist in overcoming technological issues in traditional methods, in this specific case, interlayer diffusion in heterogeneous structure obtained by layer-by-layer deposition. BioLBL uses engineered ferritin nanoparticles decorated with sequence RKLPDA (TBP) as building blocks. TBP was identified as both a good binder and able to mediate the mineralization of materials including titania, silica, and silver (Fig. 6.9).

As a guide, is a summary evaluation of key techniques that have been used to study interactions of biomolecules with ZnO, TiO_2, SiO_2, and GeO_2, where a description of the principle of the method, information that can be obtained, and factors to consider when using the techniques are given alongside examples of studies that have used the techniques. As these techniques have different fundamental principles and measurement modes, they will therefore have different advantages and disadvantages associated with their use. A thorough evaluation is required to identify the appropriate areas of application of these techniques depending on the MO.

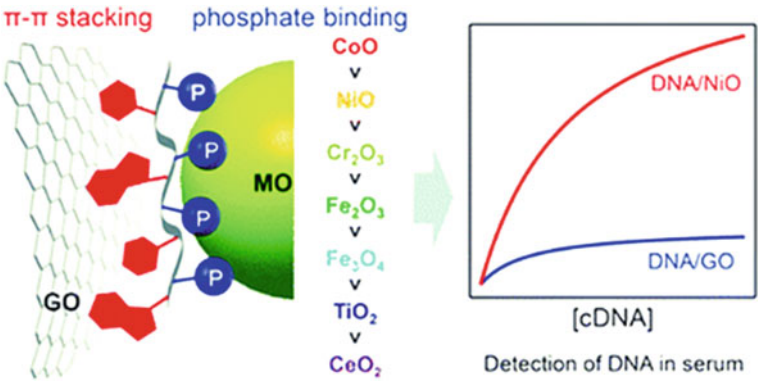

Fig. 6.7 Nanoparticle interaction with cells

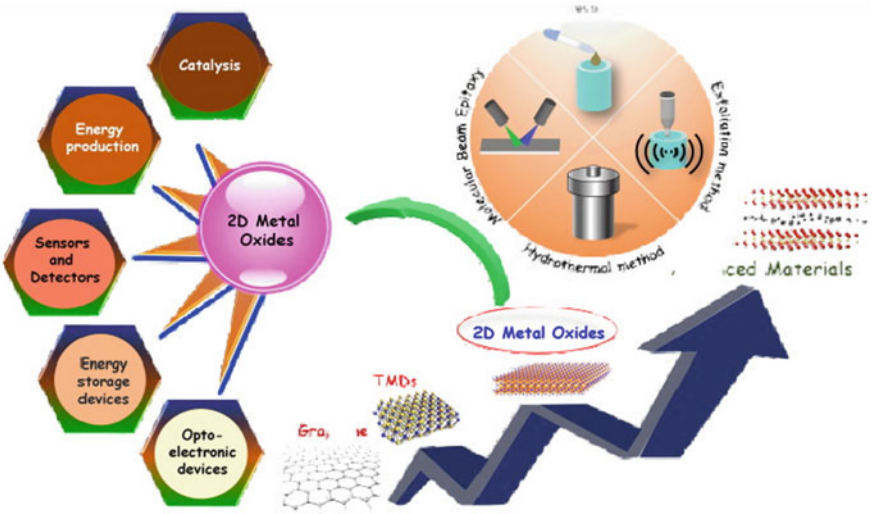

Fig. 6.8 Applications of nanomaterials

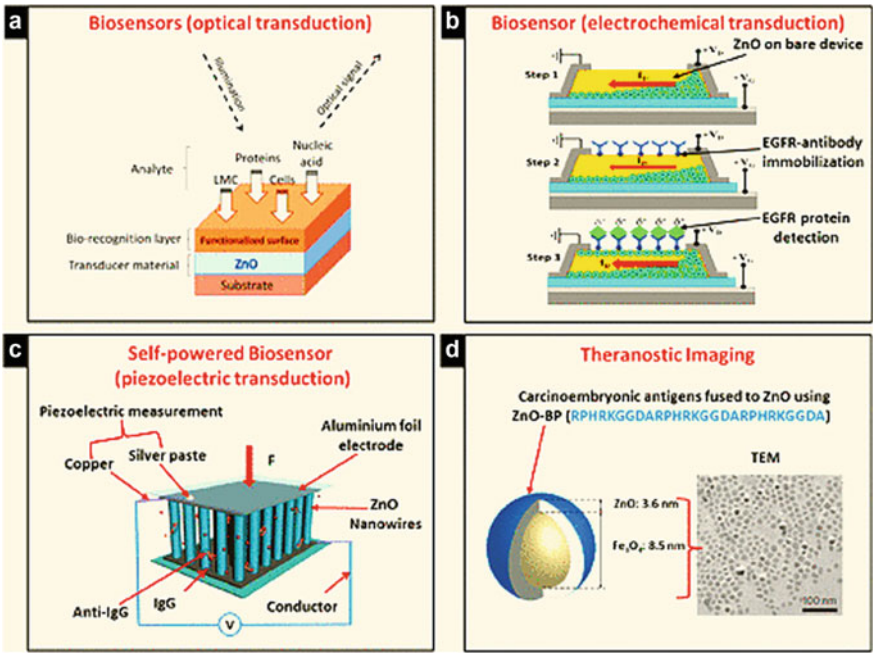

Fig. 6.9 Study interactions of biomolecules with metal oxides

Right Standard for Dose

Nanoparticle toxicity has been shown to function in a concentration-dependent manner. As a result, the determination of an appropriate nanoparticle dose to utilize in a cytotoxicity assay is a key to understanding the toxic effects of the nanoparticles under real-world conditions. The nanoparticle dosage employed should be based on how and in what quantity people are exposed to the nanoparticles. Examining the effects of a realistic dose of nanoparticles limits the probability of observing artificial toxicity induced by an unrealistically high dose and allows for the observation of the actual toxic effects of the nanoparticles. The concentration of particles introduced into the cell cultures of cytotoxicity assays widely varies depending on the parameter used to determine the dose of nanoparticles. In most studies, the dose has been expressed as mass per unit volume (e.g. μg/ml). However, in contrast to soluble chemicals, the nanoparticles have a tendency to diffuse, settle, and agglomerate in dispersion media. The extent of these processes depends on the nanoparticle size, shape, charge, and density, as well as the viscosity and density of the solution. These properties influence the transportation rate of nanoparticles to adherent cells on the culture plate and therefore affect the effective dose within cells.

As a result, defining the dose for in vitro study is rather complicated. Considering the gravitational settling and expressing the dose in terms of mass per unit surface area of the culture dish (μg/cm^2) may alleviate one of the discrepancies among doses. Moreover, the impact of cell density on cell behaviour should be considered as it affects the actual dose of particles that reach each cell. The dose could be expressed in terms of mass per cell number (μg/106 cells) to account for this effect. In addition to stating the mass of nanoparticles administered to the cell media, the number of nanoparticles administered is also important to note during the cytotoxicity assay. Thus, in our previous study on the cytotoxicity of silica nanotubes, the mass per unit volume concentration was converted to the number of particles and reported in the article. At equivalent concentrations, the number of 200 nm nanotubes was approximately 2.5-times higher than that of 500 nm nanotubes. We hypothesized that the increased number of 200 m nanotubes, along with the Kong et al. Page 6 Nanomedicine (Lond). Author manuscript; available in PMC 2012 May 1 smaller size, contributed to the increased toxicity observed. Indicating the dose in numerous forms concerning the property of the nanoparticle may be helpful for the quantitative estimation of particle–cell interaction and may improve the comparability among cytotoxicity assays. Although the metrics mentioned above allow for a better description of the administered nanoparticle concentration, they can only represent the nominal media concentration. None of these methods can accurately reflect the concentration of nanoparticles directly delivered to the cells. For the precise identification of cellular dose rather than exposure, systematic consideration of dose–response assessment is required. The transport of nanoparticles to cells is influenced by factors such as the diffusion rate, gravitational settling, and agglomeration of the particle. These factors are determined by the size, shape, and surface charge of the particle and the density and viscosity of the media. Numerous analytical tools, including microscopy, mass spectrometry (MS), inductively coupled

plasma MS (ICPMS), liquid chromatography MS (LC-MS), and radioactive isotope, are used to estimate the cellular dose of nanoparticles. In addition to estimating the in vivo dose of particles, these computational dosimetry methods have also been proposed as a promising tool to describe the kinetics of nanoparticles in biological systems. To estimate the cellular dose of nanoparticles more accurately, the concerted tools of the above-mentioned methods are thought to be helpful. For example, the MS could quantitatively measure the dose and the microscopic method would qualitatively visualize the translocation of nanoparticles throughout the cell organelles. The absence of an agreed definition of dose concerning mass, volume, number, and surface area also hinders the ability to achieve the objective analysis and comparison of toxicity between various nanoparticles. To overcome this obstacle, stating the dose of nanoparticles with at least two metrics would be beneficial in generating a more standardized concept of dose. Especially, indicating the parameter of dose both in mass per unit volume (μg/ml) and number of particle per unit volume (number of particles/ml) would be helpful to have a sense of the density of particle and quantity of cell–particle interactions.

Food Packaging Applications

Protection of food from microbial pollution is one of the main purposes in food packaging. The emergence of nanotechnology assisted to present novel food packaging materials with antimicrobial properties and with novel nanosensors to trace and monitor the food. Several studies have addressed the antibacterial properties and potential applications of ZnO-NPs in food processing. For example, ZnO has been included in a number of food linings in packaging to avoid spoilage plus it maintains colours. ZnO-NPs provides antimicrobial activity for food packaging. Once they are introduced in a polymeric matrix, it permits the interaction of food with the packaging possessing a functional part in the conservation. Other benefits also are achieved such as the barrier properties, constancy, and mechanical capability. The use of polymer nanotechnology in packaging was introduced by Silvestre et al. to achieve a novel way of packaging that mainly meets the requirements of protection against bacteria. These new 236 Nano-Micro Lett. (2015) 7(3):219–242 materials with improved antimicrobial properties permit also tracking of food during storage and transfer.

Bibliography

1. Saravanan, M., S.K. Barik, D. MubarakAli, P. Prakash, and A. Pugazhendhi. 2018. Synthesis of silver nanoparticles from Bacillus brevis (NCIM 2533) and their antibacterial activity against pathogenic bacteria. *Microbial Pathogenesis* 116: 221–226.
2. Samuel, M.S., S. Jose, E. Selvarajan, T. Mathimani, and A. Pugazhendhi. 2020. Biosynthesized silver nanoparticles using Bacillus amyloliquefaciens; Application for cytotoxicity effect on A549 cell line and photocatalytic degradation of p-nitrophenol. *Journal of Photochemistry and Photobiology, B: Biology* 202: 111642.

3. Hosseini-Koupaei, M., B. Shareghi, A.A. Saboury, F. Davar, V.A. Sirotkin, M.H. Hosseini-Koupaei, and Z. Enteshari. 2019. Catalytic activity, structure and stability of proteinase K in the presence of biosynthesized CuO nanoparticles. *International Journal of Biological Macromolecules* 122: 732–744.
4. Rahman, A., A. Ismail, D. Jumbianti, S. Magdalena, and H. Sudrajat. 2010. Synthesis of copper oxide nano particles by using *Phormidium cyanobacterium. Indonesian Journal of Chemistry* 9: 355–360.
5. Ghasemi, N., F. Jamali-Sheini, and R. Zekavati. 2017. CuO and Ag/CuO nanoparticles: Biosynthesis and antibacterial properties. *Materials Letters* 196: 78–82.
6. Saif Hasan, S., S. Singh, R.Y. Parikh, M.S. Dharne, M.S. Patole, M.L.V. Prasad, et al. 2008. Bacterial synthesis of copper/copper oxide nanoparticles. *Journal of Nanoscience and Nanotechnology* 8: 3191–3196.
7. Suresh, C. M., R. Shani, and T. Rohini. 2019. Biosynthesis of copper oxide nanoparticles using *Enicostemma axillare* (Lam.) leaf extract. *Biochemistry and Biophysics Reports 20*: 100699.
8. Duman, F., I. Ocsoy, and F.O. Kup. 2016. Chamomile flower extract-directed CuO nanoparticle formation for its antioxidant and DNA cleavage properties. *Materials Science and Engineering C* 60: 333–338.
9. Ismail, O., L.P. Mathews, A.O. Muserref, K. Sanju, C. Tao, Y. Mingxu, and T. Weihong. 2013. Nanotechnology in plant disease management: DNA directed silver nanoparticles on graphene oxide as an antibacterial against Xanthomonas perforans. *ACS Nanomaterials* 7: 8972–8980.
10. Ismail, O., G. Basri, C. Tao, Z. Guizhi, C. Zhuo, M.S. Mufrettin, P. Lu, X. Xiangling, and T. Weihong. 2013. DNA-Guided-Metal nanoparticle formation on graphene oxide surface. *Advanced Materials* 25 (16): 2319–2325.
11. Rupak, T., B. Chintan, S. Pragya, A. Suvash, and D. Pravin. 2017. Enzyme-mediated formulation of stable elliptical silver nanoparticles tested against clinical pathogens and MDR bacteria and development of antimicrobial surgical thread. *Annals of Clinical Microbiology and Antimicrobials* 16: 39.
12. Rezaie, A.B., M. Montazer, and M.M. Rad. 2017. Photo and biocatalytic activities along with UV protection properties on polyester fabric through green in-situ synthesis of cauliflower-like CuO nanoparticles. *Journal of Photochemistry and Photobiology, B: Biology* 176: 100–111.
13. Singhal, G., and R. Bhavesh. 2011. Biosynthesis of silver nanoparticles using Ocimum sanctum (Tulsi) leaf extract and screening its antimicrobial activity. *Journal of Nanoparticle Research* 13: 2981–2988.
14. Zhao, J., L. Bowman, X. Zhang, V. Vallyathan, S. Young, V. Castranova, and M. Ding. 2009. Titanium dioxide (TiO_2) nanoparticles induce JB6 Cell apoptosis through activation of the caspase-8/bid and mitochondrial pathways. *Journal of Toxicology & Environmental Health Part A: Current Issues* 72: 1141–1149.
15. Fabian, E., R. Landsiedel, L. Ma-Hock, K. Wiench, W. Wohlleben, and B. van Ravenzwaay. 2008. Tissue distribution and toxicity of intravenously administered titanium dioxide nanoparticles in rats. *Archives of Toxicology* 82: 151–157.
16. Oberdörster, G. 2000. Pulmonary effects of inhaled ultrafine particles. *International Archives of Occupational and Environmental Health 74*: 1−8.
17. Vranic, S., I. Gosens, N.R. Jacobsen, K.A. Jensen, B. Bokkers, A. Kermanizadeh, V. Stone, A. Baeza-Squiban, F.R. Cassee, L. Tran, et al. 2017. Impact of serum as a dispersion agent for in vitro Andin vivo toxicological assessments of TiO_2 nanoparticles. *Archives of Toxicology* 91: 353–363.
18. Rizk, M.Z., S.A. Ali, M.A. Hamed, N.S. El-Rigal, H.F. Aly, and H.H. Salah. 2017. Toxicity of titanium dioxide nanoparticles: Effect of dose and time on biochemical disturbance, oxidative stress and genotoxicity in mice. *Biomedicine & Pharmacotherapy* 90: 466–472.
19. Hong, F., L. Ji, Y. Zhou, and L. Wang. 2017. Chronic nasal exposure to nanoparticulate TiO_2 causes pulmonary tumorigenesis in male mice. *Environmental Toxicology* 32: 1651–1657.
20. Lin, X., J. Li, S. Ma, G. Liu, K. Yang, M. Tong, and D. Lin. 2014. Toxicity of TiO_2 nanoparticles to *Escherichia coli*: Effects of particle size, crystal phase and water chemistry. *PLoS One* 9: 0110247.

21. Zhu, Z., T. Chen, Y. Gu, J. Warren, and R. Osgood. 2005. Zinc oxide nanowires grown by vapor-phase transport using selected metal catalysts: A comparative study. *Chemistry of Materials* 17: 4227–4234.
22. Karlsson, H.L., P. Cronholm, J. Gustafsson, and L. Moller. 2008. Copper oxide nanoparticles are highly toxic: A comparison between metal oxide nanoparticles and carbon nanotubes. *Chemical Research in Toxicology* 21: 1726–1732.
23. Lai, J.C., M.B. Lai, S. Jandhyam, V.V. Dukhande, A. Bhushan, C.K. Daniels, and S.W. Leung. 2008. Exposure to titanium dioxide and other metallic oxide nanoparticles induces cytotoxicity on human neural cells and fibroblasts. *International Journal of Nanomedicine* 3: 533–545.
24. Horie, M., K. Fujita, H. Kato, S. Endoh, K. Nishio, L.K. Komaba, A. Nakamura, A. Miyauchi, S. Kinugasa, Y. Hagihara, E. Niki, Y. Yoshida, and H. Iwahashi. 2012. Association of the physical and chemical properties and the cytotoxicity of metal oxide nanoparticles: Metal ion release, adsorption ability and specific surface area. *Metallomics* 4: 350–360.
25. Ivask, A., T. Titma, M. Visnapuu, H. Vija, A. Kakinen, M. Sihtmae, S. Pokhrel, L. Madler, M. Heinlaan, V. Kisand, R. Shimmo, and A. Kahru. 2015. Toxicity of 11 metal oxide nanoparticles to three mammalian cell types in vitro. *Current Topics in Medicinal Chemistry* 15: 1914–1929.
26. Hsu, A., F. Liu, Y.H. Leung, A.P. Ma, A.B. Djurisic, F.C. Leung, W.K. Chan, and H.K. Lee. 2014. Is the effect of surface modifying molecules on antibacterial activity universal for a given material? *Nanoscale* 6: 10323–10331.
27. Ng, A.M., C.M. Chan, M.Y. Guo, Y.H. Leung, A.B. Djurisic, X. Hu, W.K. Chan, F.C. Leung, and S.Y. Tong. 2013. Antibacterial and photocatalytic activity of TiO_2 and ZnO nanomaterials in phosphate buffer and saline solution. *Applied Microbiology and Biotechnology* 97: 5565–5573.
28. Lin, S., Y. Zhao, T. Xia, H. Meng, Z. Ji, R. Liu, S. George, S. Xiong, X. Wang, H. Zhang, S. Pokhrel, L. Madler, R. Damoiseaux, S. Lin, and A.E. Nel. 2011. High contentscreening in zebra fish speeds up hazard ranking of transition metal oxide nanoparticles. *ACS Nano* 5: 7284–7295.
29. Murdock, R.C., L. Braydich-Stolle, A.M. Schrand, J.J. Schlager, and S.M. Hussain. 2008. Characterization of nanomaterial dispersion in solution prior to in vitro exposure using dynamic light scattering technique. *Toxicological Sciences* 101: 239–253.

Part IV
Future is on Cheap Metal Oxides—PbO Nanoparticles by Sol Gel Method

Chapter 7
Future is on Cheap Metal Oxides—A Review

Quantum mechanical confinement and increased availability of surface atoms than inside atoms for participating in any reaction, metal oxide nanoparticles have distinct physical, chemical, optical, and electronic properties compared to their bulk counterparts. Surface area, shape, size, stability, crystallinity, anticorrosiveness, conductivity, and photocatalytic activity are all qualities that metal oxide nanoparticles have. In general, there are two types of metal oxide nanoparticle synthesis methods: I physical methods such as ball milling, sputtering, laser ablation, electrospraying, and electron beam evaporation; and (ii) chemical processes such as sol–gel, polyol, hydrothermal, co-precipitation, microemulsion, and chemical vapour deposition, among others (Fig. 7.1). Chemical methods are mainly based on bottom to up approach, i.e. the assembly of atoms or molecules to form distribution of different sizes of nanoparticles, whereas physical methods are based on top to down strategy; i.e. the synthesis is started from the bulk counterpart of any material which gets depleted systematically for the generation of fine nanoparticles. Chemical approaches have the benefit of allowing the manufacture of particles with precise size, dimension, composition, and structure, which could be beneficial in a variety of applications such as catalysis, sensing, and electrical devices.

Furthermore, synthesis using chemical methods, notably the sol–gel route, necessitates a lower processing temperature and less energy, making this method more cost-effective than physical methods. The properties of nanoparticles are directly influenced by their form and size. They discovered that the catalytic activity of gold nanoparticles is dependent on the nanoparticle support contact; hemispherical nanoparticles outperformed spherical nanoparticles. In a similar investigation, platinum nanoparticles were found to have increased catalytic activity. Xu et al. studied the oxidation of styrene over cubic, truncated triangular nanoplates, and near-spherical Ag nanoparticles, and discovered that the rate of reaction over the nanocube particle was 14 times higher than over the nanoplates, and four times higher than over the near-spherical Ag nanoparticles. Applications in photocatalysis, photovoltaics, sensors, hydrogen production, and biomedical fields are discussed in detail.

B. Karthikeyan et al., *Nano Metal Oxides*,
https://doi.org/10.1007/978-981-19-9444-9_7

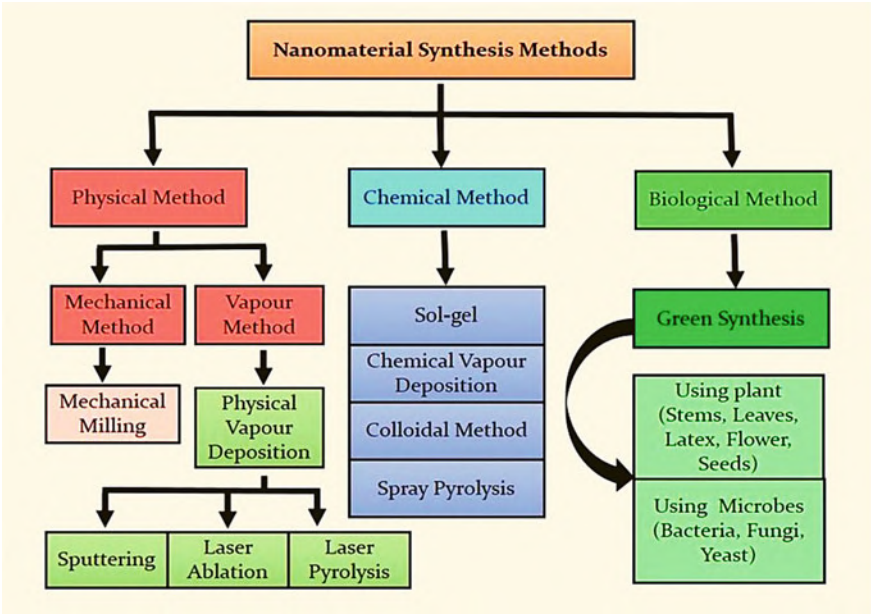

Fig. 7.1 Metal oxide nanoparticles are synthesized using a variety of physical and chemical processes

The sol–gel method is a well-known synthetic method for producing high-quality metal oxide nanoparticles and mixed oxide composites. The texture and surface qualities of the materials may be controlled very well with this procedure. As explained in, the sol–gel process can be broken down into five major steps: hydrolysis, polycondensation, ageing, drying, and heat degradation (Fig. 7.2).

Nanoparticles are a broad category of materials that includes particulate materials with at least one dimension of less than 100 nm. Nanoparticles differ from traditional, larger building blocks of substances in terms of their characteristics and behaviour. Nanotechnology is not a new concept to humanity. Noble metal colloids have a long history dating back to antiquity. Lead-based chemistry was first used in cosmetics some 4000 years ago in ancient Egypt (Fig. 7.3). When searching for the term "PbO nanoparticles" on Science Direct on 28 November 2019 shows an increase in the number of published papers, indicating that researchers' interest in PbO nanoparticles has been gradually increasing since 2010. The special properties of metal and metal oxide nanoparticles, such as catalytic activity and optical, electronic, antibacterial, and magnetic properties, are determined by their size, shape, and chemical surroundings, which can be controlled using physical, chemical, or biological methods to control the dimensions of these building blocks and their assembly.

Lead oxide electrical characteristics, such as band gap and thus colour, are heavily influenced by lead-to-oxygen ratios and crystal structures of different polymorphs.

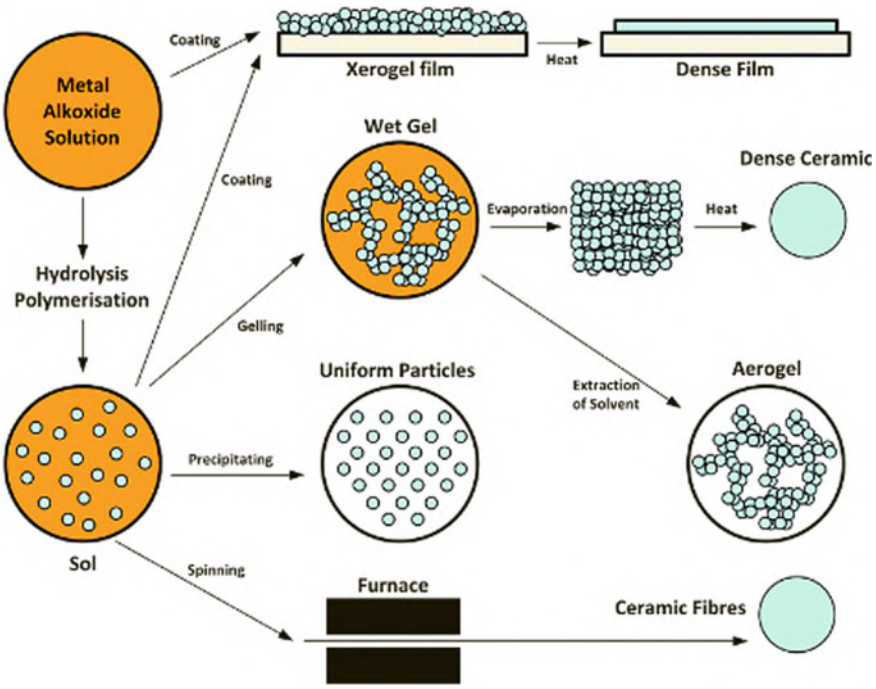

Fig. 7.2 Steps involved in making metal oxide nanoparticles using the sol–gel method

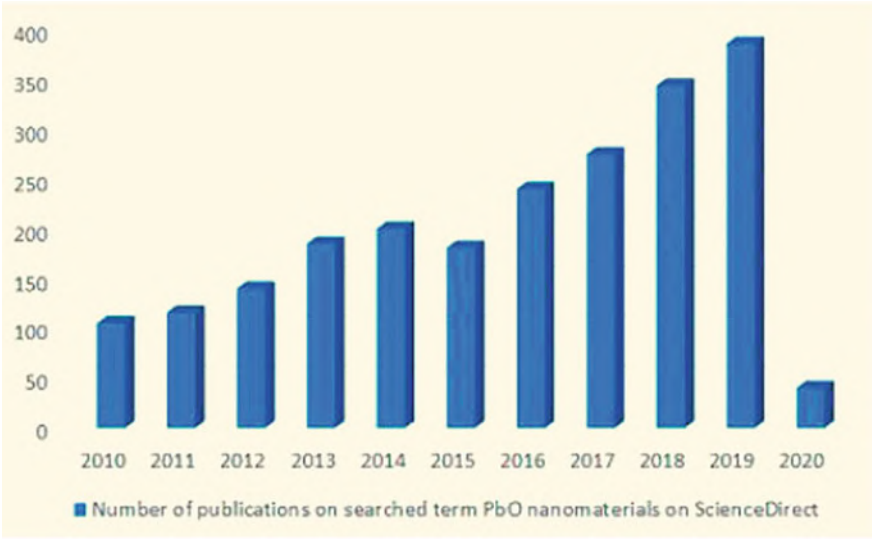

Fig. 7.3 By Googling the phrase "PbO nanoparticles" on Science Direct, you can find the results of published papers

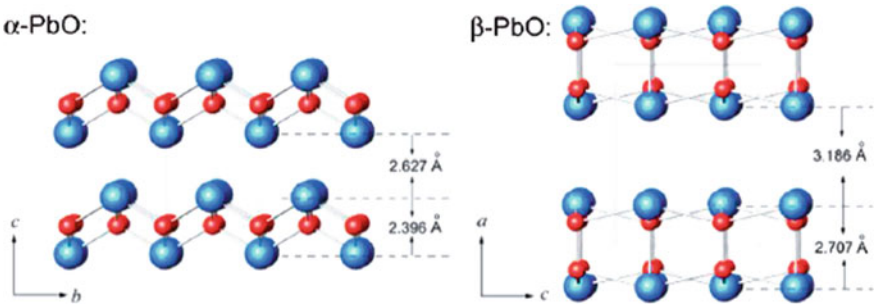

Fig. 7.4 α-PbO and β-PbO crystal formations

PbO, PbO_2 (crystalline and amorphous), Pb_2O_3, and Pb_3O_4 are some of the oxide forms of lead. The most research has been done on lead monoxide (PbO). Lead oxide is a common industrial substance that is used in batteries, gas sensors, pigments and paints, ceramics, and glass manufacturing, as well as a catalyst in synthetic organic chemistry. The morphologies of lead oxide nanoparticles can have a significant impact on their characteristics. Nanoplates, nanostars, and nanodendrites, nanorods, nanopowders, and nanosheets and nanotubes are all examples of lead oxide.

The colour of tetragonal crystalline structure is red, with a band gap of 1.9–2.2 eV and has been demonstrated to be stable at normal temperature, but the colour of orthorhombic crystalline structure is yellow, with a band gap of 2.7 eV and has been found to be stable at high temperatures, above 488 °C. The temperature at which –PbO becomes –PbO is around 490 °C. The photoconductive characteristics of the PbO yellow nanostructure. Nanomaterial synthesis is an essential study topic in a variety of scientific and industrial fields.

Researchers are interested in nanomaterials because of their unique physical and chemical properties, as well as their potential application in a variety of fields such as gas sensors, fuel cells, paints, rechargeable batteries, pigments, and so on. There are four forms of lead oxides (PbO, Pb_2O_3, PbO_2, and Pb_3O_4). Yellow b-PbO, which is stable at high temperatures, and red a-PbO, which is stable at low temperatures, is the two forms of PbO. At around 4900 °C, the a-PbO phase transforms to b-PbO. Due to its unique electronic, mechanical, and optical properties, as well as its potential applications in nanodevices and functionalized materials such as active materials for lead-acid batteries, valve-regulated lead-acid (VRLA) batteries, and lithium secondary batteries, lead oxide (PbO) is an important industrial material (Fig. 7.4).

There is a lot of interest in improving and developing lead oxide characteristics to get more discharge capacity and cycle life when compared to other electrochemical systems of lead-acid batteries because of the simplicity of design, low cost of manufacture, reliability, and relative safety when compared to other electrochemical systems of lead-acid batteries. As a result, research to improve lead oxide and lead dioxide discharge capacity is still needed. To produce nanometre-sized lead oxides,

a variety of physicochemical methods have been used, including thermal decomposition, spray pyrolysis, selected control synthesis [hydrothermal synthesis, sono chemical, microwave irradiation, synthesis by coordination polymers, and pulsed current electrochemical methods. However, the sol–gel process, which is a low-cost, easy, and non-hazardous approach for creating various nanooxides, has yet to be examined for nanosized lead oxides.

The sol–gel process has a number of advantages over traditional approaches, including the ability to control the size and morphology of crystallized particles, as well as the ability to produce powders with a higher percentage of crystallization phase and a higher density. In this study, lead oxide nanopowders were made by using a sol–gel technique to combine citric acid and lead acetate solution. FT-IR spectroscopy, TGA, XRD, and SEM were used to characterize the produced lead oxide nanopowders. Nanoplates, nanostars, nanorods, nanopowders, nanosheets, and nanotubes are among the numerous forms of lead oxide and their nanostructure compositions that have been documented. In addition, multiple oxidation states of lead have been recorded as a result of varied experimental settings. PbO is yellow, Pb_3O_4 is red, and $Pb_{12}O_{19}$ is brown, as is well known that the lead-to-oxygen ratio controls the band gap and, hence, the hue. However, because of the photoconductive features of PbO nanostructures, they have received more attention than other types of lead oxides (Fig. 7.5).

PbO is a tetragonal and orthorhombic phase semiconductor with a direct band gap. The band gaps of PbO's tetragonal and orthorhombic phases are 1.9–2.2 eV and 2.6 eV, respectively. Calcination, chemical techniques, gel combustion, anodic oxidation, hydrothermal treatment, and thermal breakdown have all recently been employed to manufacture PbO nanostructures. In general, making nanoparticles is a difficult process with a wide range of variables that might influence the end product's qualities. Some significant variables have distinct effects on the final product's qualities, while others may have relatively small impacts.

When making nanoparticles like PbO nanoparticles, it is crucial to get a limited size distribution for the end result and be able to manage the nanoparticles' morphology. In the sol–gel method, these goals can be met by utilizing an appropriate polymerization agent. For the first time, a facile sol–gel technique was developed to manufacture PbO nanoparticles in a gelatin medium. Because gelatin swells during the calcination process, making it impossible for the particles to gather together, it was utilized as a terminator for producing the PbO nanoparticles (Fig. 7.6).

The size, shape, and crystallinity of the PbO nanoparticles that resulted were studied. Nanomaterials have piqued the interest of many researchers due to their unique physical and chemical properties, as well as their prospective uses in a variety of scientific and industrial domains. Due to their small size, nanomaterials have also been employed in gas sensors, fuel cells, paints, rechargeable batteries, and pigments. Furthermore, one-dimensional (1D) nanostructures have garnered attention in solar energy conversion due to its long axis for absorbing incident sunlight. Copper doped zinc oxide nanoparticles characterization and application in energy conversion Because of their many phases, lead oxides are intriguing substances.

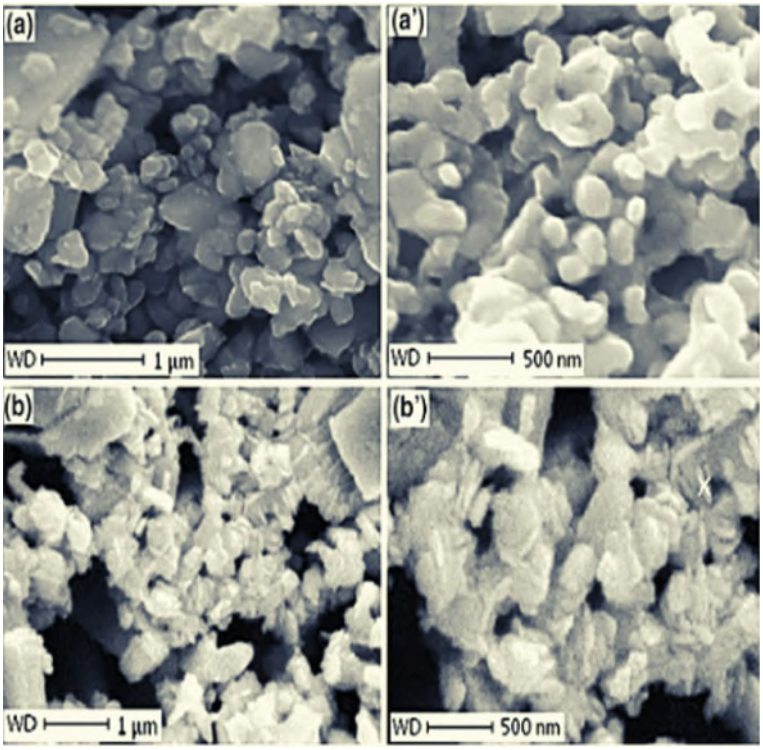

Fig. 7.5 SEM micrograph of lead oxide manufactured using **a** one-step drying (a in magnification of 15, 0009, a0 in magnification of 30, 0009) and **b** two-step drying (b in magnification of 15, 0009, b0 in magnification of 30, 0009) methods. The following conditions remained constant: MRCL = 2 and calcination temperature 4500 °C for 12 h (D and F samples, respectively)

These stages are divided into four categories: PbO (and amorphous), Pb_2O_3, Pb_3O_4 and PbO_2 (and amorphous). PbO is polymorphic and has a large band gap. The yellow –PbO is one of these two forms, and it is stable at temperatures above 425 °C. The red –PbO, which is stable at low temperatures, is the second form. At around 490 °C, the –PbO phase transforms to –PbO. The high-temperature yellow form. PbO is a transparent conducting oxide (TCO) with a high dielectric constant ($' = 525.9$) and a high dielectric constant ($' = 525.9$). It is also a substance with a high refractive index. The photoactive semiconductors –PbO and –PbO have band gaps of 1.92 and 2.7 eV, respectively. The computation of both lead citrate and lead oxalate yielded a mixture of and –PbO nanocrystals.

Due to its simplicity of production, electrical, mechanical, and optical properties, as well as its potential uses in nanodevices and functionalized materials, interest in the synthesis of PbO nanostructures has grown in recent years. PbO nanoparticles in both configurations have been employed in medical applications such as gamma ray protective garments, shielding, magnetic imaging, batteries, X-ray detection, and

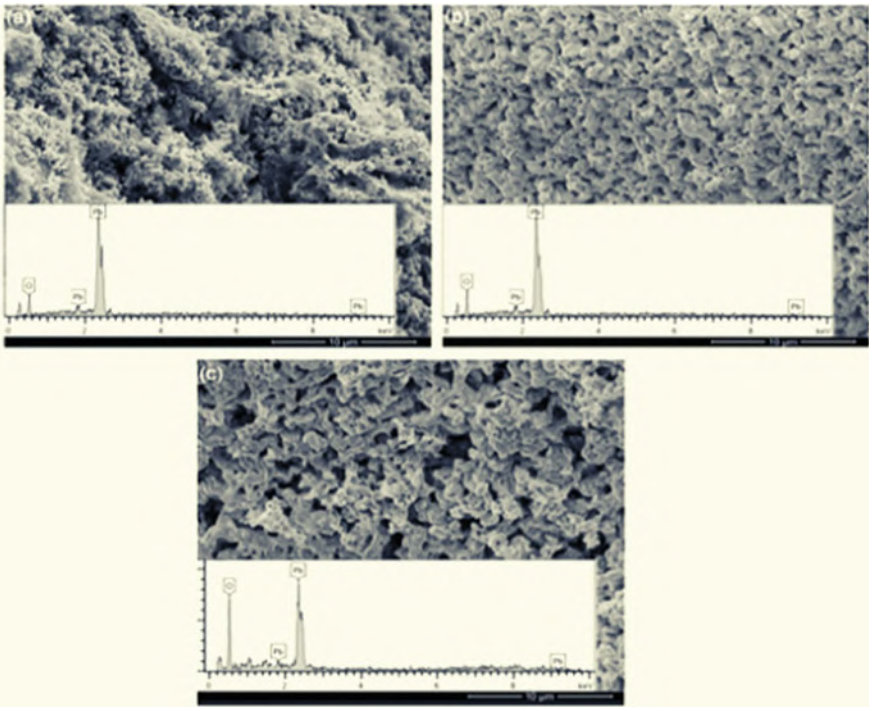

Fig. 7.6 SEM pictures and EDX spectra of nanostructures generated at **a** 5000 °C, **b** 5500 °C, and **c** 6000 °C calcination temperatures

medication delivery. Recent research has shown that nanolead oxides in rod and spherical shapes have antibacterial properties. PbO is also amphoteric, meaning it interacts readily with both acids and bases. Various approaches could be used to create lead oxide nanostructures. The sol–gel approach has a number of advantages over traditional methods, including being a low-cost, easy, and non-hazardous way for preparing various nanooxides. To produce and analyse lead oxide nanopowders, Kashani Motlagh and Mahmoudabad employed the sol–gel method. On the other hand, as the medical, pharmaceutical, nuclear, and space industries demand lighter, stronger, and greater radiation resistant materials, the need for more efficient radiation shielding and structural materials develops. Various researches have lately been conducted in this area. Because of its high density (9.53 g/cm^3), lead monoxide (PbO) proved successful in shielding radiation such as X-rays or -rays, according to the studies (Fig. 7.7).

Lead oxide nanopowders were generated in this study for usage in a variety of applications. The sol–gel approach was introduced as a reproducible process for the large-scale synthesis of PbO nanoparticles since it is simple, affordable, and economical. The produced nanoparticles were characterized using X-ray diffractometry, as well as the morphology of the particles using a transmission electron microscope.

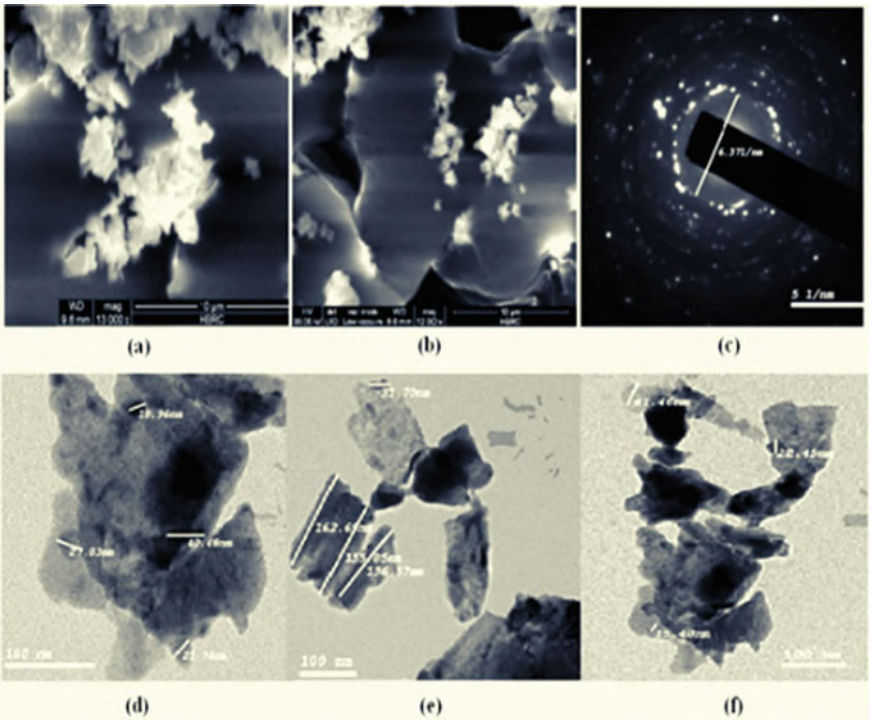

Fig. 7.7 **a, b** SEM images, **c** SAED pattern and **d**, **e**, **f** TEM images of PbO nanocrystals

Thermogravimetric analysis, differential scanning calorimetry and Fourier transform infrared spectroscopy were used to learn more about the produced particles. The produced PbO nanoparticles were X-ray diffracted (XRD) using a Phillips PW1840 X-ray diffractometer (USA) equipped with a CuK radiation anode tube (=1.54056) and operated at 40 kV and 25 mA. The difffractogram was recorded at a speed of 2 degrees per minute in the range of 2 from 5 to 70°.

After permitting the PbO sample to spread over a tiny metal circular plate at 30 kV and a magnification power of 3000×, the surface morphology was studied using scanning electron microscopy (SEM; Inspect S, FEI, Holland) in a low vacuum mode. To achieve high resolution and get bright field and dark field images of the particles, high-resolution transmission electron microscopy (HRTEM; JEM 2100, Jeol, Japan) was used.

The produced PbO nanoparticles' Fourier transform infrared (FT-IR) transmission spectrum was obtained using the potassium bromide pellet approach. 1 mg of powdered material was mixed with 100 mg of dried potassium bromide powders to make the pellets. FT-IR spectroscopy is a useful instrument for understanding the behaviour of functional groups in organic molecules (Fig. 7.8). The HRTEM picture of the as-prepared PbO revealed distinct lattice fringes. The average lattice distance was measured to be 0.31 nm, which is evident.

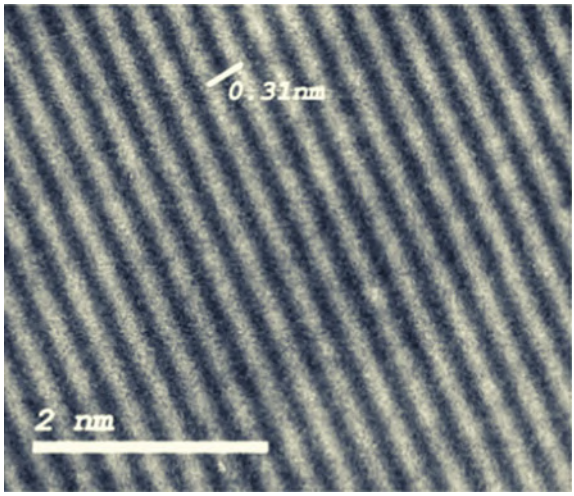

Fig. 7.8 HRTEM of PbO nanocrystals

Bibliography

1. Parashar, Mritunjaya, Vivek Kumar Shukla, and Ranbir Singh. 2020. Metal oxides nanoparticles via sol–gel method: a review on synthesis, characterization and applications. *Journal of Materials Science: Materials in Electronics*.https://doi.org/10.1007/s10854-020-02994-8
2. Bratovcic, Amra. 2020. Synthesis, characterization, applications, and toxicity of lead oxide nanoparticles. Lead chemistry edited by pipat chooto. https://doi.org/10.5772/intechopen.91362
3. Kashani-Motlagh, Mohammad Mehdi, and Masoumeh Karami Mahmoudabad. Synthesis and characterization of lead oxide nano-powders by sol–gel method. *Journal of Sol-Gel Science and Technology 59*: https://doi.org/10.1007/s10971-011-2467-y
4. Yousefi, Ramin, Ali Khorsand Zak, Farid Jamali-Sheini, Nay Ming Huang, Wan Jefrey Basirun, and M. Sookhakian. 2014. Synthesis and characterization of single crystal PbO nanoparticles in a gelatin medium. *Ceramics International*. https://doi.org/10.1016/j.ceramint.2014.03.180
5. Elawam, Sarah A., Wafaa M. Morsi, Hoda M. Abou-Shady, and Osiris W. Guirguis. 2016. Characterizations of beta-lead oxide "Massicot" nano-particles. *British Journal of Applied Science & Technology 17* (1). Article no.BJAST.28143 ISSN: 2231-0843, NLM ID: 101664541.
6. Shakeel, M., F. Jabeen, S. Shabbir, M.S. Asghar, M.S. Khan, and A.S. Chaudhry. 2016. Toxicity of nano-titanium dioxide (TiO_2-NP) through various routes of exposure: A review. *Biological Trace Element Research* 172: 1–36.
7. Norton, D.P., Y. Heo, M. Ivill, K. Ip, S. Pearton, M.F. Chisholm, and T. Steiner. 2004. ZnO: Growth, doping & processing. *Materials Today* 7: 34–40.
8. Pearton, S., D. Norton, K. Ip, Y. Heo, and T. Steiner. 2005. Recent progress in processing and properties of ZnO. *Progress on Material Science 50*: 293−340.
9. Klingshirn, C. 2007. ZnO: Material, physics and applications. *Chem. Phys. Chem.* 8: 782–803.
10. Ellmer, K., A. Klein, and B. Rech. 2007. *Transparent conductive zinc oxide: Basics and applications in thin film solar cells*. Berlin: Springer Science & Business Media.
11. Serizawa, T., T. Sawada, and H. Matsuno. 2007. Highly specific affinities of short peptides against synthetic polymers. *Langmuir* 23: 11127–11133.
12. Hirai, T., Y. Harada, S. Hashimoto, T. Itoh, and N. Ohno. 2005. Luminescence of excitons in mesoscopic ZnO particles. *Journal of Luminescence* 112: 196–199.
13. Ozgur, U., D. Hofstetter, and H. Morkoc. 2010. ZnO devices and applications: A review of current status and future prospects. *Proceedings of the IEEE* 98: 1255–1268.

14. Ahmed, M.H., T.E. Keyes, J.A. Byrne, C.W. Blackledge, and J.W. Hamilton. 2011. Adsorption and photocatalytic degradation of human serum albumin on TiO_2 and Ag-TiO_2 films. *Journal of Photochemistry and Photobiology A: Chemistry* 222: 123–131.
15. Xia, Y., J. Wang, R. Chen, D. Zhou, and L. Xiang. 2016. A review on the fabrication of hierarchical ZnO nanostructures for photo catalysis application. *Crystals* 6: 148.
16. Bunn, C. 1935. The lattice-dimensions of zinc oxide. *Proceedings of the Physical Society* 47: 835.
17. Moezzi, A., A.M. McDonagh, and M.B. Cortie. 2012. Zinc oxide particles: Synthesis, properties and applications. *Chemical Engineering Journal* 185–186: 1–22.
18. Brayner, R., R. Ferrari-Iliou, N. Brivois, S. Djediat, M.F. Benedetti, and F. Fiévet. 2006. Toxicological impact studies based on *Escherichia coli* bacteria in ultrafine ZnO nanoparticles colloidal medium, *Nano Letters 6*: 866−870.
19. Reddy, K.M., K. Feris, J. Bell, D.G. Wingett, C. Hanley, and A. Punnoose. 2007. Selective toxicity of zinc oxide nanoparticles to prokaryotic and eukaryotic systems. *Applied Physics Letters* 90: 213902.
20. Nohynek, G.J., J. Lademann, C. Ribaud, and M.S. Roberts. 2007. Grey Goo on the skin? Nanotechnology, cosmetic and sunscreen safety. *Critical Reviews in Toxicology* 37: 251–277.
21. Tankhiwale, R., and S. Bajpai. 2012. Preparation, characterization and antibacterial applications of ZnO-nanoparticles coated polyethylene films for food packaging. *Colloids and Surfaces B* 90: 16–20.
22. Espitia, P.J.P., J.S. dos Reis Coimbra, N.J. de Andrade, R.S. Cruz, E.A.A. Medeiros, and N. de Fátima Ferreira Soares. 2012. Zinc oxide nanoparticles: Synthesis, antimicrobial activity and food packaging applications. *Food Bioprocess Technology 5*: 1447−1464.
23. He, D., X. He, X. Yang, and H. Li. 2017. A Smart ZnO@ polydopamine-nucleic acid anosystem for ultrasensitive live cell mRNA imaging by the target-triggered intracellular self-assembly of active DNAzyme nanostructures. *Chemical Science* 8: 2832–2840.
24. Shanmugam, N.R., S. Muthukumar, and S. Prasad. 2017. A review on ZnO-based electrical biosensors for cardiac biomarker detection. *Future Science OA 3*: FSO196.
25. Tang, C.C., S.S. Fan, M.L.d.l. Chapelle, and P. Li. 2001. Silica-assisted catalytic growth of oxide and nitride nanowires. *Chemical Physics Letters 333*: 12−15.